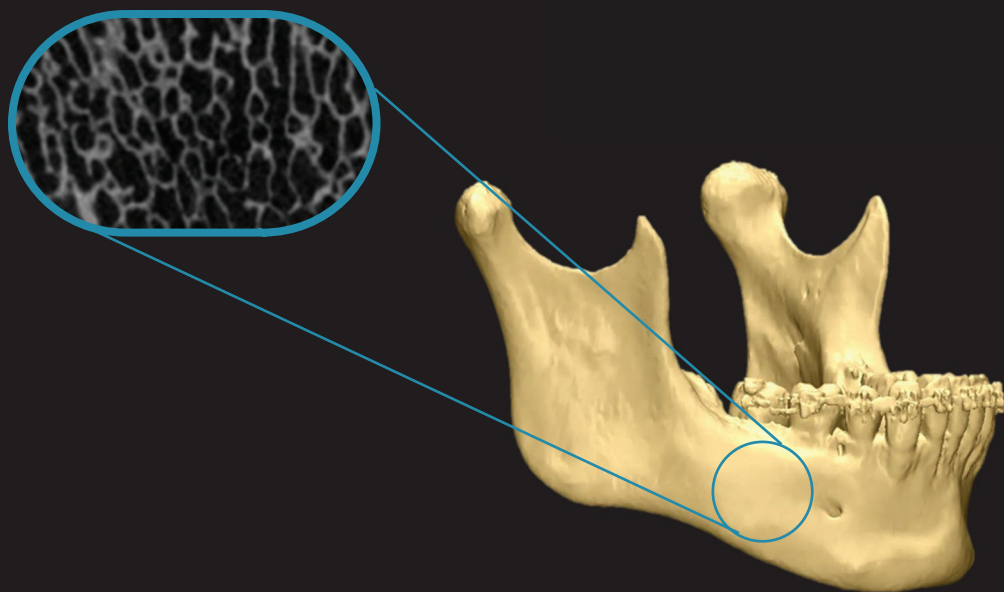




Clinical validation of cone beam computed tomography imaging for objective assessment of jaw bone quality and quantity



Laura NICOLIELO

May 2020

KU Leuven
Groep Biomedische Wetenschappen
Faculteit Geneeskunde
Departement Beeldvorming en Pathologie
Omfs impath Onderzoeksgroep



KLINISCHE VALIDATIE VAN CONE BEAM COMPUTED TOMOGRAPHY VOOR OBJECTIEVE BEPALING VAN KAAKBOT KWALITEIT EN KWANTITEIT

Laura NICOLIELO

Promotor: Prof. Dr. Reinhilde Jacobs, KU Leuven
Promotor: Prof.Dr. Ivo Lambrichts, UHasselt

Proefschrift voorgedragen tot
het behalen van de graad van
Doctor in de Biomedische
Wetenschappen

D/2020/2451/ 16

Mei 2020

KU Leuven
Biomedical Sciences Group
Faculty of Medicine
Department of Imaging & Pathology
Omfs Impath Research Group



CLINICAL VALIDATION OF CONE-BEAM COMPUTED TOMOGRAPHY IMAGING FOR OBJECTIVE ASSESSMENT OF JAW BONE QUALITY AND QUANTITY

Laura NICOLIELO

Promoter: Prof. Dr. Reinhilde Jacobs
Promoter: Prof. Dr. Ivo Lambrichts
Chair: Prof. Dr. Philippe Demaerel
Secretary: Prof. Dr. Constantinus Politis
Jury members: Prof. Dr. Antoon De Laat
Dr. Bruno Collaert
Prof. Dr. Daniel Benchimol
Prof. Dr. Esther Wolfs

Dissertation presented in partial
fulfilment of the requirements
for the degree of Doctor in
Biomedical Sciences

May 2020

Acknowledgements

“Those who pass by us, do not go alone, and do not leave us alone; they leave a bit of themselves, and take a little of us.”

— **Antoine de Saint-Exupéry**

I wish to express my deepest gratitude to:

- My supervisor:

Reinhilde Jacobs.

- My co-supervisor, collaborators and jury members:

Ivo Lambrichts, Constantinus Politis, Bruno Collaert, Antoon De Laat, Daniel Benchimol, Benjamin Salmon, Harry van Lenthe, Jeroen Van Dessel, Walter Coudyzer, Izabel Rubira-Bullen, Yan Huang, Andreas Stratis, Apoorv Kakar, Pieter Slagmolen, Marina Codari, Emmy Shaheen, Carolina Letelier and Mariana Silveira.

- All my colleagues from the OMS IMPATH Research Group and Dentistry Department at KU Leuven:

Ahmed Sobhy, Alessandro Lamira, Ademir Franco, Ana Castro, Ana Ockerman, Andres Torres, Anne Oenning, Bassant Mowafey, Berkan Celikten, Daniel Vasconcelos, Deepti Sinha, Dominique Hekner, Ellen Cloet, Emanuela Santos, Emad Albdour, Francesca Mangione, Gabriela Casteels, Karla Vasconcelos, Jimoh Agbaje, Marta Dyszki, Martine Van Vlierberghe, Myrthel Vranckx, Mostafa EzEldeen, Natalia Salvo, Omar El Mahraoui, Pisha Pittayapat, Tatiana Zogheib, Titiaan Dormaar, Ruben Pauwels, Simón Pedano and Yi Sun.

- All colleagues from the European Association of DentoMaxilloFacial Radiology.

- Brazilian financial support provided by:

CAPES - Coordination for the Improvement of Higher Education Personnel.

- KU Leuven and collaborating universities: UHasselt, Paris Descartes and Karolinska.

Finally to my family in Brazil a special thank you for the unconditional love and support.

Table of Contents

Acknowledgements	I
Table of Contents	II
List of Abbreviations	VI
Preface	VIII
CHAPTER 1 – Introduction and aims	1
1.1 General introduction	2
1.2 Jaw bone quality and quantity	2
1.2.1 Clinical radiographic methods to assess jaw bone quality and quantity	5
1.2.1.1 Conventional radiographs	5
1.2.1.2 Computed tomography	10
1.3 Assessment of bone geometry and microarchitecture	13
1.4 Aims and hypotheses	15
1.5 References	16
CHAPTER 2 – Quantification of bone quality using different CBCT devices: Accuracy assessment for edentulous human mandibles	27
2.1 Abstract	28
2.2 Introduction	30
2.3 Materials and methods	31
2.3.1 Image acquisition	32
2.3.2 Image processing	34
2.3.3 Image analysis: Bone morphometry	34
3.4 Statistical analysis	36
2.4 Results	36
2.4.1 Morphometric parameters	36
2.4.2 Segmentation accuracy on cross-sectional slices	39
2.4.3 Comparison of the 3D bone models	41
2.4.4 Correlation of morphometric indices	41
2.5 Discussion	45
	II

2.6 Conclusions	47
2.7 References	48
CHAPTER 3 – Accuracy and reliability of different CBCT devices for structural analysis of alveolar bone in comparison with multislice CT and micro-CT	53
3.1 Abstract	54
3.2 Introduction	55
3.3 Materials and methods	56
3.3.1 Image acquisitions	57
3.3.2 Image processing	59
3.3.3 Alveolar bone structural analysis	59
3.3.4 Statistical Analysis	60
3.4 Results	61
3.4.1 Quantitative morphometric analysis	61
3.4.2 Morphometric reliability	61
3.4.3 Visual 3D comparison of the alveolar bone network	66
3.5 Discussion	66
3.6 Conclusions	68
3.7 References	70
CHAPTER 4 – Computer-based automatic classification of trabecular bone pattern can assist radiographic bone quality assessment at dental implant site.	77
4.1 Abstract	78
4.2 Introduction	79
4.3 Materials and methods	80
4.3.1 Data acquisition	80
4.3.2 Image processing and quantification of morphometric parameters	80
4.3.3 Automatic trabecular bone classification	81
4.3.4 Subjective trabecular bone classification	82
4.4 Results	82
4.4.1 Automatic trabecular bone classification	82
4.4.2 Subjective trabecular bone classification	83

4.5 Discussion	87
4.6 References	90
CHAPTER 5 – Relationship between trabecular bone architecture and early dental implant failure in the posterior region of the mandible	97
5.1 Abstract	98
5.2 Introduction	99
5.3 Materials and methods	100
5.3.1 Patient selection	100
5.3.2 Image analysis	101
5.3.3 Statistical analysis	105
5.4 Results	106
5.4.1 Patient selection	106
5.4.2 Comparison of trabecular bone types	106
5.4.3 Relationship between bone type and early implant outcome	106
5.5 Discussion	108
5.6 References	111
CHAPTER 6 – Validation of a novel imaging approach using multi-slice CT and cone-beam CT to follow-up on condylar remodelling after bimaxillary surgery	119
6.1 Abstract	120
6.2 Introduction	121
6.3 Materials and methods	121
6.3.1 Clinical assessment of condylar remodelling	121
6.3.1.1 Data acquisition	121
6.3.1.2 Image analysis	122
6.3.2 Validation of method reproducibility	123
6.3.3 Validation of condylar mineralised bone assessment	123
6.3.4 Statistical analysis	124
6.4 Results	128
6.4.1 Clinical assessment of condylar remodelling	128
6.4.2 Validation of method reproducibility	128

6.4.3 Validation of condylar mineralised bone assessment	129
6.5 Discussion	129
6.6 References	133
CHAPTER 7 — General discussion and conclusions	139
7.1 General discussion	140
7.1.1 Future perspectives	143
7.1.1.1 Image analysis workflow	143
7.1.1.2 Bone vascularity	143
7.1.1.3 3D finite element models and bone printing	143
7.2 Conclusions	144
7.3 References	145
Summary	150
Samenvatting	152
Curriculum vitae	154
Scientific Acknowledgment	160
Personal Contribution	162
Conflict of Interest	163

List of Abbreviations

2D.....	Two-Dimensional
3D.....	Three-Dimensional
ANCOVA	Analysis of Covariance
ANOVA	Analysis of Variance
BIC.....	Bone-to-Implant Contact
BMD.....	Bone Mineral Density
BP.....	Bisphosphonate
BS.....	Bone Surface
BS/BV	Ratio of Bone Surface to Volume
BS/TV	Bone Surface Density
BV.....	Bone Volume
BV/TV	Bone Volume Fraction
CBCT.....	Cone Beam Computed Tomography
cc.....	canonical correlation
Conn.Dn	Connectivity Density
CT.....	Computed Tomography
Ct.BV/(Tb.TV+Ct.TV)	Cortical Bone Percentage
Ct.BV/Ct.TV	Cortical Volume Fraction
Ct.Th.....	Cortical Thickness
DA	Degree of Anisotropy
DCE-MRI	Dynamic Contrast-Enhanced MRI
DICOM.....	Digital Imaging and Communications
FD.....	Fractal Dimension
FEA.....	Finite Element Analysis
FOV	Field Of View
GPa	gigapascals
GRRAS.....	Guidelines for Reporting Reliability and Agreement Studies
HU	Hounsfield Units
ICC	Intraclass Correlation Coefficients
kV	kilovolt
kVp	peak kilovoltage
LDA.....	Linear Discriminant Analysis

mA	milliamperes
MCI	Mandibular Cortical Index
micro-CT	Microcomputed Tomography
mm.....	millimetres
MRONJ.....	Medication-Related Osteonecrosis Of The Jaw
MSCT	Multi-Slice Computed Tomography
OPG.....	Orthopantomogram
PMI	Panoramic Mandibular Index
Po(tot).....	Total Porosity Percentage
ROI	Region Of Interest
SMI	Structural Model Index
SNR.....	Signal-to-Noise Ratio
Tb.BS/Tb.TV	Trabecular Surface Density
Tb.BV/Tb.TV	Trabecular Volume Fraction
Tb.N.....	Trabecular Number
Tb.Pf.....	Trabecular Pattern Factor
Tb.Sp.....	Trabecular Separation
Tb.Th	Trabecular Thickness
TMD.....	Temporomandibular Joint Dysfunction
TMJ.....	Temporomandibular Joint
TV.....	Total Volume of interest
vBMD.....	Volumetric Bone Mineral Density
VOI	Volume Of Interest
μA.....	microamperes
μm	micrometres

Preface

This doctoral thesis is based on the following research papers:

Chapter 2:

Van Dessel, J., Nicolielo, L. F., Huang, Y., Slagmolen, P., Politis, C., Lambrichts, I., & Jacobs, R. (2016). Quantification of bone quality using different cone beam computed tomography devices: Accuracy assessment for edentulous human mandibles. *European Journal of Oral Implantology*, 9(4), 411–424.

Chapter 3:

Van Dessel, J., Nicolielo, L. F., Huang, Y., Coudyzer, W., Salmon, B., Lambrichts, I., & Jacobs, R. (2017). Accuracy and reliability of different cone beam computed tomography (CBCT) devices for structural analysis of alveolar bone in comparison with multislice CT and micro-CT. *European Journal of Oral Implantology*, 10(1), 95–105.

Chapter 4:

Nicolielo, L. F. P., Van Dessel, J., van Lenthe, G. H., Lambrichts, I., & Jacobs, R. (2018). Computer-based automatic classification of trabecular bone pattern can assist radiographic bone quality assessment at dental implant site. *The British Journal of Radiology*, 91(1092), 20180437. <https://doi.org/10.1259/bjr.20180437>.

Chapter 5:

Nicolielo, L. F. P., Van Dessel, J., Jacobs, R., Quirino Silveira Soares, M., Collaert, B. (2019). Relationship between trabecular bone architecture and early dental implant failure in the posterior region of the mandible. *Clinical Oral Implants Research*. doi: 10.1111/clr.13551.

Chapter 6:

Nicolielo, L. F. P., Van Dessel, J., Shaheen, E., Letelier, C., Codari, M., Politis, C., ... Jacobs, R. (2017). Validation of a novel imaging approach using multi-slice CT and cone-beam CT to follow-up on condylar remodeling after bimaxillary surgery. *International Journal of Oral Science*, 9(3), 139-144. <https://doi.org/10.1038/ijos.2017.22>

Chapter 1

Introduction and aims

1.1 General introduction

Radiographic assessment of the jaw bone is highly beneficial in different oral and maxillofacial procedures, including the diagnosis of bone pathologies, fractures, planning for surgery, and treatment follow-up of bone healing and remodelling. In clinical practice, conventional radiographs provide a highly effective visualization of maxillofacial bone structures, alveolar bone, among other surrounding important anatomical structures. Panoramic radiographs, as well as intraoral radiographs, are widely used in maxillofacial procedures as complementary and screening exams due to factors such as low-radiation dose, fast acquisition, relatively easy technique of use and low cost, thus providing the surgeon with valuable diagnosis of jaw bone tissue (Choi, 2011; Kim, Park, Kim, Kim, & Kim, 2011; Shah, 2014). Nevertheless, these imaging modalities cannot provide full information on three-dimensional (3D) anatomical structures and reliable measurements of jaw bone quality and quantity (Ribeiro-Rotta, Lindh, Pereira, & Rohlin, 2011). 3D imaging modalities such as Computed Tomography (CT) and Cone-Beam Computed Tomography (CBCT) have been in use for the last 20 years. The latter is increasingly being adopted as well-established, accurate and reliable method for measuring the quality and quantity of jaw bone tissue, in various maxillofacial procedures (Harris et al., 2012; Jacobs, Salmon, Codari, Hassan, & Bornstein, 2018).

1.2 Jaw bone quality and quantity

The knowledge on bone quality has increased exponentially following an increase in the demand for dental implants. For many years now, the success of implant osseointegration depended on factors such as the amount, density and primary stability of the available alveolar bone tissue. Primary stability is defined as the absence of implant mobility after being installed in the bone tissue at the implantation site (Marco, Milena, Gianluca, & Vittoria, 2005), and depends, in turn, on the implant insertion torque (Meredith, 1998). Regional differences in jaw anatomy and bone structure may explain some of the variation in clinical success rate of implant therapy. For instance, the lack of tissue in the maxilla and mandible region acts as a limiting factor for treatment success. The quantity of bone varies considerably because the edentulous regions undergo bone resorption due to disuse atrophy. This can diminish the height and thickness of the alveolar ridge substantially. After tooth loss, regions, such as the anterior part of the maxilla undergo bone resorption, resulting in a greater loss of the alveolar bone. Low quantity (volume) and poor bone density constitute one of the most negative factors in predicting the success or failure in fixing implants (Porter & Von Fraunhofer, 2005). As such, the success rate of implant treatment is considerably lower in the maxilla than the anterior region of the mandible during implant treatment, partly due low bone quality of the maxilla

(Lindh, Obrant, & Petersson, 2004). The highest failure rate has been specifically reported for the posterior region of the maxilla as it lacks sufficient volume and/or bone density (Adell, Eriksson, Lekholm, Brånemark, & Jemt, 1990; Adell, Lekholm, Rockler, & Brånemark, 1981; Bahat, 1993; Engquist, Bergendal, Kallus, & Linden, 1988; Friberg, Jemt, & Lekholm, 1991; Henry et al., 1996; Higuchi, Folmer, & Kultje, 1995; Jaffin & Berman, 1991; Jemt, 1993; Jemt & Lekholm, 1995; Spiekermann, Jansen, & Richter, 1995).

Misch and Judy (1987) utilized the regional differences of jaw bone tissue to develop a classification of residual alveolar bone, which aim to assist surgeons during planning and execution of implant treatment. This classification divided the available alveolar bone in four categories (A to D) from abundant to deficient bone (*Figure 1.1*). Regarding differences in bone density, Misch (1990b) defined four groups (D1 to D4) in all regions of the jaws that vary in both macroscopic cortical and trabecular bone types (*Figure 1.2*).

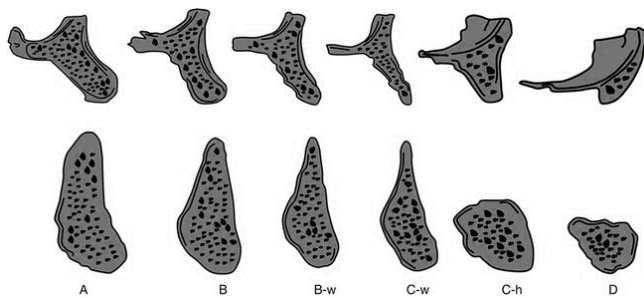


Figure 1.1. Misch and Judy (1987) classification of bone availability (Divisions A, B, C and D): Division A (abundant bone), Division B (barely sufficient bone), Division C (compromised bone), Division D (deficient bone), w (width), h (height).

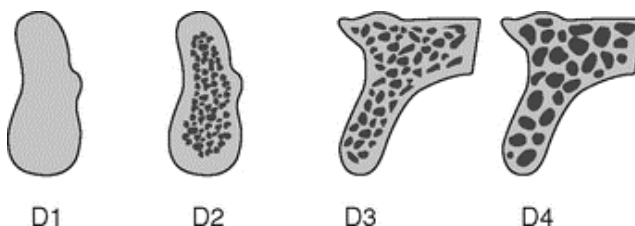


Figure 1.2. Misch bone density classification. D1 primarily dense cortical bone. D2 dense-to-porous cortical bone on the crest and, within the bone, coarse trabecular bone. D3 thinner porous cortical crest and fine trabecular bone. D4 almost no crestal cortical bone, the fine trabecular bone composes almost all of the total volume of bone. From: Misch, 1990.

Different factors can change quality and quantity of jaw bone, including medical conditions and medications. Osteoporosis is a systematic skeletal disease that presents with a decrease in bone mineral density with a concomitant change in the bone microarchitecture. This condition leads to a decrease in bone strength and an increase in the risk of fractures, primarily in the hip, spine and wrist. Osteoporosis can contribute to the manifestation of oral cavity problems that are exemplified by the resorption of the alveolar process, loss of teeth, chronic destructive periodontal disease, pain related to the maxillary sinus, fractures, and changes in the bone mineral density of the mandible and the mandibular cortex. Studies on the evaluation of the mandibular cortex in patients with osteoporosis have been extensively presented in the literature. While, studies on the other manifestations are few in the literature, as well as presenting conflicting results (Dervis, 2005; Taguchi, 2010).

Clinicians have also to be aware of the growing number of patients taking anti-resorptive agents, such as bisphosphonates (BP). BP are pyrophosphate analogues with a high affinity for bone hydroxyapatite, which is effective in the treatment of different diseases affecting bone metabolism (e.g. osteoporosis), and bone metastasis of prostate, lung and breast carcinoma (Shabestari et al., 2010). Despite the benefits associated with treatment with BP, these drugs have been related, since 2003, to a debilitating pathology, which clinical manifestations affect exclusively maxilla and mandible, called "osteonecrosis of the jaw" (Marx, Sawatari, Fortin, & Broumand, 2005; Ruggiero et al., 2006). Osteonecrosis of the jaw can be induced by radiotherapy, infections and certain drugs (Bagan et al., 2005). One of the most serious complications related to BP therapy is medication-related osteonecrosis of the jaw (MRONJ), characterized by exposed bone or bone that can be probed through an intra- or extraoral fistulas. When planning dental implants particular attention should be paid to patients undergoing BP therapy (De-Freitas et al., 2016; Madrid & Sanz, 2009). Other medical conditions that might have an influence on bone quality are osteomalacia, poorly controlled diabetes mellitus (Annibali, Pranno, Cristalli, La Monaca, & Polimeni, 2016; Naujokat, Kunzendorf, & Wiltfang, 2016) Sjögren's disease (Korfage et al., 2016).

Appropriate preoperative diagnosis of jaw bone tissue plays a critical role in decreasing treatment failure. Radiographic analysis of jaw bone quality and quantity are essential before any oral and maxillofacial procedure and can improve treatment outcome (Harris et al., 2012; Quirynen et al., 2005). Different clinical radiographic methods have been used to study the jaw bone before any maxillofacial procedure. For example, morphologic and measurements for bone density through panoramic and intraoral radiographs, as well as through more advanced imaging options, such as CT/CBCT and Quantitative CT (Lindh et al., 2004).

1.2.1 Clinical radiographic methods to assess jaw bone quality and quantity

1.2.1.1 Conventional radiographs

Two-dimensional (2D) imaging modalities, including extraoral and intraoral radiographs are the primary choice in the oral and maxillofacial procedures. Such imaging techniques meet critical characteristics such as low-radiation dose, fast acquisition, easy technique and low cost. Among extraoral radiographs, panoramic radiographs are the most clinically used for oral and maxillofacial procedures for giving an overview of maxillofacial structures, temporomandibular joints, alveolar bone (including respective dentitions) and important neurovascular bundles on a single film. As complementary exam, intraoral radiographs are used to assess details, including relation with teeth, marginal bone level and trabecular bone pattern for dental implant treatment (Lindh, Petersson, & Rohlin, 1996; Monsour & Dudhia, 2008; Mupparapu & Singer, 2004).

Literature has extensively reported subjective and quantitative methods to assess bone quality and quantity on these imaging methods (Ribeiro-Rotta et al., 2011). The most widely adopted subjective classification of bone quality and quantity in the treatment of dental implants was established by Lekholm and Zarb (1985). It is based on preoperative conventional radiographs and exploratory drilling in the preparation of the implant site, considering that the trabecular bone varies in structure and the compact layer surrounding trabecular bone varies in thickness. The evaluation of bone quality based on its structural arrangement was classified into four classes. Type 1 bone contains a significant amount of cortical bone that involves practically the entire bone area and little trabecular bone. Type 2 bone contains thick cortical bone and dense trabeculation. Type 3 bone contains thin cortical bone and dense trabeculation. Type 4 bone contains thin cortical bone that has rarefied bone trabeculation. Bone was also classified according to the available alveolar bone: A when most of the alveolar bone was present; B when there was moderate bone resorption of the residual rim; C when there was advanced resorption of the residual margin and only basal bone remained; D when there was initial resorption of the basal bone; and E when there was extreme resorption of the basal bone (*Figure 1.3*).

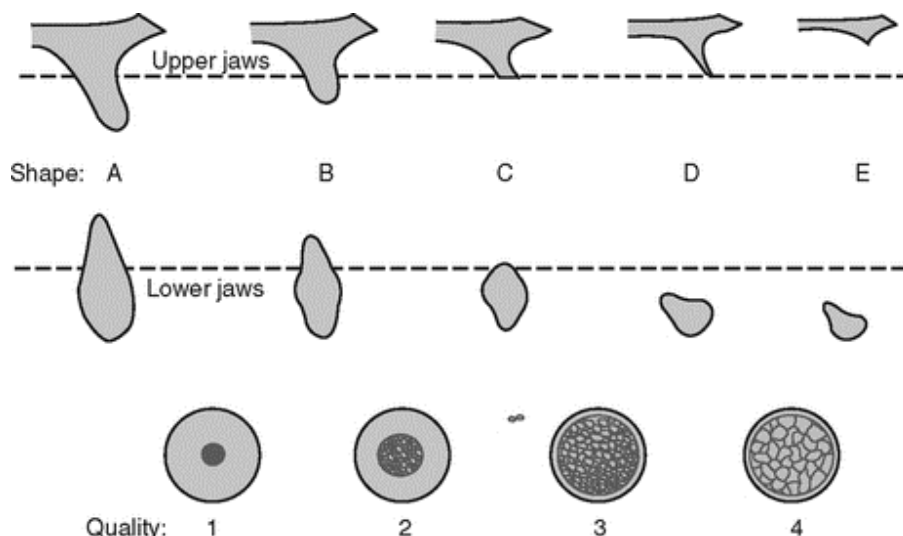


Figure 1.3. Grading system for bone quality and quantity assessment (Lekholm & Zarb, 1985).

Despite being the most widespread and used, the classification by Lekholm and Zarb has not yet been validated in any study (Ribeiro-Rotta et al., 2011).

Lindh et al. (1996) suggested a new classification of bone quality using the trabecular bone pattern assessed on 2D radiographs. This classification was based on three levels: Dense: where only dense trabeculae occurs; Dense/sparse: where trabeculae varying from dense to sparse occurs; and Sparse where only sparse trabeculae occurs (Figure 1.4). This method showed to be more reliable than the Lekholm and Zarb classification (Lindh et al., 1996).

Due to the relation between osteopenia and decrease of jaw bone mass (Kribbs, Smith, & Chesnut, 1983), panoramic radiographs have become an important tool for screening patients with osteoporosis. Many studies have shown that the mandibular cortical shape and thickness on the panoramic radiographs are correlated with bone densitometry (Ardakani & Niafar, 2004; Dervis, 2005; Tözüm & Taguchi, 2004). Some authors concluded that panoramic morphometric indices significantly correlated with mandibular bone mineral density (BMD) (Drozdowska, Pluskiewicz, & Tarnawska, 2002; Horner & Devlin, 1998a, 1998b). Therefore, this tool was previously used for developing a mandibular cortical index (MCI) for the assessment of cortical bone porosity (Klemetti et al., 1994) and panoramic mandibular index (PMI) (Benson, Prihoda, & Glass, 1991).

MCI is obtained by defining the appearance of the thickness of the inferior mandibular cortical bone as follows: C1: even and sharp endosteal margins of cortical bone on both sides; C2: semilunar defects (lacunar resorption) on the endosteal margin and/or endosteal cortical

residues on one or both sides; C3: heavy endosteal cortical residues and clearly porous on the cortical layer (Klemetti, Kolmakov, & Kröger, 1994) (*Figure 1.5*). The authors state that when the cortical height is less than 4 mm and classified as C3, the patient is at risk for the development of osteoporosis. When the cortical height is high and classified as C1, this is a patient with low risk. For Devlin and Horner (2002), a mandibular cortex smaller than 3 mm can predict low BMD. However, measuring it on panoramic radiographs can be a laborious procedure because it requires a precision calliper or a computer program for measuring digital images (Lee et al., 2005). According to these authors, visual assessment of the integrity of the mandibular cortex would be a more practical technique for the dental clinic.

On the other hand, PMI is the ratio of the thickness of mandibular cortex to the distance between the superior or inferior margin of mental foramen and the inferior mandibular cortex (Benson et al., 1991) (*Figure 1.6*). It may be considered that a PMI ratio below 0.40 may indicate an osteoporosis-related diagnosis (Klemetti, Kolmakov, Heiskanen, Vainio, & Lassila, 1993; Ledgerton, Horner, Devlin, & Worthington, 1997; Mohammad, Alder, & McNally, 1996). In addition to the cortical analysis, textural analysis to assess alterations in the trabecular bone (Apostol et al., 2006), and the evaluation of the radiographic density in periapical and panoramic radiographs can be used to compare the maxillary bones with the other skeletal bones in normal patients and with osteoporosis (Kribbs et al., 1983).

Morphometric analysis of bone texture, including fractal analysis, is a mathematical processing method using plain radiographic image and imaging processing. It expresses the roughness of the texture and characterizes the self-similarity of the texture grey-level variations over different scales, which is suitable to characterise trabecular bone microarchitecture (Amer, Heo, Brooks, & Benavides, 2012; Bhatt & Rozental, 2012; Prouteau et al., 2004) (*Figure 1.7*). Densitometric evaluation in periapical and panoramic radiographs can be performed by including and referencing an aluminium step wedge standard image with every exposure. Equal thicknesses of mineralized tissue and aluminium produce similar radiographic densities. The optical density of the jawbone site and each step of the step wedge is measured on the reference radiograph. These values are later plotted against the corresponding thickness of aluminium. The curve is obtained provided the corresponding aluminium equivalents in millimetres to the mean optical density of the jaw bone (Gulsahi et al., 2007).

Despite the great value of the conventional radiographs, the assessment of bone quality and quantity is limited by a number of disadvantages of 2D techniques, specially in relation to panoramic radiography, due to distortion, magnification and sharpness (Monsour & Dudhia, 2008). As for intraoral radiographs, the main drawback is that only restricted bone areas are visualised (De Bruyn, Vandeweghe, Ruyffelaert, Cosyn, & Sennerby, 2013), which can impair precise localization of important anatomical structures, such as mandibular canal (neurovascular bundle), maxillary sinuses, and incisive foramen. Violation or damage to these

structures can cause considerable complications (Abrahams, 2001). Furthermore, morphometric indices based on linear measurements and classificatory indexes on conventional radiographs are frequently observer-dependent, which lead to contradictory results (Correa et al., 2014; Devlin et al., 2007; Horner et al., 2007; Ishii et al., 2007; Lindh et al., 2008).



Figure 1.4. Periapical radiographs for the assessment of the trabecular pattern . A, Dense homogeneous trabecular patten in the lower jaw (left) and in the upper jaw (right). **B,** Heterogeneous trabecular pattern in the lower jaw (left) and in the upper jaw (right). **C,** Sparse homogeneous trabecular pattern in the lower jaw (left) and in the upper jaw (right). The aluminium step wedge seen in the radiographs was a reference for density measurements and not used in this particular study. From: Lindh et al., 2008.

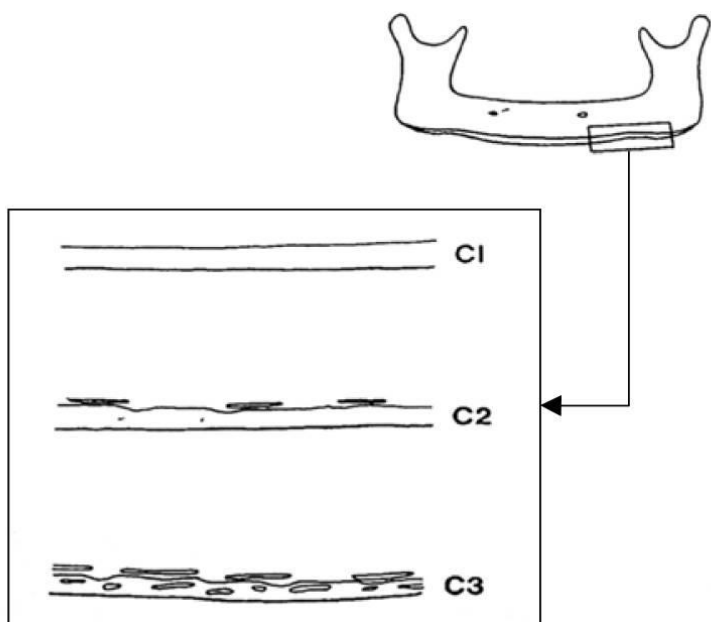


Figure 1.5. Mandibular cortical index (Klemetti 1994). From: Marandi et al., 2010.



Figure 1.6. Measurements of PMI (B/C). From: Neves et al., 2020.

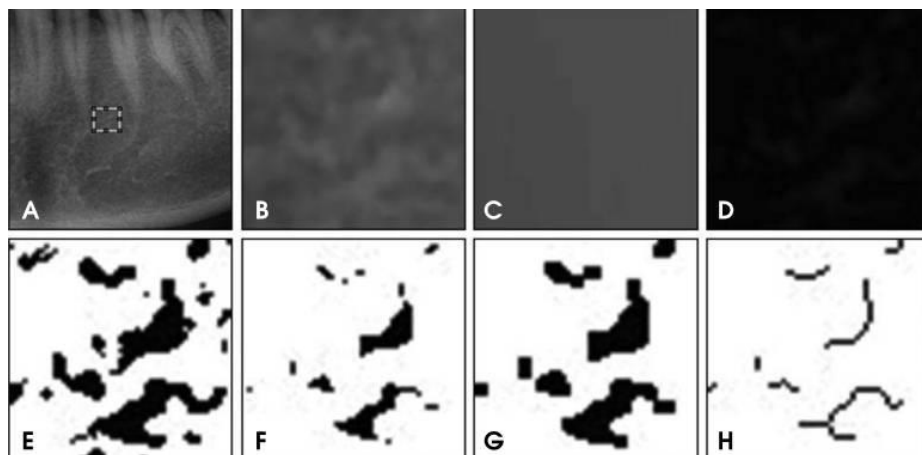


Figure 1.7. Texture analysis. A. ROI on a panoramic radiograph. B. Raw image before processing. C. Gaussian blurred image, D. Subtraction image. E. Binary image. F. Eroded image. G. Dilated image. H. Skeletonized image. From: Koh et al., 2012.

1.2.1.2 Computed tomography

The introduction of CT contributed significantly to the 3D assessment of jaw bone quality and quantity. CT employs an image formation principle that is different from conventional radiography. During CT imaging, the x-ray tube rotates around the patient and the information obtained is captured by sensors. The information is then transferred to a computer, which generates high-resolution images of sub-millimetre thickness and 3D images using programs that reconstruct the body in different planes (Scarfe & Farman, 2008).

CT carries several advantages over conventional radiography. First, CT avoids the superimposition of structures that are not within the area of interest. Secondly, contains inherent features of high contrast resolution, which allow for the effective differentiation between tissues that differ in physical density by less than 1%. Conventional radiography requires a 10% difference in physical density to distinguish between tissues. Thirdly, CT allows clinicians to assess data from a single CT imaging procedure, consisting of either multiple contiguous or one helical scan data images, using different views (including axial, sagittal and coronal, or other arbitrary planes) depending on the diagnostic task. This process is known as multiplanar reformatting imaging (Frederiksen, 2009).

Some of the outcomes of CT include 3D bone geometry with distinct cortical and trabecular bone, differentiation between soft and hard tissues, and measurement of apparent volumetric BMD (vBMD) and mass mineral or total bone volume. CT has long been the technique of choice for the standard assessment of bone mineral content, offering critical information on the

risk of osteoporotic fracture (Andresen & Nielsen, 1986; Brandi, 2009). The unit of measure of X-ray attenuation in CT is called Hounsfield Unit (HU). HU is strongly correlated to the density of biological tissues and highly reliable in the jaws (Celenk & Celenk, 2012; Shahlaie, Gantes, Schulz, Riggs, & Crigger, 2003; Shapurian, Damoulis, Reiser, Griffin, & Rand, 2006). The value of cortical bone for HU ranges from 1000-1600, although trabecular bone reveals lower values (*Figure 1.9*) (Shahlaie et al., 2003). To assist assessment of local bone density before implant placement, Misch and Kircos (1999) classified the bone density into five groups based on HU. D1 corresponds to values greater than 1250 HU, D2 has values between 850–1250 HU, D3 refers to density within 350–850 HU, D4 between 150–350 HU and D5 less than 150 HU. Although CT has been available for many years, its applications in oral and maxillofacial procedures have always been limited due to considerations of radiation dose, equipment access and cost (Farman & Scarfe, 2018). As an alternative to the slice-by-slice imaging method of conventional CT, Mozzo et al. (1998) and Arai et al. (1999) introduced CBCT in 1998. This 3D method is characterised by a cone-shaped beam and a reciprocating solid-state flat panel detector. This panel detector rotates 180-360 degrees once around the patient and covering the defined anatomical volume (complete dental/ maxillofacial volume or limited regional area of interest). The use of CBCT in dental imaging facilitates the interaction with the data and has the ability to reproduce images which are normally used in clinical settings, such as panoramic, cephalometric, or bilateral multiplanar projections of the temporomandibular joint.

Cone beam acquisition uses a beam geometry, which provides multiple transmission images that are integrated directly forming volumetric information (Sukovic, 2003). This provides an alternate method of image production ensuring more rapid data acquisition for a region of interest (ROI) and using a less expensive radiation detector than conventional CT (Farman & Scarfe, 2018) (*Figure 1.8*).

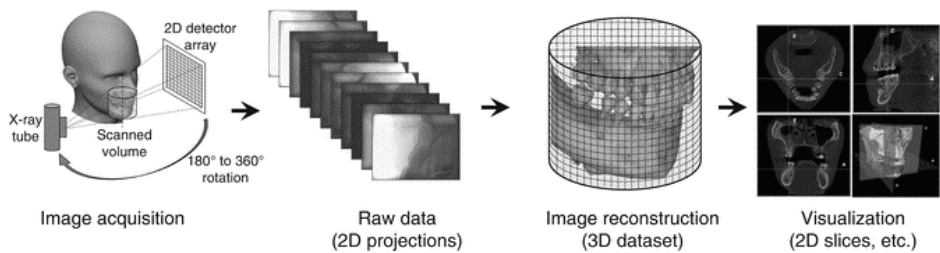


Figure 1.8. Schematic diagram showing the stages of CBCT image production. During a 180°–360° rotation of the X-ray tube and detector, multiple planar basis projections (raw data) are acquired. The raw data is then reconstructed into a volumetric dataset (primary reconstruction), which is subsequently reformatted as sequential, contiguous orthogonal slices (secondary reconstruction). The data may be further reformatted (e.g., volume rendering, curved reformatting, maximum intensity projection). From: Pauwels, 2018.

In addition to its relatively low cost, CBCT utilises reduced radiation dose. The size of irradiation can be reduced because of the CBCT machine's ability to collimate the primary X-ray beam to the area of interest. In this way, CBCT imaging meets the individual needs, cuts needless radiation exposure and diminishes scattered radiation that would affect the image quality.

CBCT units are organized according to the maximum field of view (FOV). This FOV is obtained from the scans and can be applied to different areas of dentistry (Gutierrez, Monnin, Valley, & Verdun, 2005; Palomo & Palomo, 2009). The resolution and therefore detail of CBCT imaging is determined by the individual volume elements or voxels produced from the volumetric data set. Voxel dimensions in CBCT imaging depend primarily on the pixel size on the area detector (isotropic voxels). This differs from CT imaging, which relies on slice thickness for voxel dimensions (anisotropic voxels). The resolution of the area detector is in sub-millimetres. Therefore, CBCT theoretically possesses higher resolution than CT (Scarfe & Farman, 2009; Scarfe & Farman, 2008), which is necessary for oral and maxillofacial procedures. Previous studies have shown that CBCT is more accurate for measurement of implant site dimensions than CT. (Al-Ekrish & Ekram, 2011; Kobayashi, Shimoda, Nakagawa, & Yamamoto, 2004; Loubele et al., 2008; Suomalainen, Vehmas, Kortensniemi, Robinson, & Peltola, 2008). However, CBCT lacks tissue density calibration due to the cone-beam projection geometry and detector sensitivity. As a consequence, comparing tissue density based on CT numbers generated from different CBCT units is deceptive (Venkatesh & Venkatesh Elluru, 2017). Despite the above advantages of CBCT, the assessment of bone quality and quantity on CBCT images is still largely based on subjective evaluations of bone structures and linear measurements similar to conventional 2D images. Newer products and methods developed through molecular and cellular research that focus on bone fragility have demonstrated the

importance of effective and sensitive non-invasive techniques for the assessment of bone quality (Brandi, 2009; Harvey et al., 2015). Although BMD provides objective information, bone quality is only partly resolved. Typical densitometry measurements do not take into account local variations of the trabecular structure or the non-uniform distribution of trabecular elements and failure regions. Giving a formal and complete definition of bone quality is rather ambiguous, however, it certainly includes architectural proprieties, which are of the utmost importance to bone strength (Genant et al., 1999; Harding & Beck, 2017). Yet, trabecular bone is believed to have an 8-fold higher turnover rate than cortical bone and to be highly responsive to metabolic stimuli because of its high surface area-to-volume ratio (Lang, Steiger, Faulkner, Gluer, & Genant, 1991). Therefore, earlier changes in bone quality can be first seen at the level of trabecular bone. The direct evaluation of bone microarchitecture would be considerably advantageous for the assessment of jaw bone quality. Following the advancement of 3D imaging modalities, clinical and scientific interest in 3D analysis of bone geometry and structure have become relevant, but not yet clinically applicable.

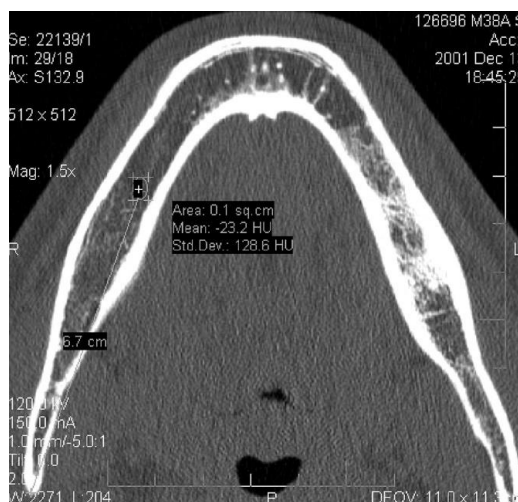


Figure 1.9. Measuring HU in axial image of the mandible. From: de Oliveira et al., 2008

1.3 Assessment of bone geometry and microarchitecture

The standard method used to assess internal bone structure is the calculation of morphometric indices through histological imaging, which provides high-resolution 2D images of tissues and bone cells (Figure 1.10). Bone trabecular pattern can be characterized by a number of

measures including area of the bony plates, circumference of the trabeculae, number of bony and marrow regions, thickness of the trabeculae, trabecular spacing, and osseous fractal dimension (Parfitt, 1987). The flaws of this method are twofold. In the first place, histological imaging is a destructive method. This means that due to the excision and sectioning of the bone, the bone sample can no longer be analysed using other methods. A second flaw related to histological imaging concerns the limits of 2D imaging of a 3D internal bone structure.

Based on the above information, a more suitable option for the 3D imaging of internal bone structures is micro-computed tomography (micro-CT). Micro-CT is a 3D x-ray imaging modality that utilizes similar methods as those used in CT scans, but on a small scale with massively increased resolution. This modality represents 3D microscopy technology, where very fine scale internal bone structures are imaged without sample preparation, staining, or thin slicing (*Figure 1.10*). Micro-CT is frequently used for imaging skeletons of small animals or bone biopsies. Thin trabecular bone structure can be easily visualised due to the high resolution of the technique, which is up to a few μm . Moreover, micro-CT imaging makes it possible to examine the bone structure in 2D or as a 3D model while simultaneously assessing quantitative aspects of morphometric parameters from the images (Boerckel, Mason, McDermott, & Alsberg, 2014; Feldkamp, Davis, & Kress, 1984). Unfortunately, due to the high radiation dose and long scanning time, this technique remains limited to laboratorial use. For a long time conventional CT was the clinical alternative for 3D assessment of jaw bone. With current CBCT machines providing sub-millimetre resolution ranging from 400 to as low as 75 μm and efficient reconstruction algorithms for noise and scatter reduction (Jia et al., 2010; Lee et al., 2016), jaw bone microstructure analysis can become promising in a clinical setting.

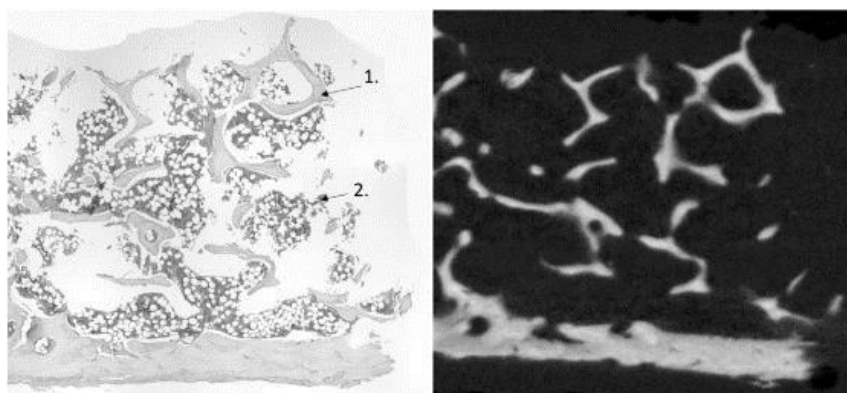


Figure 1.10. Trabecular bone showed in stained histology section (left) and corresponding micro-CT slice (right). From: Lundin et al., 2017.

Table 1.1. Clinical radiographic methods to assess jaw bone quality and quantity.

Method	Imaging modality	Category
Lekholm & Zarb classification	Conventional radiographs	Subjective
Trabecular pattern (Lindh et al., 1996)	Conventional intraoral radiographs	Subjective
MCI and PMI	Conventional radiographs	Morphometry
Texture analysis	Conventional radiographs	Morphometry
Step wedge	Conventional radiographs	Densitometry
Hounsfield units	CT	Densitometry
Bone morphometric parameters	CT, CBCT	Morphometry

1.4 Aims and hypotheses

The main aim of this thesis was to investigate the clinical applicability of CBCT imaging for objective bone quality and quantity assessment in the jaws. The differential in this project was to use post-processing methods for 3D quantification of bone structures. In order to reach the main purpose, the following sub-objectives were addressed:

- Chapters 2 & 3: To assess the accuracy and reliability of different CBCT machines to objectively assess alveolar bone geometry and microarchitecture
Hypothesis: CBCT imaging is a clinically reliable tool to assess jaw bone 3D microstructure before dental implant placement.
- Chapter 4: To develop and validate a computer-based method to assist preoperative bone quality assessment.
Hypothesis: Computer-based bone quality classification performs better than subjective classification based on examiner experience.
- Chapter 5: To investigate how morphometric parameters can correlate with dental implant survival.
Hypothesis: Extreme deviations in trabecular structure may compromise implant survival.
- Chapter 6: To describe and validate a method to follow-up condylar remodelling.
Hypothesis: 3D mandibular condyle modelling and objective bone volume quantification can assist condylar remodelling.

1.5 References

- Abrahams, J. J. (2001). Dental CT imaging: A look at the jaw. *Radiology*, 219(2), 334–345. doi:10.1148/radiology.219.2.r01ma33334
- Adell, R., Eriksson, B., Lekholm, U., Brånemark, P.-I., & Jemt, T. (1990). Long-term follow-up study of osseointegrated implants in the treatment of totally edentulous jaws. *The International Journal of Oral & Maxillofacial Implants*, 5(4), 347–359.
- Adell, R., Lekholm, U., Rockler, B., & Brånemark, P.-I. (1981). A 15-year study of osseointegrated implants in the treatment of the edentulous jaw. *International Journal of Oral Surgery*, 10(6), 387–416. doi:10.1016/S0300-9785(81)80077-4
- Al-Ekrish, A. A., & Ekram, M. (2011). A comparative study of the accuracy and reliability of multidetector computed tomography and cone beam computed tomography in the assessment of dental implant site dimensions. *Dentomaxillofacial Radiology*, 40(2), 67–75. doi:10.1259/dmfr/27546065
- Amer, M. E., Heo, M. S., Brooks, S. L., & Benavides, E. (2012). Anatomical variations of trabecular bone structure in intraoral radiographs using fractal and particles count analyses. *Imaging Science in Dentistry*, 42(1), 5–12. doi:10.5624/isd.2012.42.1.55
- Andresen, J., & Nielsen, H. E. (1986). Assessment of bone mineral content and bone mass by non-invasive radiologic methods. *Acta Radiologica - Series Diagnosis*, 27(6), 609–617. doi:10.1177/028418518602700601
- Annibali, S., Pranno, N., Cristalli, M. P., La Monaca, G., & Polimeni, A. (2016). Survival Analysis of Implant in Patients with Diabetes Mellitus: A Systematic Review. *Implant Dentistry*, 25(5), 663–674. doi:10.1097/ID.0000000000000478
- Apostol, L., Boudousq, V., Basset, O., Odet, C., Yot, S., Tabary, J., ... Peyrin, F. (2006). Relevance of 2D radiographic texture analysis for the assessment of 3D bone micro-architecture. *Medical Physics*, 33(9), 3546–3556. doi:10.1118/1.2211727
- Arai, Y., Tammisalo, E., Iwai, K., Hashimoto, K., & Shinoda, K. (1999). Development of a compact computed tomographic apparatus for dental use. *Dentomaxillofacial Radiology*,

28(4), 245–248. doi:10.1038/sj.dmf.4600448

Ardakani, F. E., & Niafar, N. (2004). Evaluation of changes in the mandibular angular cortex using panoramic images. *Journal of Contemporary Dental Practice*, 5(3), 1–15.

Bagan, J. V., Murillo, J., Jimenez, Y., Poveda, R., Milian, M. A., Sanchis, J. M., ... Scully, C. (2005). Avascular jaw osteonecrosis in association with cancer chemotherapy: Series of 10 cases. *Journal of Oral Pathology and Medicine*, 34(2), 120–123. doi:10.1111/j.1600-0714.2004.00269.x

Bahat, O. (1993). Treatment planning and placement of implants in the posterior maxillae: report of 732 consecutive Nobelpharma implants. *The International Journal of Oral & Maxillofacial Implants*, 8(2), 151–161. doi:10.1097/00008505-199404000-00012

Benson, B. W., Prihoda, T. J., & Glass, B. J. (1991). Variations in adult cortical bone mass as measured by a panoramic mandibular index. *Oral Surgery, Oral Medicine, Oral Pathology*, 71(3), 349–356. doi:10.1016/0030-4220(91)90314-3

Bhatt, R. A., & Rozental, T. D. (2012). Bone Graft Substitutes. *Hand Clinics*, 28(4), 457–468. doi:10.1016/j.hcl.2012.08.001

Boerckel, J. D., Mason, D. E., McDermott, A. M., & Alsberg, E. (2014). Microcomputed tomography: Approaches and applications in bioengineering. *Stem Cell Research and Therapy*, 5(6), 144. doi:10.1186/s13045-014-0144-4

Brandi, M. L. (2009). Microarchitecture, the key to bone quality. *Rheumatology (United Kingdom)*, 48(suppl 4), iv3–iv8. doi:10.1093/rheumatology/kep273

Celenk, C., & Celenk, P. (2012). Bone Density Measurement Using Computed Tomography. In *Computed Tomography - Clinical Applications*. doi:10.5772/22884

Choi, J. W. (2011). Assessment of panoramic radiography as a national oral examination tool: Review of the literature. *Imaging Science in Dentistry*, 41(1), 1–6. doi:10.5624/isd.2011.41.1.1

Correa, L. R., Spin-Neto, R., Stavropoulos, A., Schropp, L., da Silveira, H. E. D., & Wenzel, A. (2014). Planning of dental implant size with digital panoramic radiographs, CBCT-generated panoramic images, and CBCT cross-sectional images. *Clinical Oral Implants*

Research, 25(6), 690–695. doi:10.1111/clr.12126

- De-Freitas, N., Lima, L., De-Moura, M., Veloso-Guedes, C., Simamoto-Junior, P., & De-Magalhaes, D. (2016). Bisphosphonate treatment and dental implants: A systematic review. *Medicina Oral, Patología Oral y Cirugía Bucal*, 21(5), e644–e651. doi:10.4317/medoral.20920
- De Bruyn, H., Vandeweghe, S., Ruyffelaert, C., Cosyn, J., & Sennerby, L. (2013). Radiographic evaluation of modern oral implants with emphasis on crestal bone level and relevance to peri-implant health. *Periodontology 2000*, 62(1), 256–270. doi:10.1111/prd.12004
- de Oliveira, R. C. G., Leles, C. R., Normanha, L. M., Lindh, C., & Ribeiro-Rotta, R. F. (2008). Assessments of trabecular bone density at implant sites on CT images. *Oral Surgery, Oral Medicine, Oral Pathology, Oral Radiology and Endodontology*, 105(2), 231–238. doi:10.1016/j.tripleo.2007.08.007
- Dervis, E. (2005). Oral implications of osteoporosis. *Oral Surgery, Oral Medicine, Oral Pathology, Oral Radiology and Endodontology*, 100(3), 349–356. doi:10.1016/j.tripleo.2005.04.010
- Devlin, H., & Horner, K. (2002). Mandibular radiomorphometric indices in the diagnosis of reduced skeletal bone mineral density. *Osteoporosis International*, 13(5), 373–378. doi:10.1007/s001980200042
- Devlin, Hugh, Karayianni, K., Mitsea, A., Jacobs, R., Lindh, C., van der Stelt, P., ... Horner, K. (2007). Diagnosing osteoporosis by using dental panoramic radiographs: The OSTEODENT project. *Oral Surgery, Oral Medicine, Oral Pathology, Oral Radiology and Endodontology*, 104(6), 821–828. doi:10.1016/j.tripleo.2006.12.027
- Drozdowska, B., Pluskiewicz, W., & Tarnawska, B. (2002). Panoramic-based mandibular indices in relation to mandibular bone mineral density and skeletal status assessed by dual energy X-ray absorptiometry and quantitative ultrasound. *Dentomaxillofacial Radiology*, 31(6), 361–367. doi:10.1038/sj.dmf.4600729
- Engquist, B., Bergendal, T., Kallus, T., & Linden, U. (1988). A retrospective multicenter evaluation of osseointegrated implants supporting overdentures. *The International*

Journal of Oral & Maxillofacial Implants, 3(2), 129–134.

Farman, A. G., & Scarfe, W. C. (2018). Historical Perspectives on CBCT. In W. C. Scarfe & C. Angelopoulos (Eds.), *Maxillofacial Cone Beam Computed Tomography: Principles, Techniques and Clinical Applications* (pp. 3–11). Cham: Springer International Publishing. doi:10.1007/978-3-319-62061-9_1

Feldkamp, L. A., Davis, L. C., & Kress, J. W. (1984). Practical cone-beam algorithm. *Journal of the Optical Society of America A*, 1(6), 612. doi:10.1364/JOSAA.1.000612

Frederiksen, N. L. (2009). Advanced Imaging. In S. C. White & M. J. Pharoah (Eds.), *Oral Radiology Principles and Interpretation* (pp. 207–224). St. Louis, Missouri: Mosby, Elsevier.

Friberg, B., Jemt, T., & Lekholm, U. (1991). Early failures in 4,641 consecutively placed Brånemark dental implants: a study from stage 1 surgery to the connection of completed prostheses. *The International Journal of Oral & Maxillofacial Implants*, 6(2), 142–146.

Genant, H. K., Cooper, C., Poor, G., Reid, I., Ehrlich, G., Kanis, J., ... Khaltsev, N. (1999). Interim report and recommendations of the World Health Organization Task-Force for Osteoporosis. *Osteoporosis International*, 10(4), 259–264. doi:10.1007/s001980050224

Gulsahi, A., Paksoy, C. S., Yazicioglu, N., Arpak, N., Kucuk, N. O., & Terzioğlu, H. (2007). Assessment of bone density differences between conventional and bone-condensing techniques using dual energy x-ray absorptiometry and radiography. *Oral Surgery, Oral Medicine, Oral Pathology, Oral Radiology and Endodontology*, 104(5), 692–698. doi:10.1016/j.tripleo.2007.03.004

Gutierrez, D., Monnin, P., Valley, J. F., & Verdun, F. R. (2005). A strategy to qualify the performance of radiographic monitors. *Radiation Protection Dosimetry*, 114(1–3), 192–197. doi:10.1093/rpd/nch565

Harding, A., & Beck, B. (2017). Exercise, Osteoporosis, and Bone Geometry. *Sports*, 5(2), pii: E29. doi:10.3390/sports5020029

Harris, D., Horner, K., Gröndahl, K., Jacobs, R., Helmrot, E., Benic, G. I., ... Quirynen, M. (2012). E.A.O. guidelines for the use of diagnostic imaging in implant dentistry 2011. A

- consensus workshop organized by the European Association for Osseointegration at the Medical University of Warsaw. *Clinical Oral Implants Research*, 23(11), 1243–1253. doi:10.1111/j.1600-0501.2012.02441.x
- Harvey, N. C., Glüer, C. C., Binkley, N., McCloskey, E. V., Brandi, M. L., Cooper, C., ... Kanis, J. A. (2015). Trabecular bone score (TBS) as a new complementary approach for osteoporosis evaluation in clinical practice. *Bone*, 78, 216–224. doi:10.1016/j.bone.2015.05.016
- Henry, P. J., Laney, W. R., Jemt, T., Harris, D., Krogh, P. H. J., Polizzi, G., ... Herrmann, I. (1996). Osseointegrated implants for single-tooth replacement: a prospective 5-year multicenter study. *International Journal of Oral and Maxillofacial Implants*, 11(4), 450–455. doi:10.11607/jomi.2937
- Higuchi, K. W., Folmer, T., & Kultje, C. (1995). Implant survival rates in partially edentulous patients. A 3-year prospective multicenter study. *Journal of Oral and Maxillofacial Surgery*, 53(3), 264–268. doi:10.1016/0278-2391(95)90222-8
- Horner, K., & Devlin, H. (1998a). The relationship between mandibular bone mineral density and panoramic radiographic measurements. *Journal of Dentistry*, 26(4), 337–343. doi:10.1016/S0300-5712(97)00020-1
- Horner, K., & Devlin, H. (1998b). The relationships between two indices of mandibular bone quality and bone mineral density measured by dual energy X-ray absorptiometry. *Dentomaxillofacial Radiology*, 27(1), 17–21. doi:10.1038/sj.dmfr.4600307
- Horner, Keith, Karayianni, K., Mitsea, A., Berkas, L., Mastoris, M., Jacobs, R., ... Devlin, H. (2007). The Mandibular Cortex on Radiographs as a Tool for Osteoporosis Risk Assessment: The OSTEODENT Project. *Journal of Clinical Densitometry*, 10(2), 138–146. doi:10.1016/j.jocd.2007.02.004
- Ishii, K., Taguchi, A., Nakamoto, T., Ohtsuka, M., Sutthiprapaporn, P., Tsuda, M., ... Tanimoto, K. (2007). Diagnostic efficacy of alveolar bone loss of the mandible for identifying postmenopausal women with femoral osteoporosis. *Dentomaxillofacial Radiology*, 36(1), 28–33. doi:10.1259/dmfr/28366679

- Jacobs, R., Salmon, B., Codari, M., Hassan, B., & Bornstein, M. M. (2018). Cone beam computed tomography in implant dentistry: Recommendations for clinical use. *BMC Oral Health*, 18(1), 88. doi:10.1186/s12903-018-0523-5
- Jaffin, R. A., & Berman, C. L. (1991). The Excessive Loss of Branemark Fixtures in Type IV Bone: A 5-Year Analysis. *Journal of Periodontology*, 62(1), 2–4. doi:10.1902/jop.1991.62.1.2
- Jemt, T. (1993). Implant treatment in elderly patients. *The International Journal of Prosthodontics*, 6(5), 456–461. doi:10.1097/00008505-199405000-00012
- Jemt, T., & Lekholm, U. (1995). Implant treatment in edentulous maxillae: a 5-year follow-up report on patients with different degrees of jaw resorption. *The International Journal of Oral & Maxillofacial Implants*, 10(3), 303–311.
- Jia, X., Lou, Y., Lewis, J., Li, R., Gu, X., Men, C., ... Jiang, S. (2010). GPU-based fast cone beam CT reconstruction from undersampled and noisy projection data via total variation. *Medical Physics*, 37(4), 1757–1760. doi:10.1118/1.3469447
- Kim, Y. K., Park, J. Y., Kim, S. G., Kim, J. S., & Kim, J. D. (2011). Magnification rate of digital panoramic radiographs and its effectiveness for pre-operative assessment of dental implants. *Dentomaxillofacial Radiology*, 40(2), 76–83. doi:10.1259/dmfr/20544408
- Klemetti, E., Kolmakov, S., Heiskanen, P., Vainio, P., & Lassila, V. (1993). Panoramic mandibular index and bone mineral densities in postmenopausal women. *Oral Surgery, Oral Medicine, Oral Pathology*, 75(6), 774–779. doi:10.1016/0030-4220(93)90438-A
- Klemetti, E., Kolmakov, S., & Kröger, H. (1994). Pantomography in assessment of the osteoporosis risk group. *European Journal of Oral Sciences*, 102(1), 68–72. doi:10.1111/j.1600-0722.1994.tb01156.x
- Kobayashi, K., Shimoda, S., Nakagawa, Y., & Yamamoto, A. (2004). Accuracy in measurement of distance using limited cone-beam computerized tomography. *The International Journal of Oral & Maxillofacial Implants*, 19(2), 228–231.
- Koh, K. J., Park, H. N., & Kim, K. A. (2012). Prediction of age-related osteoporosis using fractal analysis on panoramic radiographs. *Imaging Science in Dentistry*, 42(4), 231–235.

doi:10.5624/isd.2012.42.4.231

- Korfage, A., Raghoobar, G. M., Arends, S., Meiners, P. M., Visser, A., Kroese, F. G. M., ... Vissink, A. (2016). Dental Implants in Patients with Sjögren's Syndrome. *Clinical Implant Dentistry and Related Research*, 18(5), 937–945. doi:10.1111/cid.12376
- Kribbs, P. J., Smith, D. E., & Chesnut, C. H. (1983). Oral findings in osteoporosis. Part II: Relationship between residual ridge and alveolar bone resorption and generalized skeletal osteopenia. *The Journal of Prosthetic Dentistry*, 50(5), 719–724. doi:10.1016/0022-3913(83)90215-9
- Lang, P., Steiger, P., Faulkner, K., Gluer, C., & Genant, H. K. (1991). Osteoporosis: Current techniques and recent developments in quantitative bone densitometry. *Radiologic Clinics of North America*, 29(1), 49–76.
- Ledgerton, D., Horner, K., Devlin, H., & Worthington, H. (1997). Panoramic mandibular index as a radiomorphometric tool: An assessment of precision. *Dentomaxillofacial Radiology*, 26(2), 95–100. doi:10.1038/sj.dmr.4600215
- Lee, H. C., Song, B., Kim, J. S., Jung, J. J., Li, H. H., Mutic, S., & Park, J. C. (2016). An efficient iterative CBCT reconstruction approach using gradient projection sparse reconstruction algorithm. *Oncotarget*, 7(52), 87342–87350. doi:10.18632/oncotarget.13567
- Lee, K., Taguchi, A., Ishii, K., Suei, Y., Fujita, M., Nakamoto, T., ... White, S. C. (2005). Visual assessment of the mandibular cortex on panoramic radiographs to identify postmenopausal women with low bone mineral densities. *Oral Surgery, Oral Medicine, Oral Pathology, Oral Radiology and Endodontology*, 100(2), 226–231. doi:10.1016/j.tripleo.2004.11.052
- Lekholm, U., & Zarb, G. (1985). Patient selection and preparation. In P. Brånemark, G. A. Zarb, & T. Albrektsson (Eds.), *Tissue Integrated Prostheses: Osseointegration in Clinical Dentistry* (pp. 199–209). Chicago, IL: Quintessence.
- Lindh, C., Horner, K., Jonasson, G., Olsson, P., Rohlin, M., Jacobs, R., ... Devlin, H. (2008). The use of visual assessment of dental radiographs for identifying women at risk of having osteoporosis: the OSTEODENT project. *Oral Surgery, Oral Medicine, Oral Pathology*,

- Oral Radiology and Endodontology*, 106(2), 285–293. doi:10.1016/j.tripleo.2007.09.008
- Lindh, C., Obrant, K., & Petersson, A. (2004). Maxillary bone mineral density and its relationship to the bone mineral density of the lumbar spine and hip. *Oral Surgery, Oral Medicine, Oral Pathology, Oral Radiology and Endodontology*, 98(1), 102–109. doi:10.1016/S1079-2104(03)00460-8
- Lindh, C., Petersson, A., & Rohlin, M. (1996). Assessment of the trabecular pattern before endosseous implant treatment: Diagnostic outcome of periapical radiography in the mandible. *Oral Surgery, Oral Medicine, Oral Pathology, Oral Radiology, and Endodontology*, 82(3), 335–343. doi:10.1016/S1079-2104(96)80363-5
- Loubele, M., Van Assche, N., Carpentier, K., Maes, F., Jacobs, R., van Steenberghe, D., & Suetens, P. (2008). Comparative localized linear accuracy of small-field cone-beam CT and multislice CT for alveolar bone measurements. *Oral Surgery, Oral Medicine, Oral Pathology, Oral Radiology and Endodontology*, 105(4), 512–518. doi:10.1016/j.tripleo.2007.05.004
- Lundin, E. L., Stauber, M., Papageorgiou, P., Ehrbar, M., Ghayor, C., Weber, F. E., ... Goksel, O. (2017). Automatic registration of 2D histological sections to 3D microCT volumes: Trabecular bone. *Bone*, 105, 173–183. doi:10.1016/j.bone.2017.08.021
- Madrid, C., & Sanz, M. (2009). What impact do systemically administrated bisphosphonates have on oral implant therapy? A systematic review. *Clinical Oral Implants Research*, 20(SUPPL. 4), 87–95. doi:10.1111/j.1600-0501.2009.01772.x
- Marandi, S., Bagherpour, A., Imanimoghaddam, M., Hatef, M., & Haghighi, A. (2010). Panoramic-based mandibular indices and bone mineral density of femoral neck and lumbar vertebrae in women. *Journal of Dentistry (Tehran, Iran)*, 7(2), 98–106.
- Marco, F., Milena, F., Gianluca, G., & Vittoria, O. (2005). Peri-implant osteogenesis in health and osteoporosis. *Micron*, 36(7–8), 630–644. doi:10.1016/j.micron.2005.07.008
- Marx, R. E., Sawatari, Y., Fortin, M., & Broumand, V. (2005). Bisphosphonate-induced exposed bone (osteonecrosis/osteopetrosis) of the jaws: Risk factors, recognition, prevention, and treatment. *Journal of Oral and Maxillofacial Surgery*, 63(11), 1567–1575.

doi:10.1016/j.joms.2005.07.010

- Meredith, N. (1998). Assessment of implant stability as a prognostic determinant. *The International Journal of Prosthodontics*, 11(5), 491–501. doi:10.1038/sj.leu.2404246
- Misch, C. E. (1990). Divisions of available bone in implant dentistry. *The International Journal of Oral Implantology: Implantologist*, 7(1), 9–17.
- Misch, C. E., & Judy, K. W. (1987). Classification of partially edentulous arches for implant dentistry. *The International Journal of Oral Implantology: Implantologist*.
- Misch, C. E., & Kircos, L. T. (1999). Diagnostic imaging and techniques. In C. E. Misch (Ed.), *Contemporary Implant Dentistry* (2nd ed., pp. 73–87). St. Louis: Mosby.
- Mohammad, A. R., Alder, M., & McNally, M. A. (1996). A pilot study of panoramic film density at selected sites in the mandible to predict osteoporosis. *The International Journal of Prosthodontics*, 9(3), 290–294.
- Monsour, P. A., & Dudhia, R. (2008). Implant radiography and radiology. *Australian Dental Journal*, 53(SUPPL. 1), S11-25. doi:10.1111/j.1834-7819.2008.00037.x
- Mozzo, P., Procacci, C., Tacconi, A., Tinazzi Martini, P., & Bergamo Andreis, I. A. (1998). A new volumetric CT machine for dental imaging based on the cone-beam technique: Preliminary results. *European Radiology*, 8(9), 1558–1564. doi:10.1007/s003300050586
- Mupparapu, M., & Singer, S. R. (2004). Implant imaging for the dentist. *Journal of the Canadian Dental Association*, 70(1), 32.
- Naujokat, H., Kunzendorf, B., & Wiltfang, J. (2016). Dental implants and diabetes mellitus—a systematic review. *International Journal of Implant Dentistry*, 2(1), 5. doi:10.1186/s40729-016-0038-2
- Neves, F. S., Barros, A. S., Cerqueira, G. A., Cruz, G. A., Reis, A. A., Alves, L. B., & Crusoé-Rebello, I. (2020). Assessment of fractal dimension and panoramic radiomorphometric indices in women with celiac disease. *Oral Radiology*, 36(2), 141–147. doi:10.1007/s11282-019-00388-z
- Palomo, L., & Palomo, J. M. (2009). Cone Beam CT for Diagnosis and Treatment Planning in Trauma Cases. *Dental Clinics of North America*, 53(4), 717–727.

doi:10.1016/j.cden.2009.07.001

- Parfitt, A. M. (1987). Trabecular bone architecture in the pathogenesis and prevention of fracture. *The American Journal of Medicine*, 82(1B), 68–72. doi:10.1016/0002-9343(87)90274-9
- Pauwels, R. (2018). What Is CBCT and How Does It Work? In W. C. Scarfe & C. Angelopoulos (Eds.), *Maxillofacial Cone Beam Computed Tomography Principles, Techniques and Clinical Applications* (1st ed., pp. 13–42). Springer.
- Porter, J. A., & Von Fraunhofer, J. A. (2005). Success or failure of dental implants? A literature review with treatment considerations. *General Dentistry*, 53(6), 423–432.
- Prouteau, S., Ducher, G., Nanyan, P., Lemineur, G., Benhamou, L., & Courteix, D. (2004). Fractal analysis of bone texture: A screening tool for stress fracture risk? *European Journal of Clinical Investigation*, 34(2), 137–142. doi:10.1111/j.1365-2362.2004.01300.x
- Quirynen, M., Vogels, R., Alsaadi, G., Naert, I., Jacobs, R., & Steenberghe, D. Van. (2005). Predisposing conditions for retrograde peri-implantitis, and treatment suggestions. *Clinical Oral Implants Research*, 16(5), 599–608. doi:10.1111/j.1600-0501.2005.01147.x
- Ribeiro-Rotta, R. F., Lindh, C., Pereira, A. C., & Rohlin, M. (2011). Ambiguity in bone tissue characteristics as presented in studies on dental implant planning and placement: A systematic review. *Clinical Oral Implants Research*, 22(8), 789–801. doi:10.1111/j.1600-0501.2010.02041.x
- Ruggiero, S., Gralow, J., Marx, R. E., Hoff, A. O., Schubert, M. M., Hurn, J. M., ... Valero, V. (2006). Practical Guidelines for the Prevention, Diagnosis, and Treatment of Osteonecrosis of the Jaw in Patients With Cancer. *Journal of Oncology Practice*, 2(1), 7–14. doi:10.1200/jop.2006.2.1.7
- Scarfe, W. C., & Farman, A. G. (2008). What is Cone-Beam CT and How Does it Work? *Dental Clinics of North America*, 52(4), 707–730. doi:10.1016/j.cden.2008.05.005
- Scarfe, W. C., & Farman, A. G. (2009). Cone-Beam Computed Tomography. In S. C. White & M. J. Pharoah (Eds.), *Oral Radiology Principles and Interpretation* (pp. 225–243). St. Louis, Missouri: Mosby, Elsevier.

- Shabestari, G. O., Shayesteh, Y. S., Khojasteh, A., Alikhasi, M., Moslemi, N., Aminian, A., ...
Treister, N. S. (2010). Implant placement in patients with oral bisphosphonate therapy: A case series. *Clinical Implant Dentistry and Related Research*, 12(3), 175–180. doi:10.1111/j.1708-8208.2009.00150.x
- Shah, N. (2014). Recent advances in imaging technologies in dentistry. *World Journal of Radiology*, 6(10), 794–807. doi:10.4329/wjr.v6.i10.794
- Shahlaie, M., Gantes, B., Schulz, E., Riggs, M., & Crigger, M. (2003). Bone density assessments of dental implant sites: 1. Quantitative computed tomography. *The International Journal of Oral & Maxillofacial Implants*, 18(2), 224–231.
- Shapurian, T., Damoulis, P. D., Reiser, G. M., Griffin, T. J., & Rand, W. M. (2006). Quantitative evaluation of bone density using the Hounsfield index. *The International Journal of Oral & Maxillofacial Implants*, 21(2), 290–297.
- Spiekermann, H., Jansen, V. K., & Richter, E. J. (1995). A 10-year follow-up study of IMZ and TPS implants in the edentulous mandible using bar-retained overdentures. *The International Journal of Oral & Maxillofacial Implants*, 10(2), 231–243.
- Sukovic, P. (2003). Cone beam computed tomography in craniofacial imaging. *Orthodontics & Craniofacial Research*, 6(Suppl 1), 31–36. doi:10.1034/j.1600-0544.2003.259.x
- Suomalainen, A., Vehmas, T., Kortetniemi, M., Robinson, S., & Peltola, J. (2008). Accuracy of linear measurements using dental cone beam and conventional multislice computed tomography. *Dentomaxillofacial Radiology*, 37(1), 10–17. doi:10.1259/dmfr/14140281
- Taguchi, A. (2010). Triage screening for osteoporosis in dental clinics using panoramic radiographs. *Oral Diseases*, 16(4), 316–327. doi:10.1111/j.1601-0825.2009.01615.x
- Tözüm, T. F., & Taguchi, A. (2004). Role of dental panoramic radiographs in assessment of future dental conditions in patients with osteoporosis and periodontitis. *The New York State Dental Journal*, 70(1), 32–35.
- Venkatesh, E., & Venkatesh Elluru, S. (2017). Cone beam computed tomography: basics and applications in dentistry. *Journal of Istanbul University Faculty of Dentistry*, 51(3 Suppl 1), S102–S121. doi:10.17096/jiufd.00289

Chapter 2

Quantification of bone quality using different CBCT devices: Accuracy assessment for edentulous human mandibles

This chapter is based on:

Van Dessel, J., **Nicoliello, L. F.**, Huang, Y., Slagmolen, P., Politis, C., Lambrichts, I., & Jacobs, R. (2016). Quantification of bone quality using different cone beam computed tomography devices: Accuracy assessment for edentulous human mandibles. *European Journal of Oral Implantology*, 9(4), 411–424

2.1 Abstract

Purpose: To determine the accuracy of the latest cone beam computed tomography (CBCT) machines in comparison to multi-slice computer tomography (MSCT) and micro-computed tomography (micro-CT) for objectively assessing trabecular and cortical bone quality prior to implant placement.

Materials and methods: Eight edentulous human mandibular bone samples were scanned with seven CBCT scanners (3D Accuitomo 170, i-CAT Next Generation, ProMax 3D Max, Scanora 3D, Cranex 3D, Newtom GiANO and Carestream 9300) and one MSCT system (Somatom Definition Flash) using the clinical exposure protocol with the highest resolution. Micro-CT (SkyScan 1174) images served as a gold standard. A volume of interest (VOI) comprising trabecular and cortical bone only was delineated on the micro-CT. After spatial alignment of all scan types, micro-CT VOIs were overlaid on the CBCT and MSCT images. Segmentation was applied and morphometric parameters were calculated for each scanner. CBCT and MSCT morphometric parameters were compared with micro-CT using mixed-effect models. Intraclass correlation analysis was used to grade the accuracy of each scanner in assessing trabecular and cortical quality in comparison with the gold standard. Bone structure patterns of each scanner were compared with micro-CT in 2D and 3D to facilitate the interpretation of the morphometric analysis.

Results: Morphometric analysis showed an overestimation of the cortical and trabecular bone quantity during CBCT and MSCT evaluation compared to the gold standard micro-CT. The trabecular thickness (Tb.Th) was found to be significantly ($P < 0.05$) different and the smallest overestimation was found for the ProMax 3D Max (180 μm), followed by the 3D Accuitomo 170 (200 μm), Carestream 9300 (220 μm), Newtom GiANO (240 μm), Cranex 3D (280 μm), Scanora 3D (300 μm), high resolution MSCT (310 μm), i-CAT Next Generation (430 μm) and standard resolution MSCT (510 μm). The underestimation of the cortical thickness (Ct.Th) in ProMax 3D Max (-10 μm), the overestimation in Newtom GiANO (10 μm) and the high resolution MSCT (10 μm) were negligible. However, a significant overestimation ($P < 0.05$) was found for 3D Accuitomo 170 (110 μm), Scanora 3D (140 μm), standard resolution MSCT (150 μm), Carestream 9300 (190 μm), Cranex 3D (190 μm) and i-CAT Next Generation (230 μm). Comparison of the 2D network and 3D surface distance confirmed the overestimation in bone quantity, but only demonstrated a deviant trabecular network for the i-CAT Next Generation and the standard resolution MSCT. Intraclass correlation coefficients (ICCs) showed a significant ($P < 0.05$) high intra-observer reliability ($\text{ICC} > 0.70$) in morphometric evaluation between micro-CT and commercially available CBCT scanners (3D Accuitomo 170, Newtom GiANO and ProMax 3D Max). The ICC for Tb.Th and Ct.Th were 0.72 and 0.98 (3D Accuitomo 170), 0.71 and 0.96 (Newtom GiANO), and 0.87 and 0.92 (ProMax 3D Max), respectively.

Conclusions: High resolution CBCT offers a clinical alternative to MSCT to objectively determine the bone quality prior to implant placement. However, not all tested CBCT machines have sufficient resolution to accurately depict the trabecular network or cortical bone.

2.2 Introduction

Radiological bone quality evaluation is considered an essential element during the pre-surgical implant planning (Sakka & Coulthard, 2009). Bone with high cortical density and small trabecular spaces was for a long time considered the ideal anatomy to ensure osseointegration (Lekholm & Zarb, 1985). Bone quality evaluations have therefore mainly focussed on trabecular bone density calculations (González-García & Monje, 2013; Monje et al., 2014) and linear bone measurements (Guerrero et al., 2006). Nowadays, modification in implant surface characteristics have immensely changed the perception of optimal bone quality. It was reported that well-structured and vascularised trabecular bone is preferable to achieve a high implant success (Fanuscu & Chang, 2004; Wirth et al., 2011). The latter implies that increased trabecular bone density is no longer a key factor for implant success, making the need to measure multi-slice computed tomography (MSCT) based Hounsfield units to express bone density doubtful (Pauwels, Jacobs, Singer, & Mupparapu, 2015).

It is clear that implant outcome closely relates to local trabecular structure characteristics, as local osteosclerotic scar tissue (Quirynen, Gijbels, & Jacobs, 2003) and bone after high-dose intravenous bisphosphonate treatment are often dense and not well-vascularised leading to implant failure (Marx, 2014). Structural bone assessment, besides a solely bone density evaluation approach, should therefore be considered as a supplementary tool in pre-surgical implant planning and provides a better estimation of the implant success (Diederichs et al., 2009).

Bone quality evaluation is to a large extent still based on subjective visual interpretation of two-dimensional (2D) radiographs of which the reliability has often been questioned thanks to the bone structure overlap (Ribeiro-Rotta, Lindh, & Rohlin, 2007). With the development of high resolution three-dimensional (3D) imaging modalities, new methods for analysing the trabecular and cortical bone structure in 3D have made it possible to evaluate the bone quality and quantity in a quantitative and non-invasive way (Ibrahim, Parsa, Hassan, van der Stelt, & Wismeijer, 2013). Since a typical trabecular thickness is measured in micrometres (μm), the micro-CT is routinely used for structural evaluation of the individual trabeculae and is considered the reference method for assessing bone morphology (D.-G. Kim, Christopherson, Dong, Fyhrie, & Yeni, 2004). Although a resolution as small as a few μm can be achieved, the micro-CT lacks clinical applicability due to its small field of view (Burghardt, Link, & Majumdar, 2011). For a long period of time, the only available clinical alternative to estimate the bone quality was the MSCT. Nevertheless, high radiation doses and lower spatial resolution limited its use in trabecular bone structure evaluation (Loubele et al., 2009).

Over the last decade, improvements in cone beam computed tomography (CBCT) technology have yielded much higher spatial resolutions in the maxillofacial area ranging from 80 μm to

400 μm , illustrating the possibility of CBCT to quantify trabecular bone structures at the dental implant site prior to implant placement (Kothari et al., 1998) and even allow for follow-up of the peri-implant bone formation afterwards (dos Santos Corpas et al., 2011; Huang, Van Dessel, Liang, et al., 2014). Previous studies reported that trabecular morphometric parameters quantified by CBCT show strong correlations with 2D histomorphometric values (Huang, Van Dessel, Depypere, et al., 2014) and 3D morphometric micro-CT and MSCT indices (Ibrahim et al., 2014; J.-E. Kim et al., 2015; Klintström, Smedby, Klintström, Brismar, & Moreno, 2014; Panmekiate, Ngonphloy, Charoenkarn, Faruangsang, & Pauwels, 2015; Parsa, Ibrahim, Hassan, van der Stelt, & Wismeijer, 2015; Van Dessel et al., 2013). Most of these studies, however, only reported the basic trabecular morphometric parameters and neglected the cortical bone structure. Therefore limited information is provided on the overall bone structure at the dental implant site, as the decision on the most suitable implant position should rely on a combination of trabecular and cortical bone information (Ribeiro-Rotta, Lindh, Pereira, & Rohlin, 2011).

The present study mainly introduced a novel technique to objectively quantify the trabecular and cortical bone structures on pre-surgical CBCT images. Yet, the availability of a broad range of CBCT machines may pose a different set of challenges as there is a wide variation in scan parameters and voxel sizes that have a clear impact on the bone microstructural analysis (Ibrahim, Parsa, Hassan, van der Stelt, Aartman, et al., 2013; Pauwels, Faruangsang, Charoenkarn, Ngonphloy, & Panmekiate, 2015). It is therefore still unclear whether available CBCT systems can cope with such novel bone quality evaluation. Secondly, if such bone quality assessment can be done, CBCT accuracy for bone structural analysis prior to implant placement should be determined. The aims of the present study are to determine the accuracy of the latest CBCT machines in comparison to multi-slice CT (MSCT) and micro-CT for objective assessment of both trabecular and cortical bone quality prior to implant placement. Guidelines for Reporting Reliability and Agreement Studies (GRRAS) were followed (Kottner et al., 2011).

2.3 Materials and methods

Eight edentulous human mandibular bone samples from the first premolar to second molar (left and right mandible) were obtained from the Anatomy Department, KU Leuven and approved for research by the medical ethics committee of the University Hospitals KU Leuven (s55619). Sample size was calculated using the results of our previous comparison study between CBCT and micro-CT on structural trabecular bone evaluation (Van Dessel et al., 2013). The principal parameters considered were the inconsistency in trabecular thickness ($0.42\text{ mm} \pm 0.01\text{ mm}$ and $0.19\text{ mm} \pm 0.01\text{ mm}$ for the CBCT and micro-CT evaluation, respectively) and bone volume

fraction ($53.74\% \pm 5.69\%$ and $34.39\% \pm 5.41\%$ for the CBCT and micro-CT evaluation, respectively). A power analysis in G*Power 3.1 suggested a sample size of four bone specimens assuming 90% power with an α of 0.05 (Faul, Erdfelder, Buchner, & Lang, 2009). The sample was, however, increased to eight specimens due to an expected smaller difference in cortical bone assessment.

2.3.1 Image acquisition

Each sample was placed in a sponge block to prevent any movement during the scanning process. When placing the samples, the instructions for patient positioning were followed according to the different scanning devices to avoid the effect of differences in object location. Bone specimens were scanned according to a unique randomisation list with seven CBCT scanners: 1) 3D Accuitomo 170 (Morita, Kyoto, Japan), 2) i-CAT Next Generation (Imaging Sciences International, Pennsylvania, USA), 3) ProMax 3D Max (Planmeca, Helsinki, Finland), 4) Scanora 3D (Soredex, Tuusula, Finland), 5) Cranex 3D (Soredex, Tuusula, Finland), 6) Newtom GiANO (QR Verona, Verona, Italy), 7) Carestream 9300 (Carestream Health, New York, USA), using the clinical exposure protocol with the highest resolution (*Table 2.1*). Subsequently, samples were randomly scanned by one MSCT system (Somatom Definition Flash, Siemens Healthcare, Erlangen, Germany) using the clinical standard and high resolution scanning protocol (*Table 2.1*). In contrast to CBCT and micro-CT, MSCT voxel sizes were non-isotropic with a slice thickness of 250 μm . Finally, all the samples underwent micro-CT scanning in a SkyScan 1174 system (Bruker, Kontich, Belgium). The micro-CT parameters consisted of a 26 μm voxel size, 50 kVp, 800 μA , 1 mm aluminum filter, angular rotation step 0.8 degree, 360-degree scanning, 450 projections and an exposure time of 9s with a total scan duration of 2h 20min.

Table 2.1. Overview of scanning devices and scan parameters.

Scan parameters	Unit	Micro-CT	3D Accuitomo 170	Carestream 9300	Cranex 3D	i-CAT next generation	Newton GIANO	ProMax 3D Max	Scanora 3D	High resolution MSCT	Standard resolution MSCT
Voxel size	(μm)	26	80	90	85	125	100	100	130	400	700
Tube voltage	(kV)	50	90	80	90	120	90	90	90	120	12
Tube current	(mA)	800	5	3	5	37	5	11	10	250	250
Field of view	(mm)	30x50	40x40	50x50	60x40	160x40	50x50	60x40	60x40	500x500	500x500
Effective dose	(μSv)	/	43	58	51	45	41	46	45	546	474

2.3.2 Image processing

Figure 2.1 and *Figure 2.2* show an overview of the consecutive image processing steps that were followed in order to obtain the trabecular and cortical morphometric parameters of the tested CT scanners. To compare the same morphological structures on the images from different scanning devices, CBCT and MSCT images were first spatially matched to the micro-CT scans by a rigid image registration using maximisation of mutual information (Maes, Collignon, Vandermeulen, Marchal, & Suetens, 1997).

The validity of the automatic registration process was verified by checking different anatomical reference points. Afterwards, a volume of interest (VOI) comprising of only the trabecular bone in the samples was manually delineated on the micro-CT images in CT-Analyser (Bruker, Kontich, Belgium). In this way, interference of cortical bone was avoided and a realistic 3D reconstruction of the trabecular bone structure could be provided. The non-selected cortical bone was saved as a separate VOI for later cortical bone analyses. The resulting micro-CT VOIs were then overlaid on the CBCT and MSCT images of the corresponding samples. The trabecular and cortical bone within the selected VOIs were segmented by an experienced radiologist (L.F.P.N.), who was blinded for scanner type, using an automatic adaptive threshold algorithm in CT-Analyser. The intensity ranges of the images were not globally normalised by linear rescaling, but the original intensity values of the different devices were kept, in order to take into consideration the technical specification of each device on the segmentation results. Voxel radius values were kept constant at six micro-CT voxels (156 μm) and threshold values were visually validated in order to give the most accurate segmentation overlap with the original image.

2.3.3 Image analysis: Bone morphometry

Morphometric parameters were calculated automatically and independent of an operator for each scanner within the corresponding trabecular and cortical VOI, based on the segmented images in CT-Analyser. Structural parameters were calculated in 3D according to the latest recommendations of the American Society of Bone and Mineral Research (*Table 2.2*) (Dempster et al., 2013). The morphometric variables could be related to routinely used terms in clinical bone quality evaluation, namely bone density and structure.

1. Bone density is directly related to the amount of bone. It can be expected that denser bones are related to high bone volume densities ($\uparrow\text{Tb.BV/Tb.TV}$ or $\uparrow\text{Ct.BV/Ct.TV}$ or $\uparrow\text{Ct.BV}[\text{Ct.TV}+\text{Tb.TV}]$) and low bone surface densities ($\downarrow\text{Tb.BS/Tb.TV}$), explained either by the bone being thick ($\uparrow\text{Tb.Th}$ or $\uparrow\text{Ct.Th}$) or consisting of a plate-like pattern ($\downarrow\text{SMI}$).

2. Bone structure is linked to the 3D trabeculae architecture. If the trabeculae are organized into a well-connected network (\downarrow Tb.Pf and \uparrow Conn. Dn), small marrow-spaced trabeculae (\downarrow Tb.Sp and \downarrow Po[tot]) with a great amount of trabeculae (\uparrow Tb.N) is expected.

Dimensions were given in millimetres (mm). Segmented VOIs were additionally visualised in 3D using 3-Matic (Materialise, Leuven, Belgium) to facilitate the interpretation of the bone morphometric evaluation. Finally, 3D models from CBCT and MSCT were overlaid on the micro-CT model and the distance between both surfaces was colour-coded to evaluate the structural differences between scanners in 3D.

Table 2.2. Quantified morphometric parameters for regional trabecular and cortical bone evaluation.

Morphometric parameter	Abbreviation	Unit	Description
Trabecular bone morphometry			
Trabecular volume fraction	Tb.BV/Tb.TV	(%)	Ratio of the segmented trabecular bone volume to the total volume of the trabecular volume of interest
Trabecular surface density	Tb.BS/Tb.TV	(mm ³ /mm ²)	Ratio of the segmented trabecular bone surface to the total trabecular volume of the volume of interest
Trabecular thickness	Tb.Th	(mm)	Mean thickness of trabeculae
Trabecular separation	Tb.Sp	(mm)	Mean distance between trabeculae
Trabecular number	Tb.N	(1/mm)	Average number of trabeculae per millimeter
Trabecular pattern factor	Tb.Pf	(1/mm)	Index of trabecular bone connectivity
Structural model index	SMI		An indicator for the structure of trabeculae SMI will be 0 for parallel plates and 3 for cylindrical rods
Connectivity density	Conn.Dn	(1/mm ³)	Measure of the degree of connectivity of trabeculae normalised by TV
Total porosity percentage	Po(tot)	(%)	Ratio of the volume of all open plus closed pores to the total trabecular volume of interest
Cortical bone morphometry			
Cortical volume fraction	Ct.BV/Ct.TV	(%)	Ratio of the segmented cortical bone volume to the total volume of the cortical volume of interest
Cortical thickness	Ct.Th	(mm)	Mean thickness of cortical bone
Cortical bone percentage	Ct.BV/(Tb.TV+Ct.TV)	(%)	Ratio of the segmented cortical bone volume to the total volume of the sample

3.4 Statistical analysis

Descriptive analysis expressed data as mean values with standard deviations. In order to control for dependence among the repeated observations for each bone sample, a mixed-effect model with scanner type as a fixed effect was used to compare the morphometric parameters of the micro-CT with the other scanners. The intraclass correlation coefficient (ICC) was calculated to evaluate the reliability of each scanner in assessing trabecular and cortical quality in comparison with the gold standard micro-CT. The two-way mixed single measures for consistency were reported. Statistical analysis was carried out in IBM SPSS Statistics (IBM, New York, USA). The significance level for all performed tests was set at $\alpha < 0.05$.

2.4 Results

2.4.1 Morphometric parameters

Table 2.3 shows the descriptive statistics of the trabecular and cortical structural bone parameters calculated within each corresponding VOI in the different scanners. Statistically significant ($P < 0.05$) differences were found between the micro-CT and other scanning devices for all trabecular and cortical morphometric parameters, except for percentage cortical bone in the total sample ($Ct.TV/[Tb.TV+Ct.TV]$). More specifically, the trabecular volume fraction ($Tb.BV/Tb.TV$), trabecular thickness ($Tb.Th$) and cortical volume fraction ($Ct.TV/Ct.BV$) were overestimated in all MSCT and CBCT machines compared to the values obtained from the micro-CT. The smallest overestimation of the average $Tb.Th$ was found in the Promax 3D Max (180 μm), followed by the 3D Accuitomo 170 (200 μm), Care-stream 9300 (220 μm), Newtom GiANO (240 μm), Cranex 3D (280 μm), Scanora 3D (300 μm), high resolution MSCT (310 μm), i-CAT Next Generation (430 μm) and standard MSCT (510 μm) (*Table 2.3*). The average cortical thickness ($Ct.Th$) was overestimated for all MSCT and CBCT devices compared to the reference micro-CT, except for the ProMax 3D Max (-10 μm). This overestimation was negligible in Newtom GiANO (10 μm) and high resolution MSCT (10 μm). However a significant overestimation ($P < 0.05$) was found for 3D Accuitomo 170 (110 μm), Scanora 3D (140 μm), standard resolution MSCT (150 μm), Carestream 9300 (190 μm), Cranex 3D (190 μm) and i-CAT Next Generation (230 μm) (*Table 2.3*). On the other hand, the trabecular surface density ($Tb.BS/Tb.TV$) and trabecular number ($Tb.N$) were underestimated for all scan types compared to micro-CT. The structural model index (SMI) was underestimated in MSCT and CBCT, except for the Cranex 3D scanner. Connectivity density (Conn.Dn) was only underestimated in the 3D Accuitomo 170, Cranex 3D, Newtom GiANO and Promax 3D Max compared to micro-CT. Also, the trabecular pattern factor ($Tb.Pf$) was underestimated in all

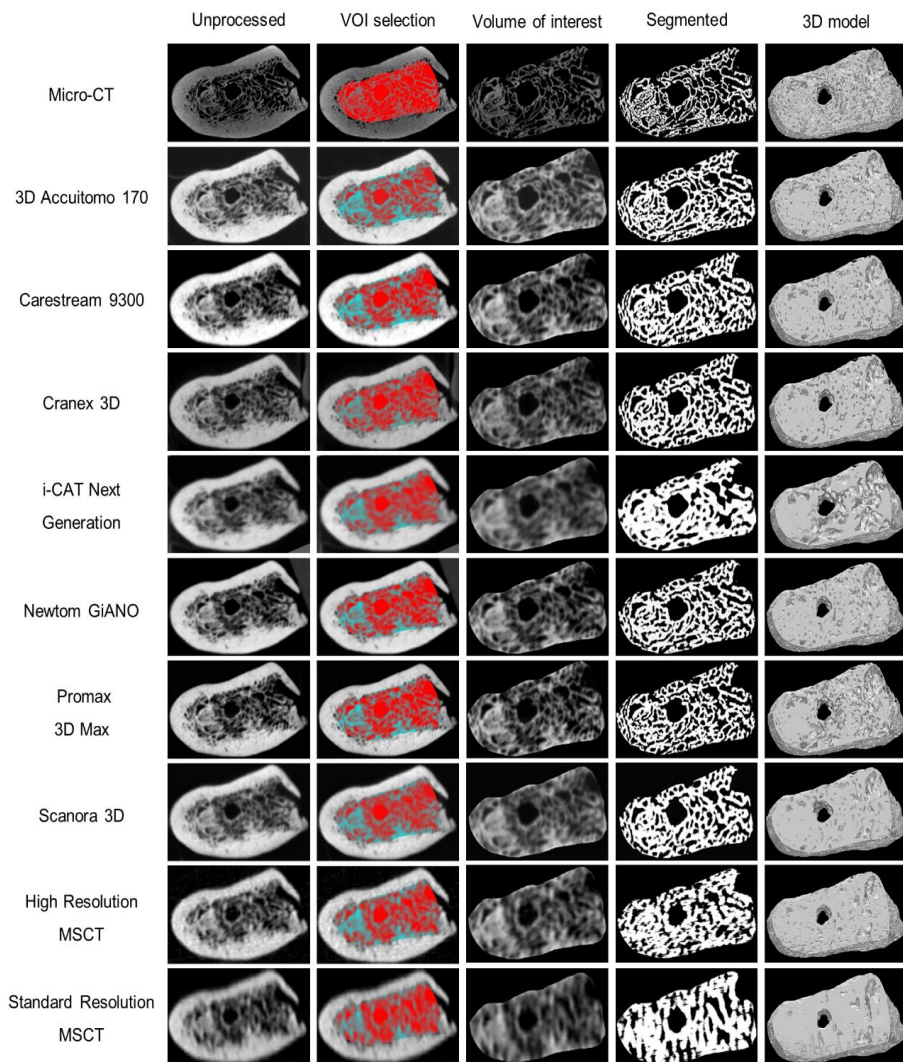


Figure 2.1. Workflow of image processing before calculation of trabecular morphometric parameters in sample 2. Multi-slice Computed Tomography (MSCT) and Cone-beam CT images were spatially aligned on the micro-CT scan. A volume of interest (VOI) was manually delineated on the micro-CT image and overlaid on the images of other scanning devices. Trabecular bone structures were extracted using the adaptive threshold. Based on the resulting segmented images automatic trabecular morphometric quantification was performed and three-dimensional models were made.

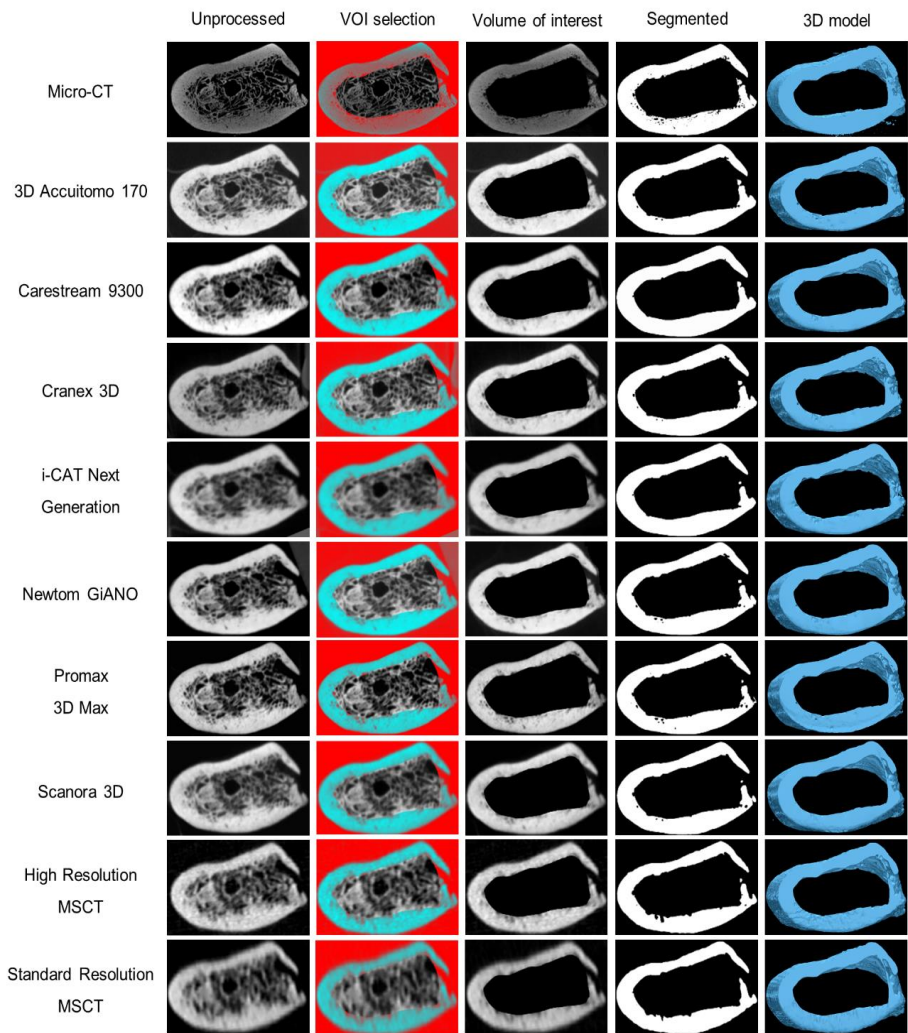


Figure 2.2. Workflow of image processing before calculation of cortical morphometric parameters in sample 2. Multi-slice Computed Tomography (MSCT) and Cone-beam CT images were spatially aligned on the micro-CT scan. The trabecular volume of interest (VOI) and black background were subtracted from the image in order to select the cortical VOI. Cortical bone structures were extracted using the adaptive threshold. Based on the resulting segmented images automatic cortical morphometric quantification was performed and three-dimensional models were made.

scanners, with the exception of ProMax 3D Max and 3D accuitomo 170. Taken together, these morphometric parameters indicated that the quantity of cortical and trabecular bone is overestimated during CBCT and MSCT assessment compared to the gold standard micro-CT (*Figure 2.3*).

2.4.2 Segmentation accuracy on cross-sectional slices

Comparison of the segmented 2D trabecular network confirmed the thicker trabeculae (\uparrow Tb.Th) on CBCT and MSCT scans compared to micro-CT, which led to an overestimation of the total amount of trabecular bone (\uparrow Tb.BV/Tb.TV and \downarrow Tb.BS/Tb.TV; *Figure 2.4*). In line with the morphometric parameters, this overestimation was the largest in the MSCT protocols and i-CAT Next Generation with significant deviations in the trabecular bone pattern when compared to the gold standard micro-CT. The trabecular structure, however, remained identical to micro-CT for the 3D Accuitomo 170, Carestream 9300, Cranex 3D, Newtom GiANO, Promax 3D Max, Scanora 3D CBCT and high resolution MSCT. For the cortical bone, the difference between tested scanners and micro-CT could be considered negligible, although the difference in cortical thickness indicated by the morphometric results may be difficult to evaluate visually in 2D only (*Figure 2.4*).

Table 2.3. Comparison of three-dimensional morphometric parameters for the different scanning devices [mean (standard deviation)].

Morphometric Parameters	Unit	micro-CT	3D Accutomo 170	Carestream 9300	Cranex 3D	i-CAT next generation	Newtom GIANO	ProMax 3D Max	Scanora 3D	High Resolution MSCT	Standard Resolution MSCT
Trabecular bone morphometry											
Trabecular volume fraction	%	34.0 (3.5)	53.0 (2.2)*	58.5 (2.5)*	54.9 (2.1)*	60.9 (6.0)*	56.5 (2.3)*	45.6 (6.5)*	59.0 (5.0)*	64.3 (1.8)*	69.8 (3.7)*
Trabecular surface density	mm ² /mm ³	6.8 (0.7)	5.0 (0.4)*	5.6 (0.4)*	4.4 (0.2)*	4.9 (0.6)*	4.9 (0.1)*	4.4 (0.6)*	5.6 (0.6)*	5.9 (0.2)*	5.7 (0.5)*
Trabecular thickness	mm	0.16 (0.02)	0.36 (0.01)*	0.38 (0.01)*	0.44 (0.01)*	0.59 (0.03)*	0.40 (0.01)*	0.34 (0.04)*	0.46 (0.01)*	0.47 (0.01)*	0.67 (0.01)*
Trabecular separation	mm	0.60 (0.12)	0.60 (0.08)	0.54 (0.11)	0.66 (0.08)	0.95 (0.22)*	0.58 (0.06)	0.72 (0.18)	0.69 (0.14)	0.52 (0.10)	0.71 (0.12)
Trabecular number	1/mm	2.1 (0.2)	1.5 (0.1)*	1.5 (0.1)*	1.3 (0.1)*	1.0 (0.1)*	1.4 (0.1)*	1.4 (0.2)*	1.3 (0.1)*	1.4 (0.1)*	1.0 (0.1)*
Trabecular pattern factor	mm ⁻¹	-8.5 (4.4)	-8.3 (1.9)	-13.9 (0.9)*	-10.4 (0.8)	-28.9 (3.3)*	-10.6 (0.7)	-5.5 (1.2)	-20.0 (2.6)*	-20.6 (0.1)*	-38.8 (1.9)*
Structural model index	(SMI)	-0.4 (0.5)	-1.3 (0.4)*	-1.9 (0.4)*	1.7 (0.3)*	-6.4 (1.2)*	-1.8 (0.4)*	-0.8 (0.4)	-2.42 (0.5)*	-3.0 (0.2)*	-8.5 (0.4)*
Connectivity density	(Conn.Dn)	60.8 (26.7)	35.1 (16.0)	76.6 (18.5)	43.6 (8.9)	145.4 (29.1)*	40.3 (5.2)	14.0 (4.1)*	138.4 (40.3)*	123.3 (8.9)*	211.0 (31.0)*
Total porosity	%	65.9 (3.5)	47.1 (2.2)*	41.5 (2.5)*	45.1 (2.1)*	39.1 (6.0)*	43.5 (2.3)*	54.4 (6.5)*	40.9 (4.95)*	35.7 (1.84)*	30.1 (3.74)*
Cortical bone morphometry											
Cortical volume fraction	%	95.0 (1.2)	99.3 (0.1)*	99.6 (0.1)*	99.4 (0.1)*	99.8 (0.7)*	99.5 (0.3)*	99.2 (0.3)*	99.6 (0.2)*	99.62 (0.2)*	99.6 (0.2)*
Cortical thickness	(Ct.Th)	1.92 (0.13)	2.03 (0.13)*	2.11 (0.15)*	2.11 (0.10)*	2.15 (0.09)*	1.93 (0.08)	1.91 (0.14)	2.06 (0.15)	1.93 (0.15)	2.07 (0.12)*
Percentage cortical bone in total sample	(Ct.TV / [Tb.TV+Ct.TV])	43.6 (2.8)	45.6 (2.7)	45.7 (2.8)	45.6 (2.7)	45.8 (2.8)	43.7 (2.8)	45.5 (2.7)	45.7 (2.8)	45.7 (2.7)	45.4 (2.7)

*Significant difference (P<0.05) with micro-CT

2.4.3 Comparison of the 3D bone models

The colour map of the mean distance between the micro-CT, and the aligned MSCT and CBCT trabecular surface visually confirmed the significant overestimation of Tb.Th obtained from the morphometric analysis (*Figure 2.4*). The colour pattern was predominantly green to yellow (difference in trabecular radius $< 125 \mu\text{m}$), except for the i-CAT Next Generation and standard resolution MSCT. This is in line with the 2D comparison and confirms that the trabecular network strongly deviated from the micro-CT pattern. The colour map of the 3D surface comparison of the cortical bone showed a higher Ct.Th (yellow and red colours; difference in trabecular thickness $> 125 \mu\text{m}$) for the Carestream 9300, Cranex 3D, i-CAT Next Generation, Scanora 3D and standard resolution MSCT compared to micro-CT. This corresponded with the significant overestimations ($P < 0.05$) in Ct.Th that were found in the morphometric analysis.

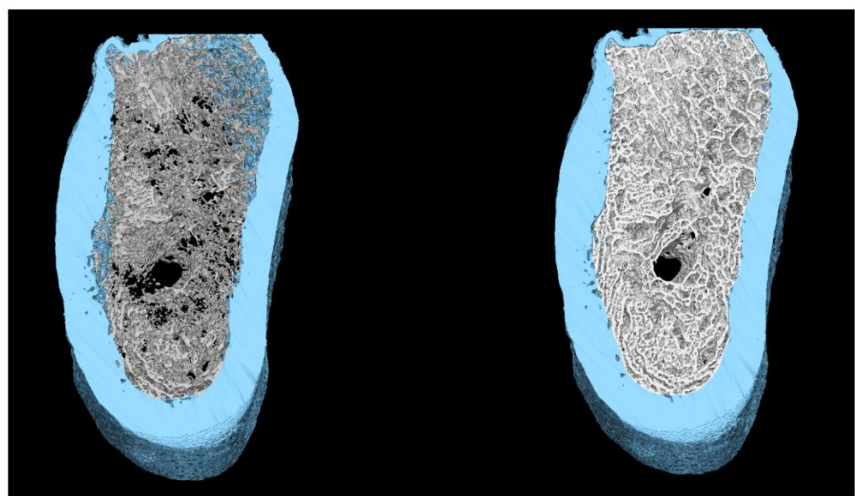
2.4.4 Correlation of morphometric indices

Although most morphometric CBCT and MSCT parameters were statistically different from micro-CT values, high ICC correlation coefficients ($\text{ICC} > 0.70$) were found (*Table 2.4*). The correlations however were strongly dependent on the scanner type. The 3D Accuitomo 170, Newtom GiANO and ProMax 3D Max had a noticeably higher ICC for structural trabecular bone parameters compared to other CBCT scanners. For the cortical bone parameters, excellent ICC were obtained for all scanners (except for Ct.BV/Ct.TV measured in Cranex 3D and i-CAT Next Generation).

Table 2.4. Intraclass correlation coefficients of morphometric parameters between micro-computed tomography and other CT modalities.

Morphometric Parameters	Unit	3D Accutomo 170	Carestream 9300	Cranex 3D	i-CAT next generation	Newtom GIANO	ProMax 3D Max	Scanora 3D	High Resolution MSCT	Standard Resolution MSCT
Trabecular bone morphometry										
Trabecular volume fraction	%	0.82*	0.77*	0.85*	0.84*	0.83*	0.87*	0.64	0.63	0.56
Trabecular surface density	mm ² /mm ³	0.52	0.39	0.47	0.54	0.55	0.67	0.91*	0.05	0.83*
Trabecular thickness	mm	0.72*	0.76*	0.36	0.58	0.75*	0.41	0.35	0.63	0.24
Trabecular separation	mm	0.76*	0.85*	0.95*	0.88*	0.71*	0.87*	0.85*	0.90*	0.76*
Trabecular number	1/mm	0.80*	0.74*	0.50	0.48	0.85*	0.83*	0.83*	0.67	0.10
Trabecular pattern factor	mm ⁻¹	0.86*	0.43	0.46	0.03	0.93*	0.74*	0.16	0.34	0.22
Structural model index		0.72*	0.67	0.61	0.55	0.86*	0.75*	0.15	0.46	0.07
Connectivity density	1/mm ³	0.75*	0.54	0.53	0.07	0.70*	0.81*	0.72*	0.26	0.44
Total porosity	%	0.82*	0.77*	0.85*	0.53	0.84*	0.67	0.64	0.63	0.56
Cortical bone morphometry										
Cortical volume fraction	%	0.96*	0.98*	0.67	0.41	0.93*	0.93*	0.72*	0.85*	0.76*
Cortical thickness	mm	0.98*	0.98*	0.92*	0.87*	0.96*	0.92*	0.95*	0.98*	0.89*
Percentage cortical bone in total sample	%	0.99*	0.99*	0.99*	0.99*	0.97*	0.99*	0.99*	0.99*	0.99*

*Intraclass correlation coefficient has a P < 0.05



Sparse trabecular bone	Morphometric parameters	Dense trabecular bone
<i>Density related parameters</i>		
↓ Tb.BV/Tb.TV	Trabecular volume fraction	↑ Tb.BV/Tb.TV
↑ Tb.BS/Tb.TV	Trabecular surface density	↓ Tb.BS/Tb.TV
↓ Tb.Th	Trabecular thickness	↑ Tb.Th
↑ Po(tot)	Total porosity percentage	↓ Po(tot)
<i>Structural related parameters</i>		
↑ Tb.Sp	Trabecular separation	↓ Tb.Sp
↓ Conn.Dn	Connectivity density	↑ Conn.Dn
↑ SMI	Structural model index	↓ SMI
↑ Tb.Pf	Trabecular pattern factor	↓ Tb.Pf
↓ Tb.N	Trabecular number	↑ Tb.N

Figure 2.3. Difference in morphometric parameters between sparse (left) and dense (right) trabecular bone.

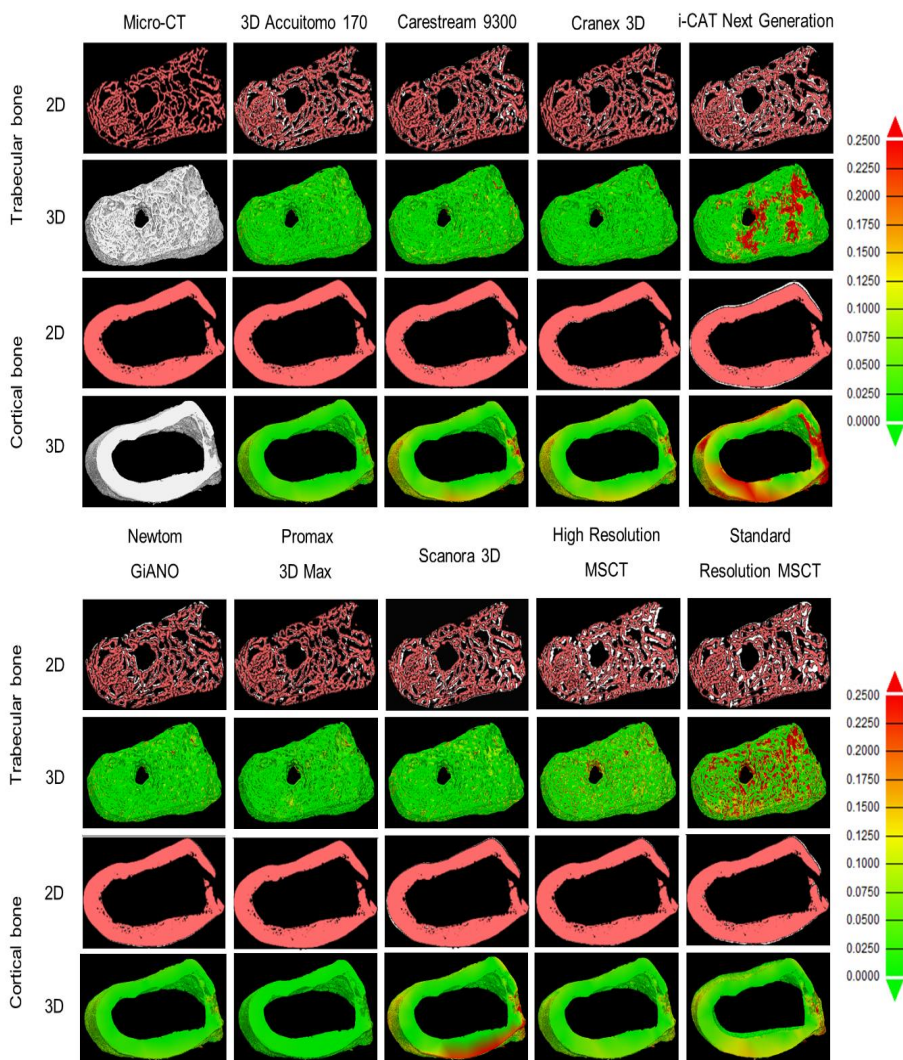


Figure 2.4. Accuracy of trabecular (top) and cortical (bottom) bone segmentation on cross-sectional images (2D) and three-dimensional (3D) bone surface comparison in sample 2. The micro-CT trabecular and cortical network was overlaid (in red) on seven cone-beam CT devices (3D Accuitomo 170®, Carestream 9300®, Cranex 3D®, i-CAT Next Generation®, Newtom GiANO®, Promax 3D Max®, Scanora 3D®) and two multi-slice CT (MSCT) protocols. The colour-coded 3D distance (in mm) between the micro-CT surface and the aligned CBCT and MSCT was in the same range as the values of the morphometric parameters. Thicker trabeculae compared to micro-CT were found in all scanners, although the trabecular structural pattern remained identical for all machines, besides for the i-CAT Next Generation® and standard resolution MSCT. For cortical bone, the difference was difficult to visualise on cross-sectional slices, but a clear difference in 3D was found for the Carestream 9300®, Cranex 3D®, i-CAT Next Generation®, Scanora 3D® and standard resolution MSCT.

2.5 Discussion

Radiographic assessment of the trabecular and cortical structure at the dental implant site is an important factor for ensuring successful rehabilitation. Despite the increasing use of CBCT for pre-surgical implant planning, implant surgeons still experience problems during the radiological determination of the appropriate trabecular and cortical bone quality required for optimal implant support (Liang et al., 2010). In the present study, a novel evaluation technique was introduced to objectively quantify the trabecular and cortical bone quality on pre-surgical CBCT images. Secondly, the accuracy of the latest CBCT machines for bone structure assessment prior to implant placement was determined in comparison with the gold standard (micro-CT) and the clinical reference standard (MSCT).

Decisions on the most suitable implant site are still often based on the combination of 2D linear measurements and subjective interpretation of various bone quality rating scales, which itself are based on the characterisation of cross-sectional trabecular morphology and cortical thickness (Ribeiro-Rotta et al., 2011). Therefore, the need arises for a 3D, objective and universally accepted system for classifying bone quality in the maxilla and mandible.

Previous studies have shown that the morphometric parameters used in this study are related to routinely used bone quality terms, such as bone density and structure (Gomes de Oliveira, Leles, Lindh, & Ribeiro-Rotta, 2012). The interpretation of the trabecular organisation is often complex, due to the large heterogeneity in individual trabecular configurations and pathologies that can alter the trabecular network. Well-structured trabecular bone ideal for implant placement is characterised by a high trabecular thickness (\uparrow Tb.Th, \downarrow Tb.N) with high trabecular interconnectivity (\uparrow Conn.Dn, \downarrow Tb.Pf) and small trabecular spaces (\downarrow Tb.Sp, \downarrow Po[tot]) (*Figure 2.3*). In turn, dense trabecular bone is related to a high bone volume density (\uparrow Tb.BV/Tb.TV) and low bone surface density (\downarrow Tb.BS/Tb.TV), explained by trabeculae being thick or having a plate-like pattern of trabeculae (\downarrow SMI) (*Figure 2.3*). This indicated the clinical application potential of structural parameters for bone quality evaluation prior to implant placement.

Benefiting from the improvement in CBCT technology, the latest CBCT devices on the market achieve higher spatial resolutions (ranging from 80 μ m to 130 μ m) in comparison with MSCT scanners, which are deemed necessary to accurately measure trabecular and cortical bone structures (Waarsing, Day, & Weinans, 2004). Previous CBCT morphometric bone evaluations have found similar values for the trabecular (Ibrahim et al., 2014; J.-E. Kim et al., 2015; Klintström et al., 2014; Panmekiate et al., 2015; Parsa et al., 2015; Van Dessel et al., 2013) and cortical (Hsu et al., 2013) parameters and obtained high Pearson correlations with micro-CT and MSCT. In the present study, the authors opted to calculate the ICC instead of the Pearson correlation coefficient, as it is a more appropriate statistical test for evaluating the reliability of CBCT in structural bone assessment (Kottner et al., 2011). Despite the high

significant ICC ($ICC > 70$) between 3D Accuitomo 170, Newtom GiANO, Promax 3D Max and micro-CT, the results support previous findings that CBCT overestimates or underestimates respective structural parameters compared to those of the gold standard micro-CT (Ibrahim et al., 2014; J.-E. Kim et al., 2015; Klintström et al., 2014; Panmekiate et al., 2015; Parsa et al., 2015; Van Dessel et al., 2013). This deviation may be caused by increased scattering, increased noise levels, lower resolution and artefacts specific to the CBCT technique, which operates at a lower kilovoltage and current tube settings in comparison to MSCT and micro-CT scanners, thereby resulting in reduced signal-to-noise ratio (SNR) (Schulze et al., 2011). Trabeculae that are thin in respect to the image resolution can appear thicker and smeared out, or a certain level completely disappears under the influence of the partial volume effect (Kothari et al., 1998). Nevertheless, the micro-CT trabecular network remained similar to that of the most tested CBCTs as well as the high resolution MSCT protocol. Only the standard resolution MSCT protocol and the i-CAT Next Generation demonstrated a deviant trabecular pattern, which was reflected by the dissimilarity in morphometric parameters.

It is important to note that the segmentation process plays a fundamental role in the reliability of the morphometric results. This sensitive step depends on various factors such as technical specifications of the scanner, the scanning protocol, movement artefacts, contrast values, reconstruction software and post-processing (Schulze et al., 2011). In the CT-Analyser software there are different possibilities for the segmentation process: global thresholding, adaptive thresholding and the Otsu method (Nackaerts et al., 2015). In the present study, the adaptive thresholding method was chosen according to the recommendations of Nackaerts et al. (2015) as it was shown to give the best segmentation results.

Previous studies that investigated the bone microarchitecture using CBCT relied on observers to manually match images obtained by different modalities (Ibrahim et al., 2014; J.-E. Kim et al., 2015; Klintström et al., 2014; Panmekiate et al., 2015; Parsa et al., 2015). This approach, however, is less accurate and inevitably leads to discrepancies between scanners for the selected VOI. To precisely compare the various devices, the same morphological structures should be compared to ensure that morphometric indices are derived from identical anatomical structures up to the voxel accuracy.

In the present study, this was achieved by fully automated and rigid registration, independent of the observer and based on mutual information (Maes et al., 1997). This allowed the authors to use an identical VOI for all images of a sample, which was selected on the micro-CT images to ensure optimal and complete selection of the trabecular and cortical bone. This was in contrast to other studies where a limited rectangular shaped VOI was used (Ibrahim et al., 2014; Klintström et al., 2014; Parsa et al., 2015). Unlike the majority of studies on bone quality, the trabecular bone sample was not harvested using a trepanation procedure, so that realistic and clinically useful 3D reconstruction of the complete bone structure could be provided. These

3D models in combination with the quantitative structural parameters could facilitate and assist the clinician in choosing the most optimal implant site and type.

Current research was however limited to an *in vitro* evaluation. Morphometric parameters obtained from a cadaver mandible may deviate from the clinical situation, as surrounding anatomical structures (tongue and vertebra) and the influence of soft tissue were not taken into consideration during the assessment. This study was restricted to the evaluation using the highest resolution scanning protocol for each scanner. Such small fields of view are not always applicable in a clinical setting and therefore the lower resolution settings are often applied. Further validation of the clinical relevance of the morphometric CBCT is required to show a relationship with clinical bone quality and existing bone classification schemes.

2.6 Conclusions

The present study demonstrated the potential of low-dose CBCT for quantitative 3D structural evaluation of the cortical and trabecular bone prior to implant placement for levels comparable to micro-CT. However, not all CBCT machines are equally reliable in displaying the trabecular and cortical bone structure. Standard resolution MSCT also performs suboptimally in this respect. Furthermore, overestimations or underestimations of respective morphometric parameters need to be taken into account.

2.7 References

- Burghardt, A. J., Link, T. M., & Majumdar, S. (2011). High-resolution Computed Tomography for Clinical Imaging of Bone Microarchitecture. *Clinical Orthopaedics and Related Research*, 469(8), 2179–2193. <https://doi.org/10.1007/s11999-010-1766-x>
- Dempster, D. W., Compston, J. E., Drezner, M. K., Glorieux, F. H., Kanis, J. A., Malluche, H., ... Parfitt, A. M. (2013). Standardized nomenclature, symbols, and units for bone histomorphometry: A 2012 update of the report of the ASBMR Histomorphometry Nomenclature Committee. *Journal of Bone and Mineral Research*, 28(1), 2–17. <https://doi.org/10.1002/jbmr.1805>
- Diederichs, G., Link, T. M., Kentenich, M., Schwieger, K., Huber, M. B., Burghardt, A. J., ... Issever, A. S. (2009). Assessment of trabecular bone structure of the calcaneus using multi-detector CT: Correlation with microCT and biomechanical testing. *Bone*, 44(5), 976–983. <https://doi.org/10.1016/j.bone.2009.01.372>
- dos Santos Corpas, L., Jacobs, R., Quirynen, M., Huang, Y., Naert, I., & Duyck, J. (2011). Peri-implant bone tissue assessment by comparing the outcome of intra-oral radiograph and cone beam computed tomography analyses to the histological standard. *Clinical Oral Implants Research*, 22(5), 492–499. <https://doi.org/10.1111/j.1600-0501.2010.02029.x>
- Fanuscu, M. I., & Chang, T.-L. (2004). Three-dimensional morphometric analysis of human cadaver bone: microstructural data from maxilla and mandible. *Clinical Oral Implants Research*, 15(2), 213–218. <https://doi.org/10.1111/j.1600-0501.2004.00969.x>
- Faul, F., Erdfelder, E., Buchner, A., & Lang, A.-G. (2009). Statistical power analyses using G*Power 3.1: Tests for correlation and regression analyses. *Behavior Research Methods*, 41(4), 1149–1160. <https://doi.org/10.3758/BRM.41.4.1149>
- Gomes de Oliveira, R. C., Leles, C. R., Lindh, C., & Ribeiro-Rotta, R. F. (2012). Bone tissue microarchitectural characteristics at dental implant sites. Part 1: Identification of clinical-related parameters. *Clinical Oral Implants Research*, 23(8), 981–986. <https://doi.org/10.1111/j.1600-0501.2011.02243.x>

- González-García, R., & Monje, F. (2013). The reliability of cone-beam computed tomography to assess bone density at dental implant recipient sites: a histomorphometric analysis by micro-CT. *Clinical Oral Implants Research*, 24(8), 871–879. <https://doi.org/10.1111/j.1600-0501.2011.02390.x>
- Guerrero, M. E., Jacobs, R., Loubele, M., Schutyser, F., Suetens, P., & van Steenberghe, D. (2006). State-of-the-art on cone beam CT imaging for preoperative planning of implant placement. *Clinical Oral Investigations*, 10(1), 1–7. <https://doi.org/10.1007/s00784-005-0031-2>
- Hsu, J.-T., Huang, H.-L., Fuh, L.-J., Li, R.-W., Wu, J., Tsai, M.-T., ... Tu, M.-G. (2013). Location of the Mandibular Canal and Thickness of the Occlusal Cortical Bone at Dental Implant Sites in the Lower Second Premolar and First Molar. *Computational and Mathematical Methods in Medicine*, 2013, 608570. <https://doi.org/10.1155/2013/608570>
- Huang, Y., Van Dessel, J., Depypere, M., EzEldeen, M., Iliescu, A. A., Dos Santos, E., ... Jacobs, R. (2014). Validating cone-beam computed tomography for peri-implant bone morphometric analysis. *Bone Research*, 2(1), 103–109. <https://doi.org/10.1038/boneres.2014.10>
- Huang, Y., Van Dessel, J., Liang, X., Depypere, M., Zhong, W., Ma, G., ... Jacobs, R. (2014). Effects of Immediate and Delayed Loading on Peri-Implant Trabecular Structures: A Cone Beam CT Evaluation. *Clinical Implant Dentistry and Related Research*, 16(6), 873–883. <https://doi.org/10.1111/cid.12063>
- Ibrahim, N., Parsa, A., Hassan, B., van der Stelt, P., Aartman, I. H. A., & Wismeijer, D. (2013). The effect of scan parameters on cone beam CT trabecular bone microstructural measurements of the human mandible. *Dentomaxillofacial Radiology*, 42(10), 20130206. <https://doi.org/10.1259/dmfr.20130206>
- Ibrahim, N., Parsa, A., Hassan, B., van der Stelt, P., Aartman, I. H. A., & Wismeijer, D. (2014). Accuracy of trabecular bone microstructural measurement at planned dental implant sites using cone-beam CT datasets. *Clinical Oral Implants Research*, 25(8), 941–945. <https://doi.org/10.1111/clr.12163>

- Ibrahim, N., Parsa, A., Hassan, B., van der Stelt, P., & Wismeijer, D. (2013). Diagnostic imaging of trabecular bone microstructure for oral implants: a literature review. *Dentomaxillofacial Radiology*, 42(3), 20120075. <https://doi.org/10.1259/dmfr.20120075>
- Kim, D.-G., Christopherson, G. T., Dong, X. N., Fyhrie, D. P., & Yeni, Y. N. (2004). The effect of microcomputed tomography scanning and reconstruction voxel size on the accuracy of stereological measurements in human cancellous bone. *Bone*, 35(6), 1375–1382. <https://doi.org/10.1016/j.bone.2004.09.007>
- Kim, J.-E., Yi, W.-J., Heo, M.-S., Lee, S.-S., Choi, S.-C., & Huh, K.-H. (2015). Three-dimensional evaluation of human jaw bone microarchitecture: correlation between the microarchitectural parameters of cone beam computed tomography and micro-computer tomography. *Oral Surgery, Oral Medicine, Oral Pathology and Oral Radiology*, 120(6), 762–770. <https://doi.org/10.1016/j.oooo.2015.08.022>
- Klintström, E., Smedby, Ö., Klintström, B., Brismar, T. B., & Moreno, R. (2014). Trabecular bone histomorphometric measurements and contrast-to-noise ratio in CBCT. *Dentomaxillofacial Radiology*, 43(8), 20140196. <https://doi.org/10.1259/dmfr.20140196>
- Kothari, M., Keaveny, T. M., Lin, J. C., Newitt, D. C., Genant, H. K., & Majumdar, S. (1998). Impact of Spatial Resolution on the Prediction of Trabecular Architecture Parameters. *Bone*, 22(5), 437–443. [https://doi.org/10.1016/S8756-3282\(98\)00031-3](https://doi.org/10.1016/S8756-3282(98)00031-3)
- Kottner, J., Audigé, L., Brorson, S., Donner, A., Gajewski, B. J., Hróbjartsson, A., ... Streiner, D. L. (2011). Guidelines for Reporting Reliability and Agreement Studies (GRRAS) were proposed. *Journal of Clinical Epidemiology*, 64(1), 96–106. <https://doi.org/10.1016/j.jclinepi.2010.03.002>
- Lekholm, U., & Zarb, G. (1985). Patient selection and preparation. In P.-I. Brånemark, G. A. Zarb, & T. Albrektsson (Eds.), *Tissue Integrated Prostheses: Osseointegration in Clinical Dentistry* (pp. 199–209). Chicago, IL: Quintessence.
- Liang, X., Jacobs, R., Hassan, B., Li, L., Pauwels, R., Corpas, L., ... Lambrichts, I. (2010). A comparative evaluation of Cone Beam Computed Tomography (CBCT) and Multi-Slice CT (MSCT) Part I. On subjective image quality. *European Journal of Radiology*, 75(2),

- 265–269. <https://doi.org/10.1016/j.ejrad.2009.03.042>
- Loubele, M., Bogaerts, R., Van Dijck, E., Pauwels, R., Vanheusden, S., Suetens, P., ... Jacobs, R. (2009). Comparison between effective radiation dose of CBCT and MSCT scanners for dentomaxillofacial applications. *European Journal of Radiology*, 71(3), 461–468. <https://doi.org/10.1016/j.ejrad.2008.06.002>
- Maes, F., Collignon, A., Vandermeulen, D., Marchal, G., & Suetens, P. (1997). Multimodality image registration by maximization of mutual information. *IEEE Transactions on Medical Imaging*, 16(2), 187–198. <https://doi.org/10.1109/42.563664>
- Marx, R. E. (2014). A Decade of Bisphosphonate Bone Complications: What It Has Taught Us About Bone Physiology. *The International Journal of Oral & Maxillofacial Implants*, 29(2), e247–e258. <https://doi.org/10.11607/jomi.te61>
- Monje, A., Monje, F., González-García, R., Galindo-Moreno, P., Rodríguez-Salvanes, F., & Wang, H.-L. (2014). Comparison between microcomputed tomography and cone-beam computed tomography radiologic bone to assess atrophic posterior maxilla density and microarchitecture. *Clinical Oral Implants Research*, 25(6), 723–728. <https://doi.org/10.1111/clr.12133>
- Nackaerts, O., Depypere, M., Zhang, G., Vandenberghe, B., Maes, F., & Jacobs, R. (2015). Segmentation of Trabecular Jaw Bone on Cone Beam CT Datasets. *Clinical Implant Dentistry and Related Research*, 17(6), 1082–1091. <https://doi.org/10.1111/cid.12217>
- Panmekiate, S., Ngonphloy, N., Charoenkarn, T., Faruangaeng, T., & Pauwels, R. (2015). Comparison of mandibular bone microarchitecture between micro-CT and CBCT images. *Dentomaxillofacial Radiology*, 44(5), 20140322. <https://doi.org/10.1259/dmfr.20140322>
- Parsa, A., Ibrahim, N., Hassan, B., van der Stelt, P., & Wismeijer, D. (2015). Bone quality evaluation at dental implant site using multislice CT, micro-CT, and cone beam CT. *Clinical Oral Implants Research*, 26(1), e1–e7. <https://doi.org/10.1111/clr.12315>
- Pauwels, R., Faruangaeng, T., Charoenkarn, T., Ngonphloy, N., & Panmekiate, S. (2015). Effect of exposure parameters and voxel size on bone structure analysis in CBCT. *Dentomaxillofacial Radiology*, 44(8), 20150078. <https://doi.org/10.1259/dmfr.20150078>

- Pauwels, R., Jacobs, R., Singer, S. R., & Mupparapu, M. (2015). CBCT-based bone quality assessment: are Hounsfield units applicable? *Dentomaxillofacial Radiology*, 44(1), 20140238. <https://doi.org/10.1259/dmfr.20140238>
- Quirynen, M., Gijbels, F., & Jacobs, R. (2003). An infected jawbone site compromising successful osseointegration. *Periodontology* 2000, 33(1), 129–144. <https://doi.org/10.1046/j.0906-6713.2002.03311.x>
- Ribeiro-Rotta, R. F., Lindh, C., Pereira, A. C., & Rohlin, M. (2011). Ambiguity in bone tissue characteristics as presented in studies on dental implant planning and placement: a systematic review. *Clinical Oral Implants Research*, 22(8), 789–801. <https://doi.org/10.1111/j.1600-0501.2010.02041.x>
- Ribeiro-Rotta, R. F., Lindh, C., & Rohlin, M. (2007). Efficacy of clinical methods to assess jawbone tissue prior to and during endosseous dental implant placement: a systematic literature review. *The International Journal of Oral & Maxillofac Implants*, 22(2), 289–300.
- Sakka, S., & Coulthard, P. (2009). Bone Quality: A Reality for the Process of Osseointegration. *Implant Dentistry*, 18(6), 480–485. <https://doi.org/10.1097/ID.0b013e3181bb840d>
- Schulze, R., Heil, U., Groß, D., Bruellmann, D. D., Dranischnikow, E., Schwanecke, U., & Schoemer, E. (2011). Artefacts in CBCT: a review. *Dentomaxillofacial Radiology*, 40(5), 265–273. <https://doi.org/10.1259/dmfr/30642039>
- Van Dessel, J., Huang, Y., Depypere, M., Rubira-Bullen, I., Maes, F., & Jacobs, R. (2013). A comparative evaluation of cone beam CT and micro-CT on trabecular bone structures in the human mandible. *Dentomaxillofacial Radiology*, 42(8), 20130145. <https://doi.org/10.1259/dmfr.20130145>
- Waarsing, J. H., Day, J. S., & Weinans, H. (2004). An Improved Segmentation Method for In Vivo μ CT Imaging. *Journal of Bone and Mineral Research*, 19(10), 1640–1650. <https://doi.org/10.1359/JBMR.040705>
- Wirth, A. J., Goldhahn, J., Flaig, C., Arbenz, P., Müller, R., & van Lenthe, G. H. (2011). Implant stability is affected by local bone microstructural quality. *Bone*, 49(3), 473–478. <https://doi.org/10.1016/j.bone.2011.05.001>

Chapter 3

Accuracy and reliability of different CBCT devices for structural analysis of alveolar bone in comparison with multislice CT and micro-CT

This chapter is based on:

Van Dessel, J., **Nicolielo, L. F.**, Huang, Y., Coudyzer, W., Salmon, B., Lambrichts, I., & Jacobs, R. (2017). Accuracy and reliability of different cone beam computed tomography (CBCT) devices for structural analysis of alveolar bone in comparison with multislice CT and micro-CT. *European Journal of Oral Implantology*, 10(1), 95–105

3.1 Abstract

Objective: The aim of this study was to assess whether Cone-Beam Computed Tomography (CBCT) may be used for the purpose of clinically reliable alveolar bone quality assessment in comparison to its clinical alternative multi-slice CT (MSCT) and gold standard (micro-CT).

Materials and methods: Six dentate mandibular bone samples were scanned with seven CBCTs devices (ProMax 3D Max®, NewTom GiANO®, Cranex 3D®, 3D Accuitomo®, Carestream 9300®, Scanora 3D®, I-CAT Next generation®), one micro-CT scanner (SkyScan 1174®) and one MSCT machine (Somatom Definition Flash®) using two protocols (standard and high-resolution). MSCT and CBCT images were automatically spatially aligned on the micro-CT scan of the corresponding sample. A volume of interest was manually delineated on the micro-CT image and overlaid on the other scanning devices. Alveolar bone structures were automatically extracted using the adaptive thresholding algorithm. Based on the resulting binary images an automatic 3D morphometric quantification was performed in CT-Analyser® (Skyscan). The reliability and measurement errors were calculated for each modality compared to the gold standard micro-CT.

Results: Both MSCT and CBCT were associated with a clinically and statistically ($P < 0.05$) significant measurement error. Bone quantity-related morphometric indices (BV/TV 8.41 % min – 17.90 % max and Tb.Th: 0.15 mm min – 0.31 mm max) were significantly ($P < 0.05$) overestimated resulting in significantly ($P < 0.05$) closer trabecular pores (Po[_{tot}] -8.41 % min – -17.90 % max and FD 0.08 min – 0.17 max) in all scanners compared to micro-CT. The structural pattern of the alveolar bone remained however similar compared to that of the micro-CT for the ProMax 3D Max®, NewTom GiANO®, Cranex 3D®, 3D Accuitomo 170® and Carestream 9300®. On the other hand, the Scanora 3D®, i-CAT Next Generation®, standard and high-resolution MSCT displayed an overrated bone quantity and aberrant structural pattern compared to other scanning devices. The calculation of morphometric indices had an overall high reliability (ICC 0.62 min – 0.99 max), except for the i-CAT Next Generation® CBCT (ICC 0.26 min – 0.86 max) and standard resolution MSCT (ICC 0.10 min – 0.62 max).

Conclusions: This study demonstrated that most CBCT machines may be able to quantitatively assess alveolar bone quality, with a level of accuracy and reliability that approaches micro-CT. One may therefore propose to extrapolate this to clinical CBCT imaging, definitely when there is a need for implant rehabilitation in dentate jaw bones.

3.2 Introduction

Alveolar bone density has been considered as one of the most important prognostic factors of successful osseointegration (Esposito, Hirsch, Lekholm, & Thomsen, 1998). Bone quality classification schemes have associated bone of thin cortical density and large alveolar spaces with poor quality for successful osseointegration (He, Zhao, Deng, Shang, & Zhang, 2015; Ihde, Kopp, & Maier, 2009). On the other hand, higher implant failure rates have been repeatedly reported in a dense sclerotic alveolar bone region in patients under bisphosphonate therapy (De-Freitas et al., 2016; Yip, Borrell, Cho, Francisco, & Tarnow, 2012) or at local chronic peri-apical lesions (Quirynen, Gijbels, & Jacobs, 2003). Hereby, it is too simplistic to link denser bone with an increased bone quality (Monje et al., 2015). Progress in surgical techniques combined with improved implant surface features have resulted in a more predictable osseointegration, regardless of bone quality type (Goiato, dos Santos, Santiago, Moreno, & Pellizzer, 2014; van Velzen, Ofec, Schulten, & ten Bruggenkate, 2015). Contrariwise, the number and distribution of blood vessels are now considered to be a more crucial factor in the bone formation and remodelling process (Brandi & Collin-Osdoby, 2006; Gerber & Ferrara, 2000; Mamalis & Cochran, 2013). Vascularisation in the alveolar bone cannot yet be visualised with clinically applicable radiological techniques. Sparse and homogeneously structured trabeculae, however, are rich vascularised in contrast to sclerotic bone with close pores that lacks vascularisation (Engelke, Lazzarini, Stühmer, & Beltrán, 2015). Presurgical radiographic evaluation of the implant site should therefore evolve from a pure density-based approach to a more structural bone analysis in order to choose the most optimal surgical protocol to avoid surgical complications and enhance implant outcome (Pauwels, Jacobs, Singer, & Mupparapu, 2015).

Intraoral and panoramic radiographs are well established tools in dentistry for two-dimensional (2D) evaluation of the width and height of alveolar ridge, and the dimensions of missing tooth area. Correct assessment of the bone structure on these 2D images however remains limited and subjective due to anatomical overlap and standardisation during follow-up in time is difficult (Ribeiro-Rotta, Lindh, & Rohlin, 2007). Various three-dimensional (3D) imaging techniques have proven to be more reliable for evaluation and monitoring of the alveolar bone remodelling (Ibrahim, Parsa, Hassan, van der Stelt, & Wismeijer, 2013). Unfortunately, current radiographic bone quality evaluations still rely on subjective grading scales that are based on the classification of cross-sectional trabecular morphology and cortical bone thickness (Lindh, Petersson, & Rohlin, 1996). Furthermore, various standards for describing the jawbone characteristics prior to implant treatment have been proposed (Lekholm & Zarb, 1985; Misch, 1990; Rao & Rao, 1999). These different classification systems for bone quality frequently lead to confusion and interfere with attempts to compare the results across studies. Therefore,

objective quantitative bone quality parameters for implant treatment in clinical practice are needed (Ribeiro-Rotta, Lindh, Pereira, & Rohlin, 2011).

Multiple structural analysis procedures have been used for the quantitative assessment of trabecular bone architecture in high-resolution 3D radiological images (Link, 2008). Most commonly used are morphological parameters based on standard histomorphometry, as they give a specific estimation of important structural properties (Dempster et al., 2013). Since the diameter of jawbone trabeculae ranges from approximately 50 – 200 μm , sufficient high-resolution imaging modalities have been considered obligatory to accurately predict the structural pattern (Kothari et al., 1998). Micro-CT systems can achieve resolutions up to 0.5 μm and are currently considered as the nondestructive gold standard measure. The use of micro-CT, however, is restricted to small animal models or human biopsy specimen evaluations due to its limited field of view (FOV) and excessive radiation dose. Making it unsuitable for clinical diagnosis.

Recent comparative studies have validated Cone-Beam CT (CBCT) as a reliable radiological technique to objectively assess bone quality by means of morphometric parameters. Most of these validation studies were however conducted using the same CBCT machine (3D Accuitomo 170®, Morita, Kyoto, Japan) using edentulous bone samples (Huang et al., 2014; Ibrahim et al., 2014; Parsa, Ibrahim, Hassan, van der Stelt, & Wismeijer, 2015; Van Dessel et al., 2013, 2016) or trephine biopsies (Ho et al., 2013; Kim et al., 2015; Klintström, Smedby, Klintström, Brismar, & Moreno, 2014; Panmekiate, Ngonphloy, Charoenkarn, Faruangsang, & Pauwels, 2015). Considering that more and more patients are getting single tooth replacements in an otherwise dental jaw bone, there is a growing need for alveolar bone quality diagnostics at the implant site and at the level of the neighboring teeth. With the CBCT technology evolving at an incredible pace, the aim of this study was to assess whether different CBCT devices may be used for the purpose of clinically reliable alveolar bone quality assessment in comparison to its clinical alternative (Multi-Slice CT) and the gold standard (micro-CT).

3.3 Materials and methods

A cadaver was obtained from the Anatomy Department, KU Leuven, Leuven, Belgium and approved for research by the medical ethics committee of the University Hospitals KU Leuven (s55619). The mandible was sectioned perpendicular to the lower jaw arch in order to include the trabecular bone of the interproximal area, totalizing six full dentate mandibular bone samples (*Figure 3.1*).

3.3.1 Image acquisitions

The bone specimens were scanned using a micro-CT scanner, seven CBCT scanners and one Multi-Slice CT (MSCT) scanner according to a computer-generated randomisation list. All scans got a unique code of which only one of the investigators (J.V.D.) was aware and had access to the file. For micro-CT scanning, each sample was individually fixed in a wax block and scanned in a SkyScan 1174[®] system (SkyScan, Kontich, Belgium) in order to obtain an accurate reference of the alveolar network. A high-resolution scan protocol was used at 50 kVp, 800 μ A and 360° rotation with an angular step of 0.8°. A 1 mm aluminum filter was used to eliminate the beam hardening effect. After scanning, the raw image stacks were reconstructed in NRecon[®] software (version 1.6.5, Bruker micro-CT) with isotropic voxel size of 30 μ m³, resulting in a total of 514 slices.

For CBCT scanning, the teeth region of each bone sample was located in the center of the field of view while keeping the mandibular base parallel to the floor to avoid effects of differences in object location. The exposure parameters for the seven CBCT scanners (1) ProMax 3D Max[®] (Planmeca, Helsinki, Finland), (2) NewTom GiANO[®] (QR Verona, Verona, Italy), (3) Cranex 3D[®] (Soredex, Tuusula, Finland), (4) 3D Accuitomo 170[®] (Morita, Kyoto, Japan), (5) Carestream 9300[®] (Carestream Health, New York, USA), (6) Scanora 3D[®] (Soredex, Tuusula, Finland), (7) i-CAT Next Generation[®] (Imaging Sciences International, Hatfield, USA) varied and were chosen according to their clinical scan protocol with the highest resolution.

Likewise, bone samples were randomly scanned by a 256-slice Somatom Definition Flash[®] (Siemens Healthcare, Erlangen, Germany) MSCT system using a clinical standard and high-resolution scanning protocol. The voxel sizes of the MSCT were not isotropic with a slice thickness of 250 μ m and a U75 kernel was used. An overview of the micro-CT, CBCT and MSCT scan protocols can be found in *Table 3.1*.

Table 3.1. Overview of micro-Computed Tomography, cone-beam CT and multi-slice CT scan protocols.

Scan parameters	Unit	Micro-CT	ProMax 3D Max	NewTom GiANO	Cranex 3D	3D Accutomo 170	Carestream 9300	Scanora 3D	i-CAT Next Generation	Standard Resolution MSCT	High Resolution MSCT
Voxel size	(µm)	30	100	100	85	80	90	130	125	700	400
Tube voltage	(kV)	50	90	90	90	90	80	90	120	120	120
Tube Current	(mA)	800	11	5	5	5	3	10	37	250	250
Field of view	(mm)	30 x 50	60 x 40	50 x 50	60 x 40	40 x 40	50 x 50	60 x 40	160 x 40	500 x 500	500 x 500

3.3.2 Image processing

All scans underwent the same image processing workflow shown in *Figure 3.2*. CBCT and MSCT images were spatially aligned on the corresponding micro-CT scans using a ridged registration step (Maes, Collignon, Vandermeulen, Marchal, & Suetens, 1997). The validity of the automatic registration process was verified by inspecting the structural compatibility at several anatomical reference points. Thereafter, only the trabecular bone in each sample was manually delineated on the micro-CT images and saved as volume of interest (VOI) in CT-Analyser® (SkyScan, Kontich, Belgium). This micro-CT VOI was then transformed on the CBCT and MSCT scans, resulting in a highly accurate delineation of the trabecular bone in the coordinate system of the CBCT and MSCT images. The alveolar bone structure was segmented by an experienced radiologist (L.F.P.N.), which was blinded for scanner type, using an automatic adaptive threshold algorithm in CT-Analyser®. This segmentation method was selected by the recommendations of Nackaerts et al. (2015), as it showed to achieve the best segmentation results for trabecular bone structures on low-resolution images (Nackaerts et al., 2015). The computer suggested bone thresholds were visually reassessed after overlapping the segmented network on the original bone structures in order to confirm the best segmented fit. From the resulting binary images, individual 3D models of the teeth and alveolar bone were made using 3-Matic® (Materialise, Leuven, Belgium). The CBCT and MSCT alveolar network were overlaid on the micro-CT model and the perpendicular distance between both surfaces was colour coded to estimate the structural discrepancy between the trabecular networks.

3.3.3 Alveolar bone structural analysis

Quantitative 3D bone morphometry was performed to assess the quantity and structural properties of the alveolar network. Morphometric indices were calculated, operator independent and blinded for the micro-CT, based on the segmented alveolar bone structure in CT-Analyser®. In order to take full advantage of volumetric measurements, model-independent 3D algorithms were used for computing trabecular bone microarchitecture and the latest recommendations of the American Society of Bone and Mineral Metabolism were followed (Dempster et al., 2013).

Basic morphometric parameters include the measurement of bone volume (BV) and the total volume of interest (TV). The ratio of these two measures is termed bone volume fraction (BV/TV) and is often considered the key parameter to evaluate the bone quantity as it indicates the portion of mineralised bone tissue. Since trabecular bone contains marrow cavities, the BV/TV should be < 100%, whereas for cortical bone it would approach 100%. Another basic measure is the bone surface (BS) and the bone surface density (BS/TV) can be easily derived

by dividing the total volume of interest (TV). Consequently, if more trabeculae are present within a certain VOI, the surface area will be larger and a higher ratio will be obtained. The normalised morphometric parameters BV/TV and BS/TV are used to be capable of comparing samples with different VOIs.

Trabecular thickness (Tb.Th), trabecular separation (Tb.Sp) and trabecular number (Tb.N) offer an inferred estimation of the spatial organization of the trabecular net configuration. Bone pattern factor (Tb.Pf), connectivity density (Conn.Dn) and total porosity percentage (Po[tot]) indicate the degree of trabecular branching. Intra-trabecular connectivity increases with decreasing Tb.Pf. The larger the Po[tot], the bigger the amount of open trabecular cavities.

The structure model index (SMI) was developed to estimate the plate- versus rod-like characteristics of the trabecular structure. This index was designed to be 0 for perfect plates, 3 for perfect rods and 4 for perfect spheres (Hildebrand & Rüegsegger, 1997). Fractal dimension (FD) is an indicator of surface complexity of an object, which quantifies how that object's surface fills space (Fazzalari & Parkinson, 1996). Degree of anisotropy (DA) is indicating the absence of preferential alignment of structures along an axis and is often considered to be one of the important determinants of mechanical strength (Odgaard, 1997). Taken together, these morphometric variables can provide important information on both bone quantity as structural organization of the trabeculae.

3.3.4 Statistical Analysis

Recommendations for description of reliability and agreement studies were taken into account during reporting (Kottner et al., 2011). The minimum required sample size was calculated using the morphometric parameters of 3 comparison studies between CBCT and micro-CT with a similar design. The primary considered parameter was discrepancy in trabecular thickness, respectively, for the CBCT and micro-CT evaluation: 0.42 mm \pm 0.01 mm and 0.19 mm \pm 0.01 mm (Van Dessel et al., 2013); 0.42 mm \pm 0.04 mm and 0.13 mm \pm 0.01 mm (Klintström et al., 2014); 1.17 mm \pm 0.30 mm and 0.24 mm \pm 0.07 mm (Kim et al., 2015). A power analysis in G*Power 3.1 suggested a minimum sample size of 4 bone specimens when assuming 95% power and α of 0.05 (Faul, Erdfelder, Lang, & Buchner, 2007). The rest of the statistical analysis was done in SPSS® (IBM, New York, USA).

All data were tested for normality using the Shapiro-Wilk test. To fully consider the influence of repeated scans for each bone sample, a general linear mixed-effects model with post-hoc Bonferroni correction for multiple comparisons was used to calculate the measurement errors between CBCT/MSCT and gold standard micro-CT as measures of accuracy and significant differences were noted at $P < 0.05$. Scanner type was considered as fixed effect. Reliability of the CBCT and MSCT quantitative morphometric analysis was estimated by computing the two-

way mixed intraclass correlation coefficient (ICC) with micro-CT assessment. Single measurements for consistency were reported using a 95% confidence interval for all parameters.

3.4 Results

3.4.1 Quantitative morphometric analysis

Morphometric measurements of alveolar bone structure were obtained in 3D and compared between gold standard micro-CT and other scanner types (*Table 3.2*). CBCT and MSCT indices showed an alveolar network with significant ($P < 0.05$) thicker trabeculae (\uparrow Tb.Th), associated with a significant ($P < 0.05$) overestimation of the bone volume (\uparrow BV/TV) and closer pores (\downarrow Po[tot] and \uparrow FD) compared to the micro-CT model. Non-significant differences between the remaining structural parameters indicated a similar structural pattern as in the micro-CT for all CBCTs and MSCTs, with exception of the standard resolution MSCT and i-CAT Next Generation®. The latter machines showed an aberrant trabecular organization and larger overestimation of bone quantity (\uparrow BV/TV, \downarrow SMI) compared to micro-CT, explained by significant ($P < 0.05$) thicker trabeculae (\uparrow Tb.Th, \downarrow Tb.N) with smaller spaces between them (\downarrow Tb.Sp, \downarrow Po[tot]). What resulted in a significantly increased connectivity (\uparrow Conn.Dn, \downarrow Tb.Pf).

3.4.2 Morphometric reliability

High structural evaluation reliability ($ICC > 0.70$) was observed for 3D Accuitomo 170®, Carestream 9300®, Cranex 3D®, NewTom GiANO®, ProMax 3D Max® and Scanora 3D® (*Table 3.3*). Bone morphometric ICC were unexpected lower for Carestream 9300® Conn.Dn ($ICC = 0.63$), Cranex 3D® BS/TV ($ICC = 0.62$), and Scanora 3D® BS/TV ($ICC = 0.55$) and Tb.N ($ICC = 0.67$). Non-significant ($P > 0.05$) ICC were found for all morphometric parameters in standard resolution MSCT and i-CAT Next Generation® (except for BS/TV). The high resolution MSCT protocol only showed significant ($P < 0.05$) ICC for BV/TV ($ICC = 0.77$), Tb.N ($ICC = 0.83$), Tb.Pf ($ICC = 0.79$), SMI ($ICC = 0.70$), DA ($ICC = 0.76$), FD ($ICC = 0.76$) and Conn.Dn ($ICC = 0.69$).

Table 3.2. Morphometric indices for all scanner types (mean ± standard deviation).

Trabecular Morphometric Parameters	Unit	Micro-CT	ProMax 3D Max	NewTom GIANO	Cranex 3D	3D Accutomo 170	Carestream 9300	Scanora 3D	i-CAT Next Generation	Standard Resolution MSCT	High Resolution MSCT
Bone volume fraction	%	30.87 ± 4.12	38.12 ± 4.92*	39.27 ± 5.08*	40.07 ± 4.55*	44.19 ± 10.86*	44.26 ± 7.5*	44.0 ± 5.42*	48.76 ± 9.7*	47.68 ± 6.54*	47.29 ± 3.82*
Bone surface density	mm ³ /mm ²	3.92 ± 0.38	3.60 ± 0.44	4.06 ± 0.56	3.45 ± 0.33	3.85 ± 0.33	3.78 ± 0.42	3.58 ± 0.36	3.81 ± 0.62	3.95 ± 0.66	4.08 ± 0.31
Trabecular thickness	mm	0.28 ± 0.03	0.39 ± 0.01*	0.44 ± 0.02*	0.43 ± 0.02*	0.43 ± 0.07*	0.46 ± 0.09*	0.45 ± 0.02*	0.59 ± 0.13*	0.58 ± 0.03*	0.48 ± 0.02*
Trabecular separation	mm	0.91 ± 0.18	0.88 ± 0.25	0.91 ± 0.21	0.89 ± 0.19	0.89 ± 0.19	0.93 ± 0.31	1.01 ± 0.25	0.68 ± 0.37*	0.61 ± 0.08*	0.87 ± 0.22
Trabecular number	1/mm	1.11 ± 0.14	0.97 ± 0.12	1.00 ± 0.12	0.92 ± 0.10	1.02 ± 0.11	0.97 ± 0.10	0.94 ± 0.11	0.83 ± 0.11*	0.82 ± 0.11*	0.99 ± 0.08
Trabecular pattern factor	1/mm	0.77 ± 1.71	0.48 ± 0.64	-0.90 ± 2.96	0.41 ± 0.82	-0.81 ± 2.27	-0.32 ± 4.90	-0.89 ± 1.31	-10.03 ± 2.64*	-7.59 ± 2.74*	-1.63 ± 0.75
Structure model index	(SMI)	1.06 ± 0.39	1.17 ± 0.29	0.49 ± 0.69	1.17 ± 0.24	1.01 ± 0.20	-0.64 ± 0.25	1.08 ± 0.33	-2.60 ± 6.16*	-1.07 ± 0.47*	1.01 ± 0.23
Degree of anisotropy	(DA)	1.85 ± 0.56	1.80 ± 0.51	1.81 ± 0.57	1.77 ± 0.55	1.81 ± 0.55	1.76 ± 0.60	1.78 ± 0.51	2.16 ± 0.71	2.50 ± 1.15	1.70 ± 0.54
Fractal dimension	(FD)	2.50 ± 0.04	2.57 ± 0.03*	2.62 ± 0.04*	2.59 ± 0.04*	2.61 ± 0.09*	2.62 ± 0.07*	2.59 ± 0.04*	2.67 ± 0.07*	2.65 ± 0.04*	2.62 ± 0.03*
Total porosity percentage	Po(10)	69.13 ± 4.12	61.88 ± 4.92*	60.73 ± 5.42*	59.93 ± 4.55*	55.81 ± 10.86*	55.74 ± 7.52*	56.00 ± 5.08*	51.24 ± 9.74*	52.32 ± 6.54*	52.71 ± 3.82*
Connectivity density	(Conn.Dn)	7.85 ± 3.16	5.53 ± 1.02	12.58 ± 14.05	5.18 ± 1.66	12.98 ± 7.08	14.50 ± 3.79	9.02 ± 4.40	42.75 ± 16.17*	46.73 ± 18.29*	12.16 ± 2.28

*Significant difference P < 0.05 with gold standard micro-CT

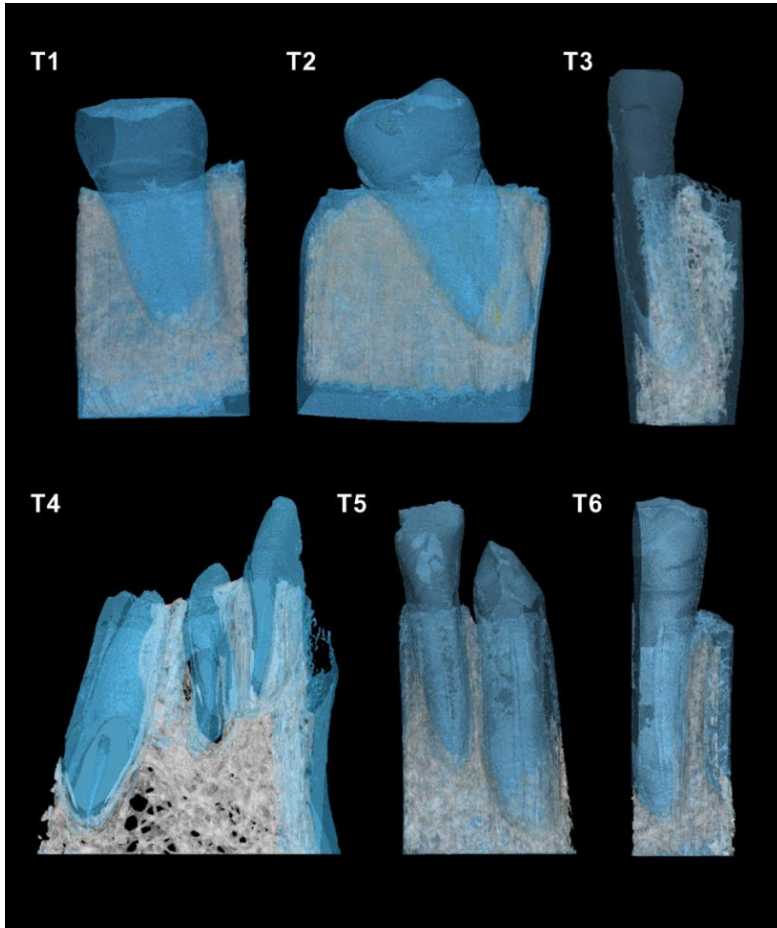


Figure 3.1. High-resolution 3D models of micro-CT image data of six mandibular bone samples containing a molar (T1), single rooted premolar (T2), lateral incisor (T3), 1 sample containing a canine, lateral and central incisor (T4), lateral incisor and canine (T5), and central incisor (T6). The alveolar bone network (grey) was saved as volume of interest and used for quantitative 3D morphometric analysis. The cortical bone and teeth (blue) were not taken into consideration during structural analysis and solely displayed for visualisation purposes.

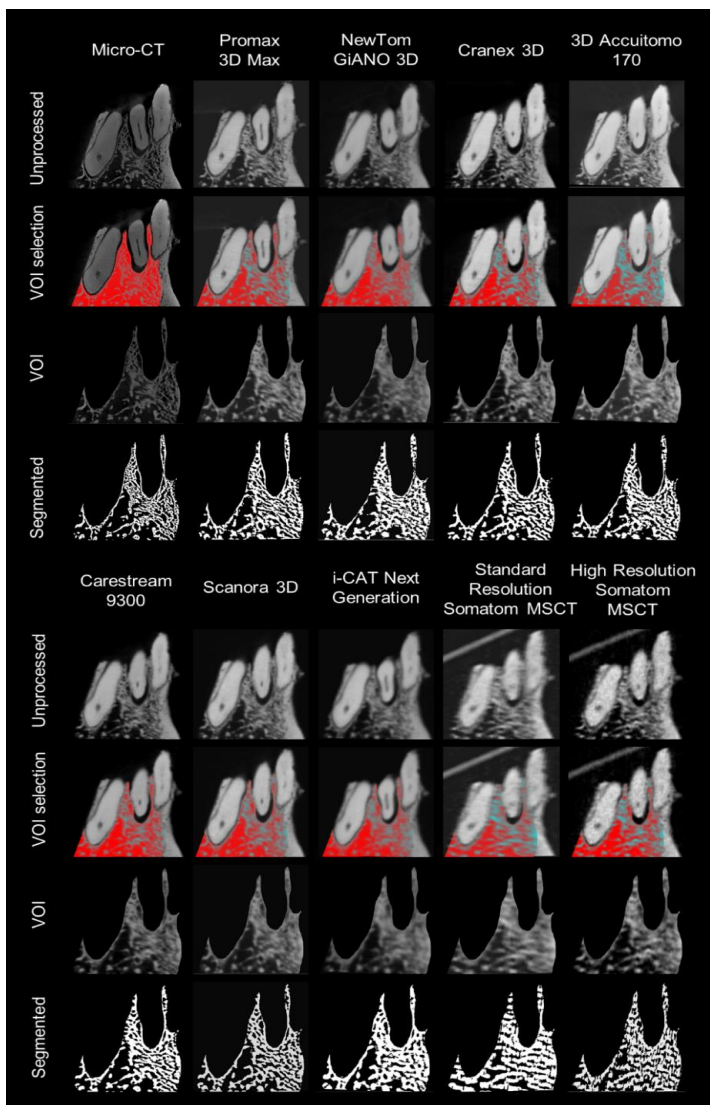


Figure 3.2. Overview of image processing steps before calculation of morphometric parameters. Cone-beam computed tomography (CBCT) and multi-slice CT (MSCT) images were spatially aligned with the gold standard micro-CT scan. A volume of interest (VOI) was manually delineated on the micro-CT image to ensure an accurate selection of only the alveolar bone. The micro-CT VOI was overlaid on the corresponding images of other scanners, allowing a reliable comparison without introducing errors by unmatched VOIs. The alveolar bone was segmented using the adaptive thresholding algorithm. Based on the resulting binary images an automatic 3D morphometric bone quantification was performed. Image showing the sample with 1 canine, 1 lateral and 1 central incisor.

Table 3.3. Intraclass correlation coefficients with micro-computed tomography to assess the reliability of each scanner type.

Trabecular Morphometric Parameters	Unit	3D Accutomo 170	Carestream 9300	Cranex 3D	i-CAT Next Generation	NewTom GIANO	ProMax 3D Max	Scanora 3D	High Resolution MSCT	Standard Resolution MSCT
Bone volume fraction	%	0.88*	0.87*	0.89*	0.26	0.87*	0.90*	0.70*	0.77*	0.46
Bone surface density	mm ³ /mm ²	0.82*	0.78*	0.62	0.86*	0.81*	0.88*	0.55	0.48	0
Trabecular thickness	mm	0.78*	0.71*	0.70*	0.24	0.79*	0.89*	0.69*	0.12	0.10
Trabecular separation	mm	0.90*	0.79*	0.99*	0.65	0.97*	0.89*	0.88*	0.61	0.44
Trabecular number	1/mm	0.93*	0.84*	0.89*	0.62	0.92*	0.91*	0.67	0.83*	0.61
Trabecular pattern factor	1/mm	0.85*	0.82*	0.84*	0.48	0.84*	0.94*	0.72*	0.79*	0.41
Structure model index	(SMI)	0.72*	0.78*	0.86*	0.10	0.81*	0.84*	0.85*	0.70*	0.62
Degree of anisotropy	(DA)	0.97*	0.95*	0.99*	0.68	0.96*	0.98*	0.98*	0.76*	0.58
Fractal dimension	(FD)	0.84*	0.75*	0.82*	0.61	0.75*	0.93*	0.81*	0.76*	0.47
Total porosity percentage	Po(tot)	0.83*	0.79*	0.81*	0.26	0.78*	0.89*	0.69*	0.62	0.45
Connectivity density	(Conn.Dn)	0.71*	0.63	0.72*	0.36	0.74*	0.85*	0.93*	0.69*	0.18

*Significant difference P < 0.05 with gold standard micro-CT

3.4.3 Visual 3D comparison of the alveolar bone network

The linear distance between the micro-CT and the aligned CBCT and MSCT trabecular surface was colour-coded in order to compare the structural organization of alveolar bone network (*Figure 3.3*). The colour pattern was mostly green (indicating a difference in Tb.Th up to 160 μm) for ProMax 3D Max[®], NewTom GiANO[®], Cranex 3D[®], 3D Accuitomo 170[®] and Carestream 9300[®]. This visually confirms similarity with the structural pattern of micro-CT and is in line with the measurement accuracy for Tb.Th for these scanners. On the other hand, the Scanora 3D[®], i-CAT Next Generation[®], standard and high-resolution MSCT display more yellow – red regions (difference in Tb.Th up to 400 μm) suggesting an even higher overrated bone quantity and aberrant structural pattern compared to other scanning devices.

3.5 Discussion

The present study evaluated the reliability and accuracy of different CBCT machines for quantitative morphometric bone analysis and alveolar network visualisation by comparing it to the reference micro-CT and its clinical MSCT alternative. The current results are strongly supportive for the use of high-resolution CBCT in structural alveolar bone assessment in three ways. First, colour-maps showed an identical trabecular pattern for most CBCTs compared to micro-CT. Secondly, these findings were confirmed by differences in mean morphometric parameters. Thirdly, high ICC values ($\text{ICC} > 0.70$) were found between the structural parameters of micro-CT and CBCT machines. These findings demonstrate the potential of CBCT machines to assess alveolar bone quality in a quantitative and objective manner, with a level of accuracy and reliability that approaches micro-CT, as such that one may therefore propose to extrapolate this to clinical CBCT imaging. This can be of paramount importance during preoperative radiographic planning of implant rehabilitation cases in dentate jaw bones. Not all CBCT machines were equally good in accurately depicting and reliably evaluating the alveolar bone structure. In general, CBCT and MSCT displayed a denser trabecular pattern compared to gold standard micro-CT. This was reflected in the morphometric analysis by significantly thicker trabeculae ($\uparrow\text{Tb.Th}$), resulting in an increased total amount of bone ($\uparrow\text{BV/TV}$) and closer pores ($\downarrow\text{Po[fo]t}$ and $\uparrow\text{FD}$). The i-CAT Next Generation[®] and standard resolution MSCT demonstrated significant differences for all morphometric parameters (except for BS/TV and DA). These morphometric results were completely in line with the visual inspection of the structural pattern.

Despite the overestimation in bone quantity, the alveolar network remained similar between the ProMax 3D Max[®], NewTom GiANO[®], Cranex 3D[®], 3D Accuitomo 170[®] and Carestream 9300[®] and reference method micro-CT. In contrast, the Scanora 3D[®], i-CAT Next Generation[®],

standard and high-resolution MSCT protocol showed a deviant alveolar network. These machines had a clinical scanning protocol with a lower resolution and larger FOV, which could explain its suboptimal performance. Studies on the effects of scanning resolution on morphometric indices have indicated that resolution dependency is especially manifested in the trabecular thickness parameter (Tb.Th) (Pauwels, Faruangsang, Charoenkarn, Ngonphloy, & Panmekiate, 2015). Trabeculae that are thin in respect to the image resolution can either appear thicker and smeared out or at a certain level completely disappear under the influence of the partial volume effect (Kothari et al., 1998). Both situations will have a large impact on the estimation of the bone quantity, but only the latter will affect the structural pattern. These results correspond with previous studies that investigated the use of morphometric parameters in evaluating trabecular structure on both *in vitro* as *in vivo* CBCT scans (Ho et al., 2013; Huang et al., 2014; Ibrahim et al., 2013; Kim et al., 2015; Klintström et al., 2014; Panmekiate et al., 2015; Parsa et al., 2015; Van Dessel et al., 2013, 2016). Yet there are important differences. Most of these studies only reported the most common morphometric indices: bone volume fraction (BV/TV), trabecular thickness (Tb.Th), trabecular separation (Tb.Sp) and trabecular number (Tb.N), and therefore provided limited information on the general trabecular structure. The interpretation of these quantitative values remained even more limited without visual information on the bone pattern in a selected implant region. It is after all possible that structural differences manifest themselves only in a specific part of the selected region, but that these values are averaged out over the whole implant site and therefore do not indicate any problems. Highlighting the importance of comparison of the 3D trabecular network using colour-maps. Alveolar bone evaluation was largely neglected and structural parameters were only calculated on either edentulous bone samples or on trephine biopsies. While in the majority of the implant cases the tooth still needs to be extracted. High Pearson correlations were found between CBCT and micro-CT morphometric parameters. However, a high Pearson correlation does not mean that the tested technique is a reliable assessment tool compared to the reference method. A more suited reliability measure is the intraclass correlation coefficient (ICC), as calculated in the present study.

Furthermore, it is important to note that there are considerable differences between reliability and agreement measures (de Vet, Terwee, Knol, & Bouter, 2006). Reliability gives us an idea on how well the parameters can be distinguished from each other despite the measurement errors. The accuracy is more related to the agreement between repeated measurements and therefore depends on the variability between the bone samples. Both need to be sufficiently high before this method can be introduced as an additional clinical measure.

A persistent obstacle in comparing various scanners is the acquisition of standardised images. Manual VOI selection on the individual images can introduce inter- and intraobserver variability that may be of the same order of magnitude as the parameter to be quantified. This variability

affects the reproducibility of the measurements and undermines the significance of the conclusions derived from them. The current study relied on a fully automated and observer independent spatial alignment of the alveolar network, ensuring that morphometric parameters could be obtained from exactly the same VOI.

In order to calculate the structural indices, the selected VOI must be converted to a binary image. Besides the registration step, also this segmentation process also has a significant impact on the reliability of the structural parameters. Different threshold techniques may lead to diverse binarised bone structures which manifests itself in distinct morphometric values. To avoid variability in segmentation, a computer-aided adaptive threshold was used as this technique showed to give the best agreement with the real situation on low-resolution images (Nackaerts et al., 2015). This automated registration and adaptive threshold procedures can facilitate the incorporation of objective bone quality classification in the clinical practice and standardisation across studies.

The present study has some limitations before the analysis method can be translated to the clinical practice. First, image quality was not assessed, but optimised through selection of the clinical scanning protocol with the highest resolution for each scanning device. In clinical situations often scan protocols with larger FOV and accompanying lower resolution are required. Further studies are needed to assess the influence of exposures settings on morphometric calculations in different scanners. Secondly, the present research involved an *in vitro* assessment. The impact of surrounding soft tissue, tongue, spine and possible movement during scanning were not taken into account. This may lead to an overestimation of the image quality compared to *in vivo* clinical scans. Finally, the relation between morphometric CBCT parameters and implant survival rate should be further investigated to confirm its clinical relevance.

3.6 Conclusions

Current results indicate that morphometric measurements by most CBCT machines and high-resolution MSCT are reliable, even though they overestimate the bone quantity compared to the gold standard micro-CT. The structural pattern of the alveolar bone, as second important factor of the bone quality, remains similar for the CBCT machines with the highest resolution. Quantitative morphometric evaluation combined with a 3D network visualisation can be a useful quantitative technique that may assist in monitoring the alveolar bone remodelling and determining the bone quality of an implant site prior tooth extraction.

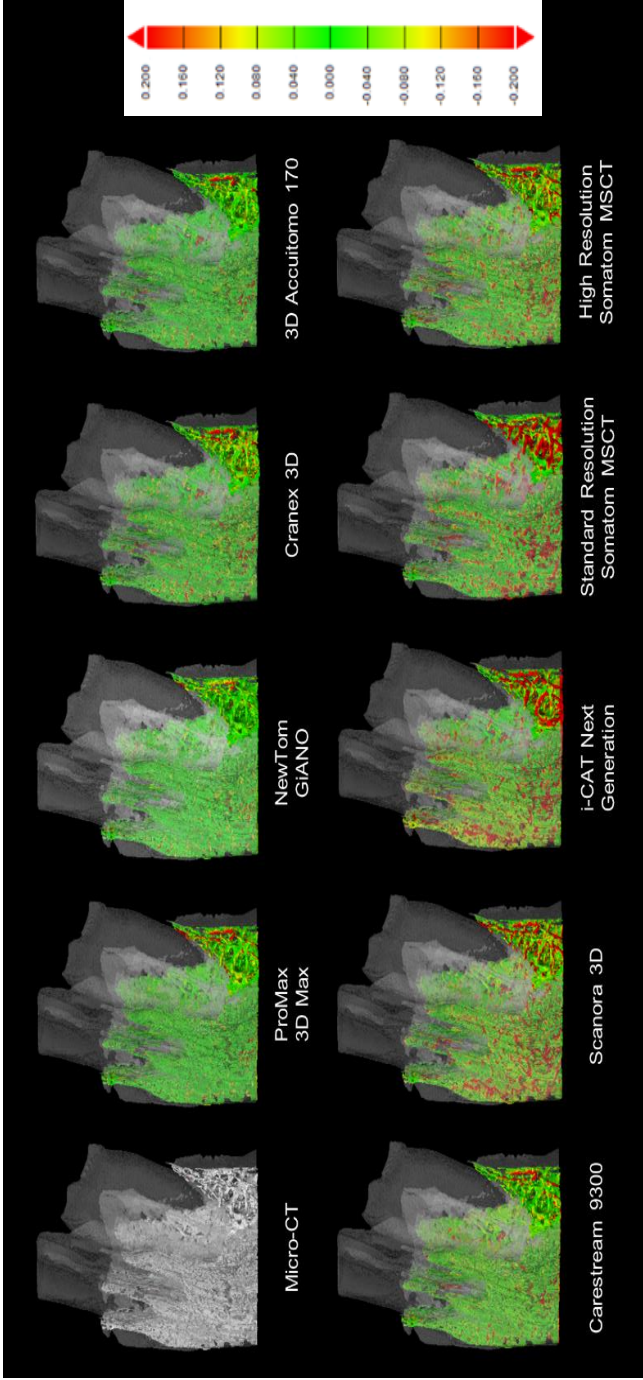


Figure 3.3. Comparison of the structural alveolar bone network between gold standard micro-CT and other scanning devices. The Skyscan 1174[®] micro-CT bone network (in grey) was overlaid on seven spatially aligned cone-beam CT devices (ProMax 3D Max[®], NewTom GiANO[®], Cranex 3D[®], 3D Accutomo 170[®], Carestream 9300[®], Scanora 3D[®] and i-CAT Next generation[®]) and two multi-slice CT (MSCT) protocols with standard (700 μ m) and high-resolution (400 μ m). The linear distance between the micro-CT and the aligned CBCT and MSCT trabecular surface was colour-coded (in mm). The colour pattern was predominantly green (< 80 μ m trabecular radius) for ProMax 3D Max[®], NewTom GiANO[®], Cranex 3D[®], 3D Accutomo 170[®] and Carestream 9300[®]. The Scanora 3D[®], i-CAT Next Generation[®], standard and high-resolution MSCT displayed more yellow – red regions (> 80 μ m trabecular radius) suggesting that the trabecular thickness was more overestimated and revealed a deviating alveolar network (red) compared to the micro-CT reference method.

3.7 References

- Brandi, M. L., & Collin-Osdoby, P. (2006). Vascular Biology and the Skeleton. *Journal of Bone and Mineral Research*, 21(2), 183–192. <https://doi.org/10.1359/JBMR.050917>
- De-Freitas, N., Lima, L., De-Moura, M., Veloso-Guedes, C., Simamoto-Junior, P., & De-Magalhaes, D. (2016). Bisphosphonate treatment and dental implants: A systematic review. *Medicina Oral, Patología Oral y Cirugía Bucal*, 21(5), e644–e651. <https://doi.org/10.4317/medoral.20920>
- de Vet, H. C. W., Terwee, C. B., Knol, D. L., & Bouter, L. M. (2006). When to use agreement versus reliability measures. *Journal of Clinical Epidemiology*, 59(10), 1033–1039. <https://doi.org/10.1016/j.jclinepi.2005.10.015>
- Dempster, D. W., Compston, J. E., Drezner, M. K., Glorieux, F. H., Kanis, J. A., Malluche, H., ... Parfitt, A. M. (2013). Standardized nomenclature, symbols, and units for bone histomorphometry: A 2012 update of the report of the ASBMR Histomorphometry Nomenclature Committee. *Journal of Bone and Mineral Research*, 28(1), 2–17. <https://doi.org/10.1002/jbmr.1805>
- Engelke, W., Lazzarini, M., Stühmer, W., & Beltrán, V. (2015). Support Immersion Endoscopy in Post-Extraction Alveolar Bone Chambers: A New Window for Microscopic Bone Imaging In Vivo. *PLOS ONE*, 10(12), e0145767. <https://doi.org/10.1371/journal.pone.0145767>
- Esposito, M., Hirsch, J.-M., Lekholm, U., & Thomsen, P. (1998). Biological factors contributing to failures of osseointegrated oral implants, (II). Etiopathogenesis. *European Journal of Oral Sciences*, 106(3), 721–764. <https://doi.org/10.1046/j.0909-8836..t01-6-.x>
- Faul, F., Erdfelder, E., Lang, A.-G., & Buchner, A. (2007). G*Power 3: A flexible statistical power analysis program for the social, behavioral, and biomedical sciences. *Behavior Research Methods*, 39(2), 175–191. <https://doi.org/10.3758/BF03193146>
- Fazzalari, N. L., & Parkinson, I. H. (1996). Fractal dimension and architecture of trabecular bone. *The Journal of Pathology*, 178(1), 100–105. [https://doi.org/10.1002/\(SICI\)1096-](https://doi.org/10.1002/(SICI)1096-)

9896(199601)178:1<100::AID-PATH429>3.0.CO;2-K

- Gerber, H., & Ferrara, N. (2000). Angiogenesis and Bone Growth. *Trends in Cardiovascular Medicine*, 10(5), 223–228. [https://doi.org/10.1016/S1050-1738\(00\)00074-8](https://doi.org/10.1016/S1050-1738(00)00074-8)
- Goiato, M. C., dos Santos, D. M., Santiago, J. F. J., Moreno, A., & Pellizzer, E. P. (2014). Longevity of dental implants in type IV bone: a systematic review. *International Journal of Oral and Maxillofacial Surgery*, 43(9), 1108–1116. <https://doi.org/10.1016/j.ijom.2014.02.016>
- He, J., Zhao, B., Deng, C., Shang, D., & Zhang, C. (2015). Assessment of Implant Cumulative Survival Rates in Sites with Different Bone Density and Related Prognostic Factors: An 8-Year Retrospective Study of 2,684 Implants. *The International Journal of Oral & Maxillofacial Implants*, 30(2), 360–371. <https://doi.org/10.11607/jomi.3580>
- Hildebrand, T., & Rüegsegger, P. (1997). Quantification of Bone Microarchitecture with the Structure Model Index. *Computer Methods in Biomechanics and Biomedical Engineering*, 1(1), 15–23. <https://doi.org/10.1080/01495739708936692>
- Ho, J.-T., Wu, J., Huang, H.-L., Chen, M. Y., Fuh, L.-J., & Hsu, J.-T. (2013). Trabecular bone structural parameters evaluated using dental cone-beam computed tomography: cellular synthetic bones. *BioMedical Engineering OnLine*, 12(1), 115. <https://doi.org/10.1186/1475-925X-12-115>
- Huang, Y., Van Dessel, J., Depypere, M., EzEldeen, M., Iliescu, A. A., Dos Santos, E., ... Jacobs, R. (2014). Validating cone-beam computed tomography for peri-implant bone morphometric analysis. *Bone Research*, 2(1), 103–109. <https://doi.org/10.1038/boneres.2014.10>
- Ibrahim, N., Parsa, A., Hassan, B., van der Stelt, P., Aartman, I. H. A., & Wismeijer, D. (2014). Accuracy of trabecular bone microstructural measurement at planned dental implant sites using cone-beam CT datasets. *Clinical Oral Implants Research*, 25(8), 941–945. <https://doi.org/10.1111/clr.12163>
- Ibrahim, N., Parsa, A., Hassan, B., van der Stelt, P., & Wismeijer, D. (2013). Diagnostic imaging of trabecular bone microstructure for oral implants: a literature review.

- Dentomaxillofacial Radiology*, 42(3), 20120075. <https://doi.org/10.1259/dmfr.20120075>
- Ihde, S., Kopp, S., & Maier, T. (2009). Comparison of implant survival with implants placed in acceptable and compromised bone: a literature review. *Journal of Maxillofacial and Oral Surgery*, 8(1), 1–7. <https://doi.org/10.1007/s12663-009-0001-3>
- Kim, J.-E., Yi, W.-J., Heo, M.-S., Lee, S.-S., Choi, S.-C., & Huh, K.-H. (2015). Three-dimensional evaluation of human jaw bone microarchitecture: correlation between the microarchitectural parameters of cone beam computed tomography and micro-computer tomography. *Oral Surgery, Oral Medicine, Oral Pathology and Oral Radiology*, 120(6), 762–770. <https://doi.org/10.1016/j.oooo.2015.08.022>
- Klintström, E., Smedby, Ö., Klintström, B., Brismar, T. B., & Moreno, R. (2014). Trabecular bone histomorphometric measurements and contrast-to-noise ratio in CBCT. *Dentomaxillofacial Radiology*, 43(8), 20140196. <https://doi.org/10.1259/dmfr.20140196>
- Kothari, M., Keaveny, T. M., Lin, J. C., Newitt, D. C., Genant, H. K., & Majumdar, S. (1998). Impact of Spatial Resolution on the Prediction of Trabecular Architecture Parameters. *Bone*, 22(5), 437–443. [https://doi.org/10.1016/S8756-3282\(98\)00031-3](https://doi.org/10.1016/S8756-3282(98)00031-3)
- Kottner, J., Audigé, L., Brorson, S., Donner, A., Gajewski, B. J., Hróbjartsson, A., ... Streiner, D. L. (2011). Guidelines for Reporting Reliability and Agreement Studies (GRRAS) were proposed. *Journal of Clinical Epidemiology*, 64(1), 96–106. <https://doi.org/10.1016/j.jclinepi.2010.03.002>
- Lekholm, U., & Zarb, G. (1985). Patient selection and preparation. In P.-I. Brånemark, G. A. Zarb, & T. Albrektsson (Eds.), *Tissue Integrated Prostheses: Osseointegration in Clinical Dentistry*. Chicago, IL: Quintessence.
- Lindh, C., Petersson, A., & Rohlin, M. (1996). Assessment of the trabecular pattern before endosseous implant treatment: Diagnostic outcome of periapical radiography in the mandible. *Oral Surgery, Oral Medicine, Oral Pathology, Oral Radiology, and Endodontology*, 82(3), 335–343. [https://doi.org/10.1016/S1079-2104\(96\)80363-5](https://doi.org/10.1016/S1079-2104(96)80363-5)
- Link, T. M. (2008). Structure Analysis Using High-Resolution Imaging Techniques. In A. L. Baert, M. Knauth, K. Sartor, & S. Grampp (Eds.), *Radiology of osteoporosis* (2nd ed).

Berlin: Springer.

- Maes, F., Collignon, A., Vandermeulen, D., Marchal, G., & Suetens, P. (1997). Multimodality image registration by maximization of mutual information. *IEEE Transactions on Medical Imaging*, 16(2), 187–198. <https://doi.org/10.1109/42.563664>
- Mamalis, A. A., & Cochran, D. L. (2013). The Role of Hypoxia in the Regulation of Osteogenesis and Angiogenesis Coupling in Intraoral Regenerative Procedures: A Review of the Literature. *The International Journal of Periodontics and Restorative Dentistry*, 33(4), 519–524. <https://doi.org/10.11607/prd.0868>
- Misch, C. E. (1990). Density of bone: effect on treatment plans, surgical approach, healing, and progressive bone loading. *The International Journal of Oral Implantology: Implantologist*, 6(2), 23–31.
- Monje, A., Chan, H.-L., Galindo-Moreno, P., Elnayef, B., Suarez-Lopez del Amo, F., Wang, F., & Wang, H.-L. (2015). Alveolar Bone Architecture: A Systematic Review and Meta-Analysis. *Journal of Periodontology*, 86(11), 1231–1248. <https://doi.org/10.1902/jop.2015.150263>
- Nackaerts, O., Depypere, M., Zhang, G., Vandenberghe, B., Maes, F., & Jacobs, R. (2015). Segmentation of Trabecular Jaw Bone on Cone Beam CT Datasets. *Clinical Implant Dentistry and Related Research*, 17(6), 1082–1091. <https://doi.org/10.1111/cid.12217>
- Odgaard, A. (1997). Three-dimensional methods for quantification of cancellous bone architecture. *Bone*, 20(4), 315–328. [https://doi.org/10.1016/S8756-3282\(97\)00007-0](https://doi.org/10.1016/S8756-3282(97)00007-0)
- Panmekiate, S., Ngonphloy, N., Charoenkarn, T., Faruangsang, T., & Pauwels, R. (2015). Comparison of mandibular bone microarchitecture between micro-CT and CBCT images. *Dentomaxillofacial Radiology*, 44(5), 20140322. <https://doi.org/10.1259/dmfr.20140322>
- Parsa, A., Ibrahim, N., Hassan, B., van der Stelt, P., & Wismeijer, D. (2015). Bone quality evaluation at dental implant site using multislice CT, micro-CT, and cone beam CT. *Clinical Oral Implants Research*, 26(1), e1–e7. <https://doi.org/10.1111/clr.12315>
- Pauwels, R., Faruangsang, T., Charoenkarn, T., Ngonphloy, N., & Panmekiate, S. (2015). Effect of exposure parameters and voxel size on bone structure analysis in CBCT.

- Dentomaxillofacial Radiology*, 44(8), 20150078. <https://doi.org/10.1259/dmfr.20150078>
- Pauwels, R., Jacobs, R., Singer, S. R., & Mupparapu, M. (2015). CBCT-based bone quality assessment: are Hounsfield units applicable? *Dentomaxillofacial Radiology*, 44(1), 20140238. <https://doi.org/10.1259/dmfr.20140238>
- Quirynen, M., Gijbels, F., & Jacobs, R. (2003). An infected jawbone site compromising successful osseointegration. *Periodontology* 2000, 33(1), 129–144. <https://doi.org/10.1046/j.0906-6713.2002.03311.x>
- Rao, T., & Rao, W. (1999). Bone classification: clinical-histomorphometric comparison. *Clinical Oral Implants Research*, 10(1), 1–7. <https://doi.org/10.1034/j.1600-0501.1999.100101.x>
- Ribeiro-Rotta, R. F., Lindh, C., Pereira, A. C., & Rohlin, M. (2011). Ambiguity in bone tissue characteristics as presented in studies on dental implant planning and placement: a systematic review. *Clinical Oral Implants Research*, 22(8), 789–801. <https://doi.org/10.1111/j.1600-0501.2010.02041.x>
- Ribeiro-Rotta, R. F., Lindh, C., & Rohlin, M. (2007). Efficacy of clinical methods to assess jawbone tissue prior to and during endosseous dental implant placement: a systematic literature review. *The International Journal of Oral & Maxillofac Implants*, 22(2), 289–300.
- Van Dessel, J., Huang, Y., Depypere, M., Rubira-Bullen, I., Maes, F., & Jacobs, R. (2013). A comparative evaluation of cone beam CT and micro-CT on trabecular bone structures in the human mandible. *Dentomaxillofacial Radiology*, 42(8), 20130145. <https://doi.org/10.1259/dmfr.20130145>
- Van Dessel, J., Nicolielo, L. F., Huang, Y., Slagmolen, P., Politis, C., Lambrichts, I., & Jacobs, R. (2016). Quantification of bone quality using different cone beam computed tomography devices: Accuracy assessment for edentulous human mandibles. *European Journal of Oral Implantology*, 9(4), 411–424.
- van Velzen, F. J., Ofec, R., Schulten, E. A., & ten Bruggenkate, C. M. (2015). 10-year survival rate and the incidence of peri-implant disease of 374 titanium dental implants with a SLA surface: a prospective cohort study in 177 fully and partially edentulous patients. *Clinical Oral Implants Research*, 26(10), 1121–1128. <https://doi.org/10.1111/clr.12499>

Yip, J. K., Borrell, L. N., Cho, S.-C., Francisco, H., & Tarnow, D. P. (2012). Association between oral bisphosphonate use and dental implant failure among middle-aged women. *Journal of Clinical Periodontology*, 39(4), 408–414. <https://doi.org/10.1111/j.1600-051X.2012.01854.x>

Chapter 4

Computer-based automatic classification of trabecular bone pattern can assist radiographic bone quality assessment at dental implant site.

This chapter is based on:

Nicolielo, L. F. P., Van Dessel, J., van Lenthe, G. H., Lambrichts, I., & Jacobs, R. (2018). Computer-based automatic classification of trabecular bone pattern can assist radiographic bone quality assessment at dental implant site. *The British Journal of Radiology*, 91(1092), 20180437. <https://doi.org/10.1259/bjr.20180437>

4.1 Abstract

Objectives: To develop and validate an automated classification method that determines the trabecular bone pattern at implant site based on 3D bone morphometric parameters derived from CBCT images.

Methods: Twenty-five human cadaver mandibles were scanned using CBCT clinical scanning protocol. Volumes-of-interest comprising only the trabecular bone of the posterior regions were selected and segmented for 3D morphometric parameters calculation. Three experts rated all bone regions into one of the three trabecular pattern classes (sparse, intermediate and dense) to generate a reference classification. Morphometric parameters were used to automatically classify the trabecular pattern with linear discriminant analysis statistical model. The discriminatory power of each morphometric parameter for automatic classification was indicated and the accuracy compared to the reference classification. Repeated-measures ANOVAs were used to statistically compare morphometric indices between the three classes. Finally, the outcome of the automatic classification was evaluated against a subjective classification performed independently by four different observers.

Results: 86% correct classification was achieved with only structure-related parameters. Cross-validation showed a 79% model prediction accuracy. Bone-volume-fraction had the most discriminatory power in the automatic classification. Trabecular bone patterns could be distinguished based on most morphometric parameters, except for trabecular-thickness and degree-of-anisotropy. The inter-observer agreement between the subjective observers was fair (0.25), while the test-retest agreement was moderate (0.46). In comparison with the reference standard, the overall agreement was moderate (0.44).

Conclusion: Automatic classification performed better than subjective classification with a prediction model comprising only structure-related parameters.

Advances in knowledge: Computer-aided trabecular bone pattern assessment based on morphometric parameters could assist objectivity in clinical bone quality classification.

4.2 Introduction

Bone quality assessment prior implant placement is an important step to predict treatment prognosis. For many years, the ideal implant site was solely associated with primary implant stability linked to bone density and quantity. Thanks to the continuous improvement of implants' surface and a better understanding of implant osseointegration mechanism, vascularisation of alveolar bone has become an important factor related to long-term implant survival. While a well-vascularised bone can promote faster peri-implant healing (Davies, 2003; Laroche, 2002), compact bone with small trabecular spaces and sclerotic areas could indicate poor vascularisation and a higher risk of implant failure (Laroche, 2002; Madrid & Sanz, 2009; Quirynen, Gijbels, & Jacobs, 2003; Simons, De Smit, Duyck, Coucke, & Quirynen, 2015; Trisi, Berardini, Falco, Podaliri Vulpiani, & Perfetti, 2014). Because bone vascularisation cannot be directly assessed, one should look to the medullar area of the bone (Simons et al., 2015).

Between the methods to assess bone quality, radiographic evaluation is certainly an important preoperative tool to assist tactile perception during preparation of implant bed. This evaluation, is frequently based on the subjective assessment of cortical thickness and medullar bone space using two-dimensional (2D) conventional radiographs. Nevertheless, it often leads to discrepancies between clinicians, what in turn makes comparisons across studies difficult (Fu et al., 2017; Ribeiro-Rotta, Lindh, Pereira, & Rohlin, 2011).

As a three-dimensional (3D) structure, bone architecture cannot be fully visualised on conventional 2D radiographs (Bouxsein et al., 2010). With the rapid advancement of radiographic technology, Cone-Beam Computed Tomography (CBCT) scans became an attractive method for implant planning, especially in cases of complex anatomy or risk factor. The full potential of the obtained 3D information, however, is in most cases not entirely exploited and bone quality radiographic evaluation often remains based on subjective 2D measurements and visual judgement. Recently, morphometric bone parameters derived from CBCT scans have been validated for standardised trabecular structure assessment by comparison with the gold standard histomorphometry (Huang et al., 2014), micro-CT (J.-E. Kim et al., 2015; Van Dessel et al., 2017, 2016) and clinical multi-slice CT alternative (Van Dessel et al., 2017, 2016). High-resolution CBCT scans showed accurate visualisation of the trabecular network in the mandible (Van Dessel et al., 2017, 2016). These morphometric bone parameters can be automatically and operator-independent calculated and comprise relevant aspects for bone quality evaluation - namely quantity and structure - which are difficult to visually evaluate.

Therefore, the aim of the present study was to develop and validate an automatic method to assist bone quality classification at the implant site based on 3D morphometric characteristics

of the trabecular bone. The efficiency of this computer-based classification was then compared with the traditional subjective evaluation performed by oral radiologists.

4.3 Materials and methods

4.3.1 Data acquisition

Twenty-five Caucasian adult human mandibles (16 males and 9 females) were obtained from the Anatomy Department of the University of Hasselt, Diepenbeek, Belgium and approved for research by the medical bioethics committee of the KU Leuven, Leuven, Belgium (s55619). Each mandible was scanned with a NewTom VGi evo CBCT (QR Verona, Verona, Italy) using a clinical scanning protocol (125 μm) containing the entire mandible in the field of view (FOV: 10 cm x 5 cm) and with the occlusal plane parallel to the floor. The tube voltage was fixed at 110 kV, while the tube current was modulated to reduce the dose yet maintain the image quality. Anatomical structures (tongue and skin) made from Mix-D were placed around the mandible to simulate soft tissue radiation attenuation (Oenning et al., 2018).

4.3.2 Image processing and quantification of morphometric parameters

The DICOM images with isotropic voxel size of 125 μm were imported in CT-Analyser (Bruker, Kontich, Belgium) where after the posterior part of the mandible was divided per tooth position (premolar and molar region), resulting in a total of 100 bone regions with an average volume of $1507.7 \pm 821.7 \text{ mm}^3$. Within each region, the trabecular bone in the consecutive slices was segmented using the computer-suggested bone threshold and morphometric parameters were calculated following a previously described methodology (Van Dessel et al., 2017, 2016). *Figure 4.1* shows an overview of the image processing steps prior morphometric analysis implemented in CT-Analyser. Routinely used morphometric indices were calculated following the recommendations of the American Society for Bone and Mineral Research (Dempster et al., 2013). Bone volume fraction (BV/TV in %) is seen as the main parameter to evaluate bone quantity as it indicates the proportion of mineralised bone tissue. Bone surface density (BS/TV in mm^2/mm^3) and the ratio of bone surface to volume (BS/BV in mm^2/mm^3) are useful parameters for characterising the complexity of bone structures. Parameters such as trabecular separation (Tb.Sp in mm), trabecular thickness (Tb.Th in mm) and trabecular number (Tb.N in mm^{-1}) provide information on the spatial distribution of the bone, which enables the contribution of microstructure to bone strength to be assessed (Klintström et al., 2018). Connectivity density (Conn.Dn in mm^{-3}) represents the trabeculae connections divided by the total volume. Trabecular pattern factor (Tb.Pf in mm^{-1}) calculates an index of relative

connectivity or isolated disconnected structures of the total bone surface. Structure model index (SMI) indicates the relative prevalence of rod-like and plate-like trabeculae. An ideal trabecular plate, cylinder and sphere have SMI values of respectively 0, 3 and 4. Negative values indicate a more concave or closed structure; positive values indicate a more convex and open structure. Fractal dimension (FD) is an indicator of trabecular complexity. Higher the FD, the more the morphological complexity at the ultrastructural level (Zeytinoğlu, İlhan, Dündar, & Boyacıoğlu, 2015). Degree of anisotropy (DA) describes the preferential alignment of the bone trabecular structure. Values higher than one represents a highly-oriented structure whereas equals to one represents an isotropic structure without a preferred orientation (Bruker MicroCT, 2015).

4.3.3 Automatic trabecular bone classification

Three observers with expertise in oral implant and dentomaxillofacial radiology (L.F.P.N., J.V.D. and R.J.) classified together the 100 bone regions in three classes: an sparse class was assigned to regions with very large medullar spaces containing few trabeculae (hollow bone); intermediate was given to regions with medium to large trabecular spaces; and dense regions were characterised by very close trabecular spaces (*Figure 4.2*). Classifications were based on visualisation of the full CBCT images of each tooth region, previously selected for image processing. The images were visualised in a dark room on a radiological screen Barco MDRC-2221 (Barco, Kortrijk, Belgium) with a 54 cm diagonally viewable size and 1600 x 1200 pixels. The experts were able to deliberately scroll through the slices until a consensus was reached. This joint classification served as reference standard to feed into a Linear Discriminant Analysis (LDA). This statistical model searches for a linear combination of morphometric parameters that best separates the trabecular bone in three types. The strength of the canonical correlation (cc) in the structure matrix was used to indicate the discriminatory power of each morphometric parameter for trabecular pattern classification. A repeated-measures ANOVA was used to compare morphometric indices between the three classes. Mean and standard deviations of each parameters for the three trabecular pattern classes were reported. Leave-one-out cross-validation was used to assess model prediction performance and how the results of LDA will generalise to an independent dataset. All statistical tests were performed in IBM SPSS Statistics (IBM corp., New York, USA).

4.3.4 Subjective trabecular bone classification

After reading a printed instruction, four observers with four to six years' experience in dentomaxillofacial radiology visually classified the trabecular structure using the same methodology described for the experts. Additionally, five randomly selected scans were duplicated to assess misclassification of the same region. Evaluators were able to use the CBCT scan as much as necessary to make a conclusive decision. One month later, trabecular pattern classification was repeated, and the Cohen's Kappa was calculated for each observer to assess the general test-retest reliability. The inter-rater reliability was assessed by Fleiss Kappa and the validity of the subjective classification for each examiner was assessed by comparing them with the reference standard classification. Finally, their ratings were compared with the computer-based classification.

4.4 Results

4.4.1 Automatic trabecular bone classification

The overall correct classification was 83% for quantity-, 86% for structure-related parameters and 84% for the parameters combined (*Table 4.1*). The highest accuracy was achieved for the sparse bone class (100%), followed by the intermediate (92%) and dense bone (74%). Cross-validation showed a 79% model prediction accuracy. Morphometric parameters were ranked according to distinctive importance: BV/TV (cc = 0.74), Tb.N (cc = 0.71), Tb.Pf (cc = -0.65), FD (cc = 0.65), Tb.Sp (cc = 0.61), SMI (cc = 0.60), BS/TV (cc = -0.59), Conn.Dn (cc = -0.27), BS/BV (cc = 0.15), Tb.Th (cc = -0.07) and DA (cc = -0.04). Variables with stronger canonical correlations can be considered more important for the performance of the given discriminant model. BV/TV accounted for 100% of variance within the quantity-related model. *Figure 4.3* shows differentiating bone type limits with 95% confidence intervals. There were statistically significant differences ($P < 0.05$) between the three classes for all bone parameters, except for trabecular thickness (Tb.Th) and degree of anisotropy (DA). These cut-off values differentiated between visual distinctive sparse, intermediate and dense bone regions. Sparse bone regions were associated with a lower bone volume density (\downarrow BV/TV) a lower bone surface density (\downarrow BS/TV) but higher specific surface (\uparrow BS/BV), described by a decreased trabecular complexity (\uparrow SMI; \downarrow FD), wide-spaced (\uparrow Tb.Sp; \downarrow Tb.N) and less connected trabeculae (\uparrow Tb.Pf; \downarrow Conn.Dn), while for dense bone it was the exact opposite for all parameters.

4.4.2 Subjective trabecular bone classification

The inter-observer agreement between the four observers was 0.25 (fair), while the test-retest agreement was 0.46 (ranging from fair 0.21 to moderate 0.57). In comparison with the reference standard, the overall agreement was 0.44 (ranging from fair 0.24 to moderate 0.60).

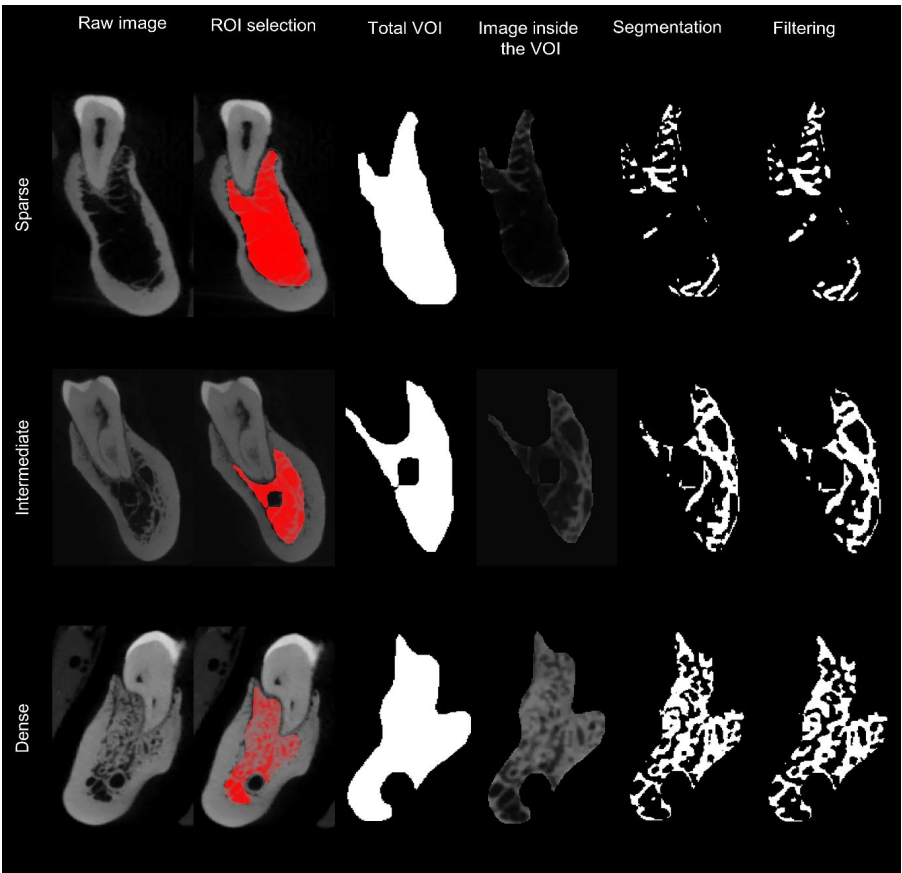


Figure 4.1. Overview of the image processing steps for each class of trabecular pattern. Only the trabecular bone, excluding teeth root and alveolar canal, was selected in the coronal view (Second column) and saved as a volume of interest (Third column). Trabecular bone was segmented based on histogram selection (Fifth column). The computer-suggested threshold value was visually reassessed in order to give a perfect overlap with the original image. The segmented images were subsequently smoothed using a Gaussian filter with a radius size of one voxel (125 μm³) (Sixth column).

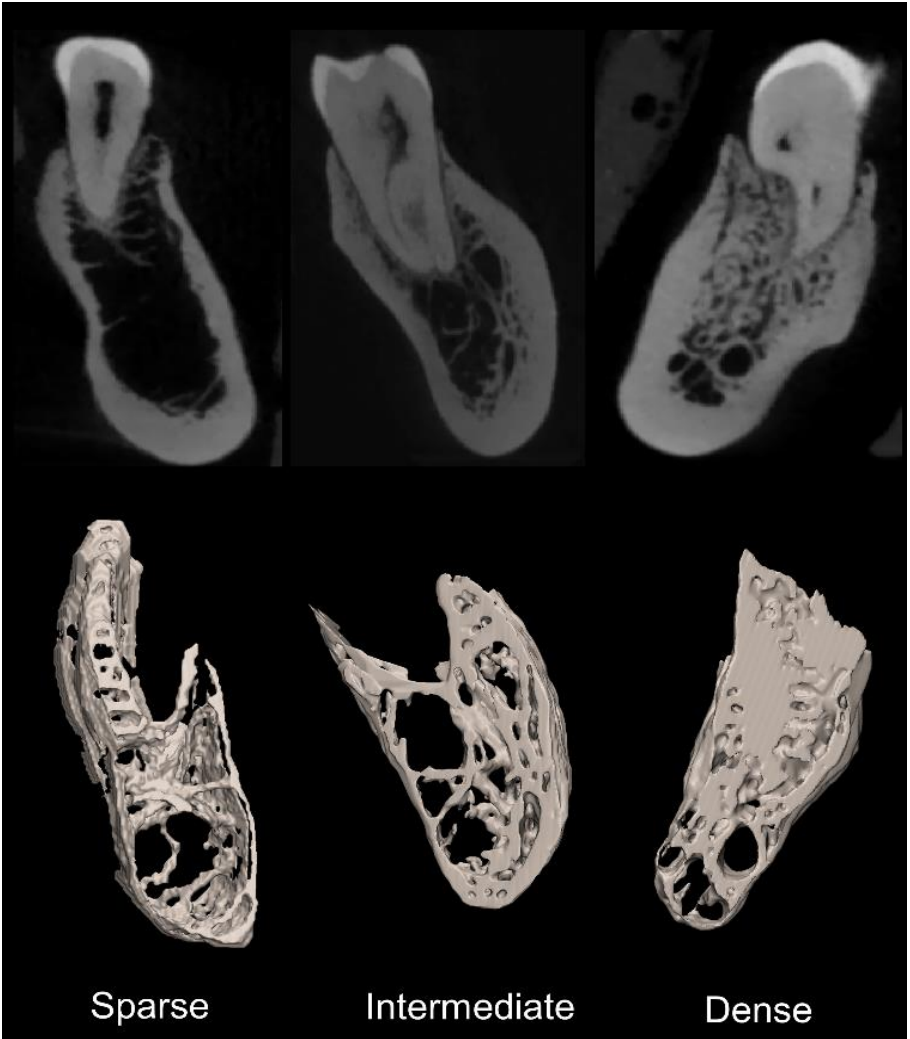


Figure 4.2. *Three-dimensional models of three classes of trabecular pattern in the posterior regions of the mandible.*

Table 4.1. Prediction results of the trabecular pattern classification using linear discriminant analysis.

	Predicted group membership (%)		
Quantity-related parameters	Sparse (n = 11)	Intermediate (n = 51)	Dense (n = 38)
Sparse	90.9	9.1	0
Intermediate	2.0	93.7	4.3
Dense	0	36.8	63.2
Structure-related parameters	Sparse (n = 11)	Intermediate (n = 51)	Dense (n = 38)
Sparse	100.0	0	0
Intermediate	3.9	92.2	3.9
Dense	0	26.3	73.7
All parameters combined	Sparse (n = 11)	Intermediate (n = 51)	Dense (n = 38)
Sparse	90.9	9.1	0
Intermediate	3.9	90.2	5.9
Dense	0	26.3	73.7

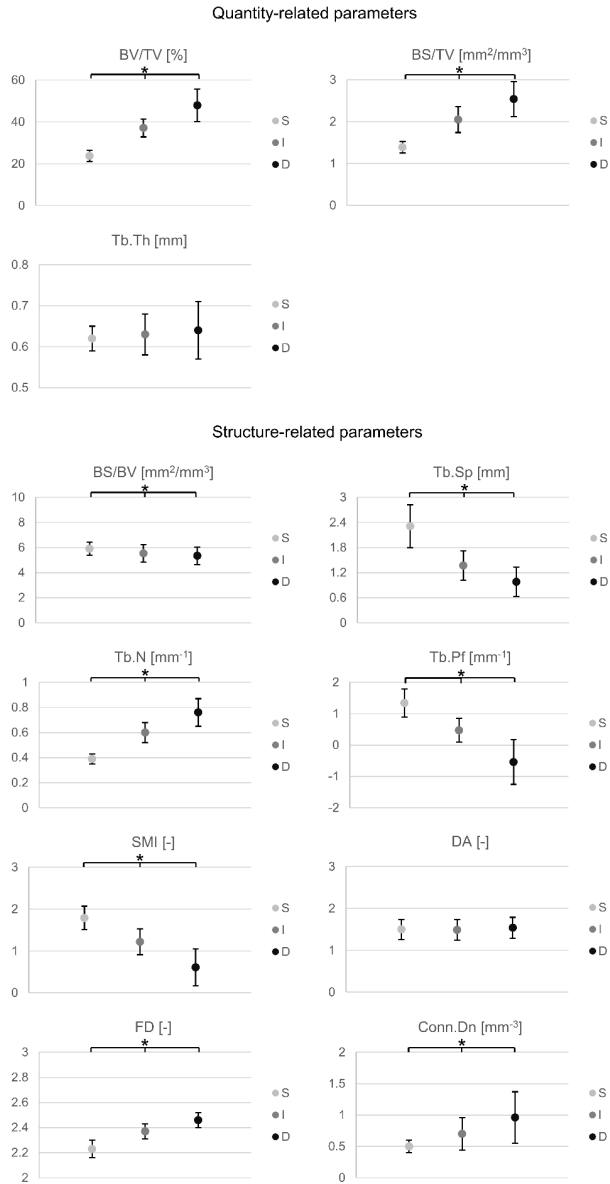


Figure 4.3. Mean and standard deviations of quantity- and structure-related morphometric parameters for the three trabecular pattern classes. The classes were statistically significant different for all parameters besides Tb.Th and DA. S: sparse; I: intermediate, D: dense.

4.5 Discussion

Although multiple subjective classification schemes and analytical methods exist to evaluate bone quality prior to implant surgery, none of these methods provide a standardised follow-up nor are they validated as prognostic test (Lindh, Petersson, & Rohlin, 1996; Ribeiro-Rotta et al., 2011; Ribeiro-Rotta, Lindh, & Rohlin, 2007). In the present study, an automatic computer-aided method was used to assist classification of trabecular bone pattern based on 3D morphometric parameters derived from CBCT images of alveolar regions. This computer-based process showed a two-fold higher accuracy in predicting trabecular bone pattern compared to a visual classification performed by oral radiologists. Computer-aided applications of structural pattern recognition are already often used in clinical radiological applications, such as screening for cervical cancer, breast tumors and cardiovascular diseases (Shameer, Johnson, Glicksberg, Dudley, & Sengupta, 2018; Torheim et al., 2017; Yassin, Omran, El Houby, & Allam, 2018). Pairing machine learning expertise with a radiologist, whether it is through an imaging platform, could help prediction of bone quality, augment the consenting process with higher expected implant treatment outcome, and reduce the cost of multiple expert diagnostic opinions.

Evidence concerning accuracy of currently used radiographic methods for bone quality assessment is scarce. Previous studies have classified bone in two, three or four bone types suggesting that there is no overall consensus in how many classes bone quality should be distinguished in order to help predicting implant survival (Lindh, Oliveira, Leles, do Carmo Matias Freire, & Ribeiro-Rotta, 2014; Ribeiro-Rotta et al., 2011). From a clinical point of view, oral implant surgeons want to avoid extremities. Sparse bone may hamper primary stability (Merheb et al., 2016), while compact bone with reduction of trabecular spaces may show impaired vascularization (Mikami, Miake, Bologna-Molina, & Takeda, 2016). The ideal bone for implant placement lies somewhere in between these two types. This intermediate type is, however, more difficult to visually differentiate (Fu et al., 2017; Norton & Gamble, 2001; Rao & Rao, 1999), especially if trabecular bone structure is not homogeneous in a particular dental implant site. In this context, Lindh et al. (1996) showed that 2D radiographic assessment of trabecular pattern in the jaw bone was more reliable when using a classification with three classes than with four classes from Lekholm and Zarb index, which is based on schematic drawings of homogeneous trabecular network (Lindh et al., 1996). This complexity becomes even higher when the bone structure is analysed in 3D. Differently from 2D images, 3D visualisation may display an association of more than one trabecular pattern in a particular implant region that will decrease pattern recognition and variable interaction. Consequently, our subjective evaluation showed lower reliability when compared with traditional 2D evaluation (Lindh et al., 1996).

Since clinical quantification of morphometric parameters became feasible with an adequate CBCT scanner and protocol (Panmekiate, Ngonphloy, Charoenkarn, Faruangsang, & Pauwels, 2015; Van Dessel et al., 2017, 2016), the 3D information of the trabecular bone structure could help objective classification of bone type. The present results indicate that the trabecular regions could be automatically categorized by specific morphometric parameters. Structural parameters (Tb.N, Tb.Sp, FD, Tb.Pf, SMI, Conn.Dn, DA, BS/BV) showed to be as important as quantity-related parameters (BV/TV, BS/TV, Tb.Th) for the bone type prediction (Van Dessel et al., 2016). However, the classification of sparse bone type reached 100% when considering structure-related parameters alone. The most difficult class to predict was dense bone, even quantity-related parameters (63%) were not able to estimate it better the correct class compared to structure-related parameters (74%). Still, all parameters combined did not performed better than structural parameters alone. Although more parameters give more information about the data, a complex model with more parameters can cause overfitting due to high variance of the parameters (Claeskens & Hjort, 2008).

BV/TV accounted for 100% of the variance within the prediction model. This can be explained by the fact that Tb.Th was not different between the bone types (*Figure 4.3*) and BS/TV that is closely linked with BV/TV (Parkinson & Fazzalari, 2003). Also, some structural-related parameters contributed little to the class prediction, including connectivity density (Conn.Dn.), ratio of bone surface to volume (BS/BV) and degree of anisotropy (DA). Interestingly, these parameters have been shown to be closely related to mechanical bone properties (Kersh et al., 2013; D.-G. Kim, Shertok, Ching Tee, & Yeni, 2011; Oravec, Kim, Flynn, & Yeni, 2018), which may indicate that more sparse structures are not always associated with poor mechanical properties and vice-versa. This is in agreement with previous studies on *in vivo* and *ex vivo* jaw bone biopsies that found a dependency of bone quality on BV/TV, Tb.Pf, Tb.N Tb.Sp and SMI and a less influence from Tb.Th (Lee, Kim, & Yun, 2017; Ribeiro-Rotta, de Oliveira, Dias, Lindh, & Leles, 2014).

Computer algorithms make use of the various parameters to find high dimensional interactions between multiple data points, that can provide the optimal solution (Murphy, 2012). These algorithms work as statistical models recognising subgroups with same patterns in the full data (clustering) or using a specific clinical information to make predictions (supervised learning) (Wang & Summers, 2012). The LDA belongs to the latter and builds a predictive model based on linear combinations of features of a known dataset that will be used to maximise separation between classes. Among other classification methods, such as logistic regression, LDA is more robust because requires continuous and normally distributed data, while performing better with small sample sizes.

Despite the clear advantage of computer-aided classifications, there are however also a number of limitations. First, LDA techniques require a gold standard set of predictor variables

to accurately classify groups. Currently, no objective ground truth in bone quality type exists. We have opted for a classification generated by experts' combined responses, which may serve as reasonable reference standard (Alonso, Vasconcelos, Lopes, Watanabe, & Freitas, 2016; Hripcsak & Wilcox, 2002). Secondly, the groups were unequal in sample size, of the 100 bone regions only 11 sparse zones were found. LDA priors were therefore based on group sizes instead of equal groups. Future studies with larger sample sizes may help overcome this problem. Thirdly, bone mineral density is also an important parameter to determine bone strength and quality. This index could not be taken into account, as grey values on CBCT do not correspond with multi-slice CT derived Hounsfield units needed to predict bone mineral density (Nackaerts et al., 2011; Pauwels et al., 2013). Lastly, although several variables related to bone structure and quantity appeared as significant predictors in LDA model, future work is needed to establish their direct clinical impact in implant treatment outcome.

The present method was able to remove the subjectivity in evaluating trabecular pattern using computer-aided image processing and categorisation using morphometric bone parameters. This could be a step forward in the development of a more predictable and standardised bone quality evaluation techniques, which eventually could be incorporated in implant planning software's and in the computer-aided design and manufacture of implant prosthetics.

4.6 References

- Alonso, M. B. C. C., Vasconcelos, T. V., Lopes, L. J., Watanabe, P. C. A., & Freitas, D. Q. (2016). Validation of cone-beam computed tomography as a predictor of osteoporosis using the Klemetti classification. *Brazilian Oral Research*, 30(1). <https://doi.org/10.1590/1807-3107BOR-2016.vol30.0073>
- Bouxsein, M. L., Boyd, S. K., Christiansen, B. A., Guldberg, R. E., Jepsen, K. J., & Müller, R. (2010). Guidelines for assessment of bone microstructure in rodents using micro-computed tomography. *Journal of Bone and Mineral Research*, 25(7), 1468–1486. <https://doi.org/10.1002/jbmr.141>
- Bruker MicroCT. (2015). Bruker Micro-CT Academy. *Bruker Micro-CT Academy*, 2(11), 1–2.
- Claeskens, G., & Hjort, N. L. (2008). *Model selection and model averaging*. Cambridge: Cambridge University Press.
- Davies, J. (2003). Understanding peri-implant endosseous healing. *Journal of Dental Education*, 67(8), 932–949.
- Dempster, D. W., Compston, J. E., Drezner, M. K., Glorieux, F. H., Kanis, J. A., Malluche, H., ... Parfitt, A. M. (2013). Standardized nomenclature, symbols, and units for bone histomorphometry: A 2012 update of the report of the ASBMR Histomorphometry Nomenclature Committee. *Journal of Bone and Mineral Research*, 28(1), 2–17. <https://doi.org/10.1002/jbmr.1805>
- Fu, M.-W., Fu, E., Lin, F.-G., Chang, W.-J., Hsieh, Y.-D., & Shen, E.-C. (2017). Correlation Between Resonance Frequency Analysis and Bone Quality Assessments at Dental Implant Recipient Sites. *The International Journal of Oral & Maxillofacial Implants*, 32(1), 180–187. <https://doi.org/10.11607/jomi.4684>
- Hripcsak, G., & Wilcox, A. (2002). Reference Standards, Judges, and Comparison Subjects: Roles for Experts in Evaluating System Performance. *Journal of the American Medical Informatics Association*, 9(1), 1–15. <https://doi.org/10.1136/jamia.2002.0090001>
- Huang, Y., Van Dessel, J., Depypere, M., EzEldeen, M., Iliescu, A. A., Dos Santos, E., ...

- Jacobs, R. (2014). Validating cone-beam computed tomography for peri-implant bone morphometric analysis. *Bone Research*, 2(1), 103–109. <https://doi.org/10.1038/boneres.2014.10>
- Kersh, M. E., Zysset, P. K., Pahr, D. H., Wolfram, U., Larsson, D., & Pandy, M. G. (2013). Measurement of structural anisotropy in femoral trabecular bone using clinical-resolution CT images. *Journal of Biomechanics*, 46(15), 2659–2666. <https://doi.org/10.1016/j.jbiomech.2013.07.047>
- Kim, D.-G., Shertok, D., Ching Tee, B., & Yeni, Y. N. (2011). Variability of tissue mineral density can determine physiological creep of human vertebral cancellous bone. *Journal of Biomechanics*, 44(9), 1660–1665. <https://doi.org/10.1016/j.jbiomech.2011.03.025>
- Kim, J.-E., Yi, W.-J., Heo, M.-S., Lee, S.-S., Choi, S.-C., & Huh, K.-H. (2015). Three-dimensional evaluation of human jaw bone microarchitecture: correlation between the microarchitectural parameters of cone beam computed tomography and micro-computer tomography. *Oral Surgery, Oral Medicine, Oral Pathology and Oral Radiology*, 120(6), 762–770. <https://doi.org/10.1016/j.oooo.2015.08.022>
- Klintström, E., Klintström, B., Pahr, D., Brismar, T. B., Smedby, Ö., & Moreno, R. (2018). Direct estimation of human trabecular bone stiffness using cone beam computed tomography. *Oral Surgery, Oral Medicine, Oral Pathology and Oral Radiology*, 126(1), 72–82. <https://doi.org/10.1016/j.oooo.2018.03.014>
- Laroche, M. (2002). Intraosseous circulation from physiology to disease. *Joint Bone Spine*, 69(3), 262–269. [https://doi.org/10.1016/S1297-319X\(02\)00391-3](https://doi.org/10.1016/S1297-319X(02)00391-3)
- Lee, J.-H., Kim, H.-J., & Yun, J.-H. (2017). Three-dimensional microstructure of human alveolar trabecular bone: a micro-computed tomography study. *Journal of Periodontal & Implant Science*, 47(1), 20–29. <https://doi.org/10.5051/jpis.2017.47.1.20>
- Lindh, C., Oliveira, G. H. C., Leles, C. R., do Carmo Matias Freire, M., & Ribeiro-Rotta, R. F. (2014). Bone quality assessment in routine dental implant treatment among Brazilian and Swedish specialists. *Clinical Oral Implants Research*, 25(9), 1004–1009. <https://doi.org/10.1111/clr.12221>

- Lindh, C., Petersson, A., & Rohlin, M. (1996). Assessment of the trabecular pattern before endosseous implant treatment: Diagnostic outcome of periapical radiography in the mandible. *Oral Surgery, Oral Medicine, Oral Pathology, Oral Radiology, and Endodontology*, 82(3), 335–343. [https://doi.org/10.1016/S1079-2104\(96\)80363-5](https://doi.org/10.1016/S1079-2104(96)80363-5)
- Madrid, C., & Sanz, M. (2009). What impact do systemically administrated bisphosphonates have on oral implant therapy? A systematic review. *Clinical Oral Implants Research*, 20, 87–95. <https://doi.org/10.1111/j.1600-0501.2009.01772.x>
- Merheb, J., Temmerman, A., Rasmusson, L., Kübler, A., Thor, A., & Quirynen, M. (2016). Influence of Skeletal and Local Bone Density on Dental Implant Stability in Patients with Osteoporosis. *Clinical Implant Dentistry and Related Research*, 18(2), 253–260. <https://doi.org/10.1111/cid.12290>
- Mikami, T., Miake, Y., Bologna-Molina, R., & Takeda, Y. (2016). Ultrastructural Analyses of Alveolar Bone in a Patient With Osteomyelitis Secondary to Osteopetrosis: A Review of the Literature. *Journal of Oral and Maxillofacial Surgery*, 74(8), 1584–1595. <https://doi.org/10.1016/j.joms.2016.02.016>
- Murphy, K. P. (2012). *Machine learning: a probabilistic perspective (adaptive computation and machine learning series)*. New York, NY: The MIT Press.
- Nackaerts, O., Maes, F., Yan, H., Couto Souza, P., Pauwels, R., & Jacobs, R. (2011). Analysis of intensity variability in multislice and cone beam computed tomography. *Clinical Oral Implants Research*, 22(8), 873–879. <https://doi.org/10.1111/j.1600-0501.2010.02076.x>
- Norton, M. R., & Gamble, C. (2001). Bone classification: an objective scale of bone density using the computerized tomography scan. *Clinical Oral Implants Research*, 12(1), 79–84. <https://doi.org/10.1034/j.1600-0501.2001.012001079.x>
- Oenning, A. C., Salmon, B., Vasconcelos, K. de F., Pinheiro Nicolielo, L. F., Lambrichts, I., Sanderink, G., ... Jacobs, R. (2018). DIMITRA paediatric skull phantoms: development of age-specific paediatric models for dentomaxillofacial radiology research. *Dentomaxillofacial Radiology*, 47(3), 20170285. <https://doi.org/10.1259/dmfr.20170285>
- Oravec, D., Kim, W., Flynn, M. J., & Yeni, Y. N. (2018). The relationship of whole human

- vertebral body creep to geometric, microstructural, and material properties. *Journal of Biomechanics*, 73, 92–98. <https://doi.org/10.1016/j.jbiomech.2018.03.021>
- Panmekiate, S., Ngonphloy, N., Charoenkarn, T., Faruangaeng, T., & Pauwels, R. (2015). Comparison of mandibular bone microarchitecture between micro-CT and CBCT images. *Dentomaxillofacial Radiology*, 44(5), 20140322. <https://doi.org/10.1259/dmfr.20140322>
- Parkinson, I. H., & Fazzalari, N. L. (2003). Interrelationships Between Structural Parameters of Cancellous Bone Reveal Accelerated Structural Change at Low Bone Volume. *Journal of Bone and Mineral Research*, 18(12), 2200–2205. <https://doi.org/10.1359/jbmr.2003.18.12.2200>
- Pauwels, R., Nackaerts, O., Bellaiche, N., Stamatakis, H., Tsiklakis, K., Walker, A., ... Horner, K. (2013). Variability of dental cone beam CT grey values for density estimations. *The British Journal of Radiology*, 86(1021), 20120135. <https://doi.org/10.1259/bjr.20120135>
- Quirynen, M., Gijbels, F., & Jacobs, R. (2003). An infected jawbone site compromising successful osseointegration. *Periodontology* 2000, 33(1), 129–144. <https://doi.org/10.1046/j.0906-6713.2002.03311.x>
- Rao, T., & Rao, W. (1999). Bone classification: clinical-histomorphometric comparison. *Clinical Oral Implants Research*, 10(1), 1–7. <https://doi.org/10.1034/j.1600-0501.1999.100101.x>
- Ribeiro-Rotta, R. F., de Oliveira, R. C., Dias, D. R., Lindh, C., & Leles, C. R. (2014). Bone tissue microarchitectural characteristics at dental implant sites part 2: Correlation with bone classification and primary stability. *Clinical Oral Implants Research*, 25(2), e47–e52. <https://doi.org/10.1111/clr.12046>
- Ribeiro-Rotta, R. F., Lindh, C., Pereira, A. C., & Rohlin, M. (2011). Ambiguity in bone tissue characteristics as presented in studies on dental implant planning and placement: a systematic review. *Clinical Oral Implants Research*, 22(8), 789–801. <https://doi.org/10.1111/j.1600-0501.2010.02041.x>
- Ribeiro-Rotta, R. F., Lindh, C., & Rohlin, M. (2007). Efficacy of clinical methods to assess jawbone tissue prior to and during endosseous dental implant placement: a systematic literature review. *The International Journal of Oral & Maxillofac Implants*, 22(2), 289–300.

- Shameer, K., Johnson, K. W., Glicksberg, B. S., Dudley, J. T., & Sengupta, P. P. (2018). Machine learning in cardiovascular medicine: are we there yet? *Heart*, 104(14), 1156–1164. <https://doi.org/10.1136/heartjnl-2017-311198>
- Simons, W.-F., De Smit, M., Duyck, J., Coucke, W., & Quirynen, M. (2015). The proportion of cancellous bone as predictive factor for early marginal bone loss around implants in the posterior part of the mandible. *Clinical Oral Implants Research*, 26(9), 1051–1059. <https://doi.org/10.1111/clr.12398>
- Torheim, T., Malinen, E., Hole, K. H., Lund, K. V., Indahl, U. G., Lyng, H., ... Futsaether, C. M. (2017). Autodelineation of cervical cancers using multiparametric magnetic resonance imaging and machine learning. *Acta Oncologica*, 56(6), 806–812. <https://doi.org/10.1080/0284186X.2017.1285499>
- Trisi, P., Berardini, M., Falco, A., Podaliri Vulpiani, M., & Perfetti, G. (2014). Insufficient irrigation induces peri-implant bone resorption: an in vivo histologic analysis in sheep. *Clinical Oral Implants Research*, 25(6), 696–701. <https://doi.org/10.1111/clr.12127>
- Van Dessel, J., Nicolielo, L. F., Huang, Y., Coudyzer, W., Salmon, B., Lambrichts, I., & Jacobs, R. (2017). Accuracy and reliability of different cone beam computed tomography (CBCT) devices for structural analysis of alveolar bone in comparison with multislice CT and micro-CT. *European Journal of Oral Implantology*, 10(1), 95–105.
- Van Dessel, J., Nicolielo, L. F., Huang, Y., Slagmolen, P., Politis, C., Lambrichts, I., & Jacobs, R. (2016). Quantification of bone quality using different cone beam computed tomography devices: Accuracy assessment for edentulous human mandibles. *European Journal of Oral Implantology*, 9(4), 411–424.
- Wang, S., & Summers, R. M. (2012). Machine learning and radiology. *Medical Image Analysis*, 16(5), 933–951. <https://doi.org/10.1016/j.media.2012.02.005>
- Yassin, N. I. R., Omran, S., El Houbay, E. M. F., & Allam, H. (2018). Machine learning techniques for breast cancer computer aided diagnosis using different image modalities: A systematic review. *Computer Methods and Programs in Biomedicine*, 156, 25–45. <https://doi.org/10.1016/j.cmpb.2017.12.012>

Zeytinoğlu, M., İlhan, B., Dünder, N., & Boyacıoğlu, H. (2015). Fractal analysis for the assessment of trabecular peri-implant alveolar bone using panoramic radiographs. *Clinical Oral Investigations*, 19(2), 519–524. <https://doi.org/10.1007/s00784-014-1245-y>

Chapter 5

Relationship between trabecular bone architecture and early dental implant failure in the posterior region of the mandible

This chapter is based on:

Nicolielo, L.F.P., Van Dessel J., Jacobs, R., Quirino Silveira Soares, M., Collaert, B. (2019). Relationship between trabecular bone architecture and early dental implant failure in the posterior region of the mandible. *Clinical Oral Implants Research*. doi: 10.1111/clr.13551

5.1 Abstract

Objective: To investigate the relationship between preoperative trabecular bone structure and implant outcome based on bone morphometric bone parameters from CBCT scans.

Material and Methods: Twenty consecutive cases with early implant failure in the posterior region of the mandible were matched with 20 control patients with a successful implant osseointegration selected. All patients had taken a preoperative CBCT image according to a standardized acquisition protocol. On these CBCT scans, the trabecular bone of each implantation site was selected and segmented, after which 3D morphometric bone parameters were calculated and used in a cluster analysis to objectively differentiate trabecular bone patterns. Fisher's exact test was used to determine whether there is a significant association between trabecular pattern and implant outcome.

Results: A sparse, intermediate and dense trabecular bone pattern was distinguished by cluster analysis. The relationship between the trabecular bone pattern and early implant failure was significant ($z = 9.6$; $P < 0.05$). Early implant failure was more likely to occur in the sparse bone types, while implant survival was associated with intermediate bone types.

Conclusion: Prior to implant placement, attention should be given to extreme deviations in trabecular structure at the planned implant sites. Very sparse or very dense bone should be carefully evaluated at the potential implant site, while intermediate bone types seem favorable for implant survival.

5.2 Introduction

For a long time, a favorable implant fixation was directly related to a high bone quantity and density (Kang et al., 2016), with higher incidence of implant failure occurring in poorly dense bone such as the posterior maxilla (Adell, 1981; Henry et al., 1996; Monje et al., 2015). Currently, the success rate of rehabilitation with implants in the posterior maxilla has become more predictable due to changes in implant surface treatments and new surgical techniques (Goiato, Dos Santos, Santiago, Moreno, & Pellizzer, 2014; Vervaeke, Collaert, Cosyn, Deschepper, & De Bruyn, 2015). This has led to an evolution in the way of thinking about bone quality. Bone quality is not only a question of mineral content or quantity, but also of structure (Lindh, Petersson, & Rohlin, 1996). Sclerotic bone caused by chronic infections or treatment with bisphosphonates is not the ideal site for implantation, while it still has a higher bone density (Madrid & Sanz, 2009; Quiryen, Gijbels, & Jacobs, 2003). In contrast, a well-structured thin trabecular bone may indicate a highly vascularized area, which may promote faster bone regeneration around the implant (Davies, 2003; Monje et al., 2015). Therefore, other parameters, such as the trabecular organization at the site of the implant before surgery, should be considered to assist the clinician in choosing the appropriate implantation protocol (Fanuscu & Chang, 2004; Ibrahim, Parsa, Hassan, van der Stelt, & Wismeijer, 2013; Minkin & Marinho, 1999; Traini et al., 2006).

The most used clinical method to assess trabecular bone is based on the subjective assessment of inter-trabecular spaces (small to large) and degree of trabeculation (sparse to dense) on two-dimensional (2D) radiographies (Ibrahim et al., 2013; Jonasson, Jonasson, & Kiliaridis, 2007; Lindh et al., 2008; Pham, Jonasson, & Kiliaridis, 2010). This method, however, can lead to biased conclusions, since it is fully dependent on the observer experience (Chrcanovic, Kisch, Albrektsson, & Wennerberg, 2016; Ibrahim et al., 2013; Ribeiro-Rotta, de Oliveira, Dias, Lindh, & Leles, 2014), while not providing the fully 3D aspect of the trabecular bone structure. Three-dimensional (3D) analysis of the bone structure became feasible with the introduction of microcomputed tomography (micro-CT), which allows bone morphometry quantification with parameters originally developed in histomorphometry (Van Dessel et al., 2013). This method objectively shows structure bone changes after a specific drug treatment (Borah et al., 2004), and differences between healthy and osteoporotic bone (McDonnell, McHugh, & O'Mahoney, 2007; Soares et al., 2018). In implantology, trabecular bone morphometric parameters were shown to be associated with implant stability (Kang et al., 2016; Ribeiro-Rotta et al., 2014), indicating its importance for bone quality assessment before implant placement. However, because of scanning range restrictions and excessive radiation doses, micro-CT is unsuitable for clinical diagnose. Clinically applicability of this method only became possible after latest advances in CBCT technology, allowing enough resolution to depict trabecular structure (Ho

et al., 2013; Huang et al., 2014; Klintström et al., 2018; Panmekiate, Ngonphloy, Charoenkarn, Faruangsang, & Pauwels, 2015). CBCT-derived trabecular bone parameters showed significant correlations with the gold standard micro-CT, when adequate scanning protocols are used (Van Dessel et al., 2016, 2017). A recent study has shown that when these morphometric parameters are linked to machine learning algorithms, they can be used to automatically distinguish three types of trabecular networks on CBCT scans of cadavers, for example, sparse, intermediate and dense trabecular bone structures. In contrast to a subjective radiological evaluation performed by dentomaxillofacial radiologists, this automatic computer-assisted method is objective and achieves a two to three times higher accuracy (Nicolielo, Van Dessel, van Lenthe, Lambrichts, & Jacobs, 2018). However, it remains a matter of debate how the trabecular pattern can influence the outcome of the implant.

The aim of this study was to investigate the relationship between preoperative trabecular bone structure in the posterior region of the mandible and early implant failure/short-term implant survival based on morphometric bone parameters derived from CBCT scans. Our hypothesis was that the three trabecular patterns can also be automatically determined on preoperative CBCT scans of patients and extreme trabecular bone conditions (very sparse versus very dense bone) are associated with a higher risk of early implant failure.

5.3 Materials and methods

A retrospective case-control design was used to assess the association between preoperative trabecular bone quality and early implant failure (< 6 months). This protocol was approved by the medical ethics committee of the University Hospital Leuven, Leuven Belgium (S57587).

5.3.1 Patient selection

The dental records of 493 consecutive patients that received 787 dental implants in the dorsal region of the mandible between January 2014 and January 2018 were screened for early implant failure from the database of a private periodontology clinic in Leuven. The selected cases with early implant failure were matched based on gender, age, medical status and implant site with control patients with implant survival. Patients were excluded if they had no standardized preoperative CBCT scan, with movement artefacts, not fully healed extraction socket or presence of tooth at the implant site at the moment CBCT image was acquired; underwent bone augmentation procedure; lost their implant due to mechanical trauma; used bisphosphonates, needed to start chemotherapy, radiotherapy, or immunosuppression treatment after implant placement; or did not stop smoking during healing phase. The following

was recorded: parafunctional habits, controlled diabetes, previous history of local perio-endo infection, implant site and size (*Table 5.1*).

All implants were placed after extraction socket healing by the same surgeon following a standard one-stage surgical protocol with the same implant system (Astra EV, Dentsply Sirona, Mölndal, Sweden). In soft bone, the osteotomy was underprepared, while in dense bone the osteotomy was overprepared. Implants were placed with a maximum torque value of 30 Ncm.

5.3.2 Image analysis

All preoperative CBCT images were taken with the same machine, ProMax® 3D Mid (Planmeca Oy, Helsinki, Finland) using a standardized acquisition protocol at 90 kV, 11 mA, 80 x 80 mm field of view and 160 µm isotropic voxel size. Scans were imported in MeVisLab software (MeVis Medical Solutions AG, Bremen, Germany) for position alignment and pre-selection of the dental implant site (*Figure 5.1*). For selection of exact implant position for further bone analysis on the preoperative CBCT images, image registration was performed to match the postoperative periapical image to the preoperative CBCT images using ImageJ software 2.0.0-rc-59/1.52i (National Institutes of Health Image program). As our samples included only implants in the posterior region, the patients had neighboring teeth that were used as anatomical landmarks for the image registration. A square was used to draw the mesial-distal, buccal-lingual and occlusal-apical limits. The mesial-distal limits corresponded to the size of the implant diameter plus 1mm mesially and 1mm distally. Buccal and lingual walls were fully included. Apical limit was the roof of the mandibular canal. Afterward, the volumes of interest (VOI) were imported into CT Analyser (Bruker, Kontich, Belgium) for trabecular bone segmentation and quantification of 3D morphometric parameters (*Figure 5.1*). The trabecular bone was first separated from the cortical bone and segmented by means of an adaptive threshold algorithm recommended by Nackaerts et al., 2015. From these binary images, the morphometric bone parameters were automatically calculated in 3D according to the latest recommendations of the American Society for Bone and Mineral Research (*Table 5.2*).

The morphometric bone parameters selection was based on our previous work (Nicolielo et al., 2018) in which Linear Discriminant Analysis was used to find the best combination of morphometric parameters separating trabecular bone in three bone types: (1) sparse – related to a loose bone structure, (2) intermediate – related to a well-structured trabecular bone and (3) dense bone types – related to a massive bone area with little space between the trabeculae (*Figure 5.2*).

Table 5. 1. Descriptive statistics from cases and control groups.

		Cases (n=20)	Controls (n=20)
Age (Mean \pm SD)		57 \pm 11.7	62.3 \pm 8.7
Gender (♂/ ♀)		10/8	10/8
Implant site	35	5	4
	36	5	4
	37	0	1
	45	6	4
	46	3	6
	47	1	1
Implant length (mm)	6	1	0
	8	15	12
	11	4	8
Implant diameter (mm)	3.6	4	7
	4.2	14	11
	4.8	2	2
Controlled diabetes		1	1
Bruxism		1	1
Previous local perio-endo infection		1	0

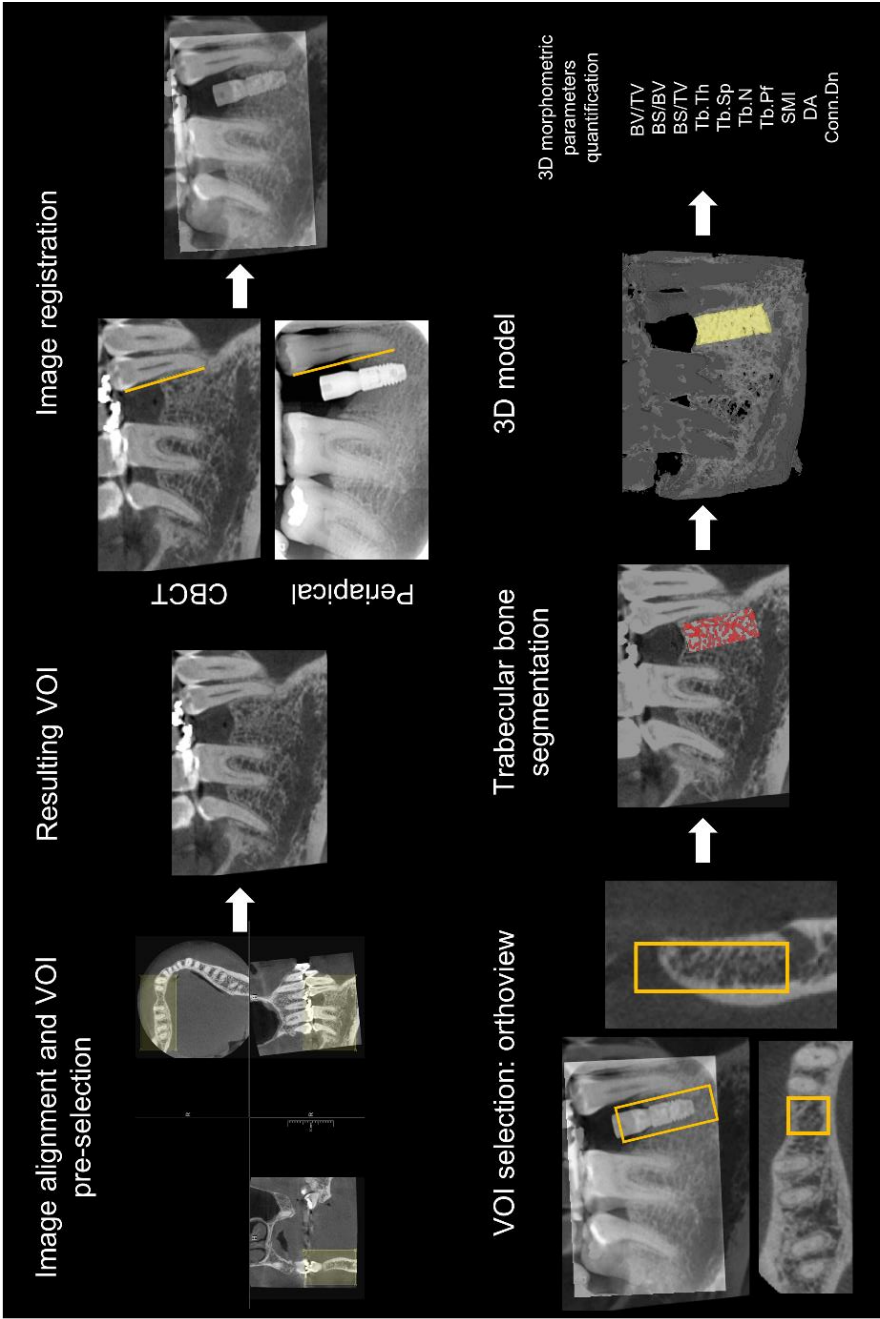


Figure 5.1. First row: Pre-selection of the implant site and image registration. **Second row:** Implant site selection, trabecular bone segmentation and 3D morphometric parameters quantification.

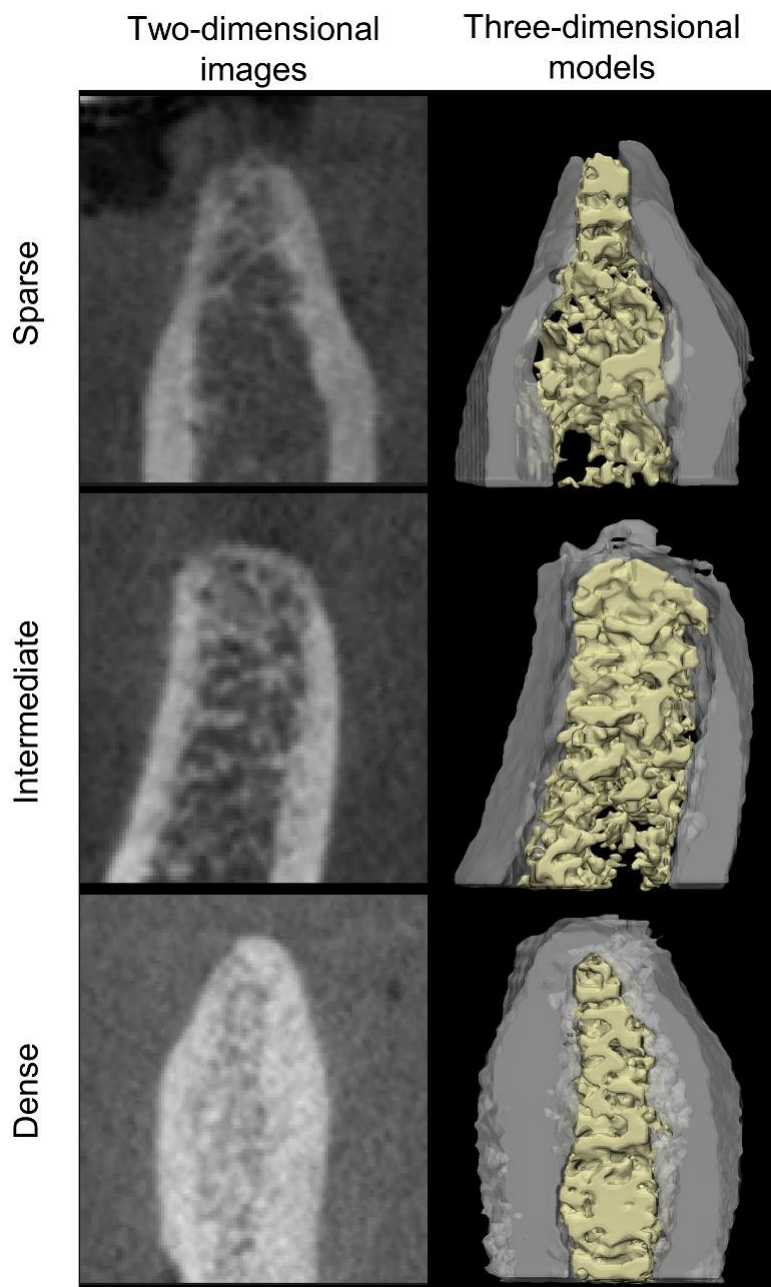


Figure 5.2. Examples of the three trabecular bone clusters. **First column.** Two-dimensional cross-sectional images of the implant site. **Second column.** Three-dimensional models.

Table 5.2. Quantified morphometric parameters of the local trabecular bone.

Morphometric parameter	Abbreviation	Unit	Description
Bone volume fraction	BV/TV	%	Ratio of the segmented trabecular bone volume to total volume of trabecular volume of interest
Specific bone surface	BS/BV	mm ² /mm ³	Ratio of the segmented bone surface to segmented bone volume. Characterises the complexity of bone structures
Bone surface density	BS/TV	mm ² /mm ³	Ratio of segmented trabecular bone surface to the total trabecular volume of the volume of interest
Trabecular thickness	Tb.Th	mm	Mean thickness of trabeculae
Trabecular separation	Tb.Sp	mm	Mean distance between trabeculae
Trabecular number	Tb.N	1/mm	Average number of trabeculae per millimeter
Trabecular pattern factor	Tb.Pf	1/mm	Index of trabecular bone connectivity
Structural model index	SMI	-	An indicator for the structure of trabeculae. SMI will be 0 for parallel plates and 3 for cylindrical rods
Degree of anisotropy	DA	-	Describes preferential alignment of the bone trabecular structure. Values higher than one represents a highly-oriented structure whereas equals to one represents an isotropic structure without a preferred orientation
Connectivity density	Conn.Dn	1/mm ³	Measure of degree of connectivity of trabeculae normalised by TV

5.3.3 Statistical analysis

Morphometric bone parameters were transformed in z-scores that specify how far a given raw score lies from the mean of a nominal distribution in terms of standard deviation. Morphometric z-scores were used in a k-mean cluster analysis to classify preoperative dental implant site of all subjects in three trabecular patterns.

A between-subject ANOVA was conducted to compare the morphometric parameters of the three trabecular bone types. Post-hoc Tukey tests were performed to explore significant effects. The F distribution had 2 degrees of freedom numerator (groups – 1) and 37 degrees of freedom denominator (patients – groups). Fisher's exact test was used to determine whether there is a significant association between trabecular pattern and implant outcome. The adjusted standardized residuals were used as post-hoc analysis to assess the significance in each cell. All statistical analyses were performed in IBM SPSS Statistics 22 (IBM Corp, Somers, NY). A p value less than 0.05 was considered statistically significant for all analyses.

5.4 Results

5.4.1 Patient selection

Thirty-two patients had 39 early failure implants in the posterior region of the mandible (95% survival rate), of which 14 patients were excluded considering a lack of preoperative CBCT. Eighteen patients (10♂/ 8♀) with 20 early failure implants were selected for the case group. The average time between implant placement and failure was 6.2 ± 4.5 weeks. For the matched-control group, eighteen patients (10♂/ 8♀) with 20 survival implants were selected (*Table 5.1*).

5.4.2 Comparison of trabecular bone types

The three bone clusters showed a clear and consistent pattern for all morphometric parameters. The sparse bone type was related to the cluster with lower bone volume densities ($\downarrow BV/TV$) and high bone surface densities ($\uparrow BS/BV$), consisting of a rod-like trabecular pattern ($\uparrow SMI$) in comparison with the intermediate bone type. The trabeculae are organised into a sparse-connected network ($\uparrow Tb.Pf$ and $\downarrow Conn.Dn$) with large marrow-spaced trabeculae ($\uparrow Tb.Sp$) and a lower number of trabeculae ($\uparrow Tb.N$) compared to the intermediate type. Exactly the opposite pattern occurred for the dense bone type when compared with the intermediate bone type (*Figure 5.3*).

An analysis of variance showed that the effect of bone volume fraction (BV/TV ; $F = 36.1$; $P < 0.001$), specific bone surface (BS/BV ; $F = 26.5$; $P < 0.001$), bone surface density (BS/TV ; $F = 21.2$; $P < 0.001$), trabecular thickness ($Tb.Th$; $F = 13.8$; $P < 0.001$), trabecular separation ($Tb.Sp$; $F = 23.6$; $P < 0.001$), trabecular number ($Tb.N$; $F = 90.5$; $P < 0.001$), trabecular pattern factor ($Tb.Pf$; $F = 22.4$; $P < 0.001$), structural model index (SMI ; $F = 25.8$; $P < 0.001$), degree of anisotropy (DA ; $F = 5.0$; $P < 0.05$) and connectivity density ($Conn.Dn$; $F = 5.4$; $P < 0.01$) was statistically significant different. Post-hoc analyses indicated significant differences in morphometric parameters between cluster types, except between sparse and intermediate trabecular pattern for BS/TV , $Tb.Sp$, DA and $Conn.Dn$, dense and intermediate for BS/BV and DA , and sparse and dense for $Tb.Th$ and $Conn.Dn$.

5.4.3 Relationship between bone type and early implant outcome

Fisher's exact test of independence showed a significant relationship between trabecular bone patterns and implant outcome ($z = 9.6$; $P < 0.05$). Early implant failure was more likely to occur in the sparse bone types (adjusted residual = 2.4), while implant survival was associated with

intermediate bone types (adjusted residual = 2.9). The proportions of early implant failure and success are shown in *Figure 5.4*.

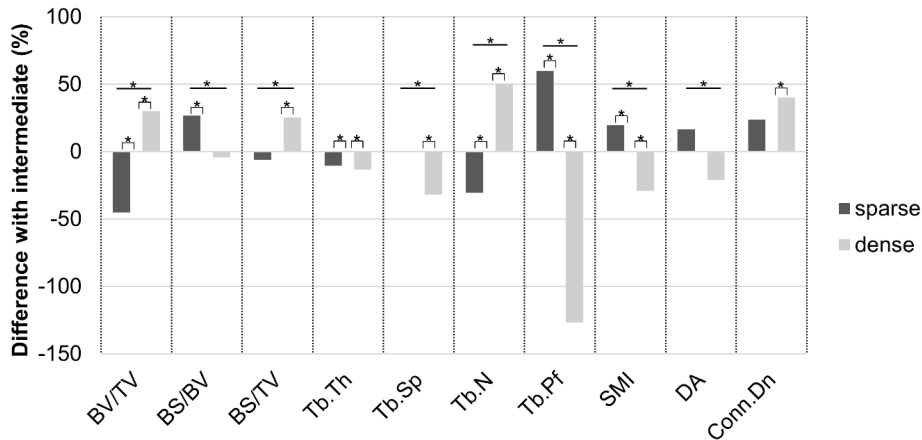


Figure 5.3. Percentage difference of the sparse and dense clusters in comparison with the intermediate for each morphometric parameter. *Significant difference between groups.

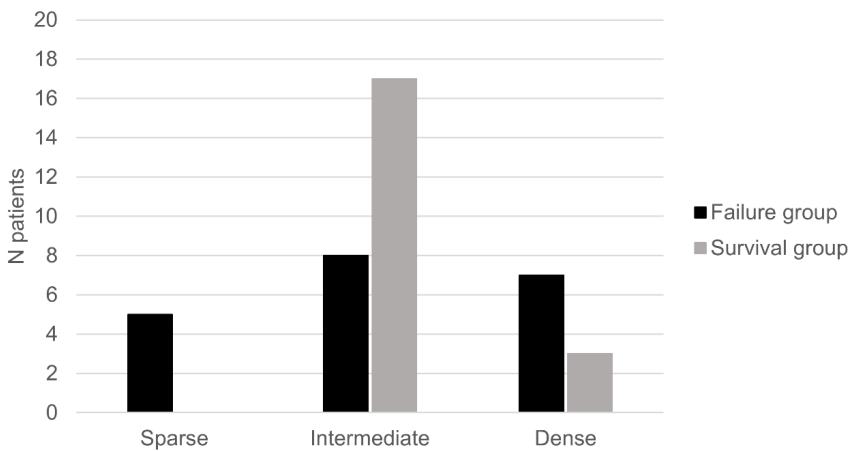


Figure 5.4. Occurrence of trabecular bone pattern per patient group.

5.5 Discussion

Lack of reliability in assessing bone quality has led to controversial results in how it can influence implant outcome (Aranyarachkul et al., 2005; Balshi, Wolfinger, Stein, & Balshi, 2015; Chrcanovic, Albrektsson, & Wennerberg, 2017; Merheb et al., 2015; Shahlaie, Gantes, Schulz, & Riggs, 2003). Previous studies have shown a variable interexaminer repeatability for bone tissue qualitative analysis in 2D radiographs (Lindh et al., 1996) and tactile perception (Trisi & Rao, 1999). Furthermore, quantitative assessment of bone density is often performed on MSCT images, but it does not account for density variations within a specific implant site (Bassi, Procchio, Fava, Schierano, & Preti, 1999) and is associated with higher radiation dose compared with the CBCT (Pauwels et al., 2013). Studies have shown that not only bone density is important to accurately predict implant survival, but also structural and biological properties (e.g., bone vascularization) play an important role in the osseointegration outcome (Chrcanovic et al., 2017). Considering this, Lindh et al. proposed a qualitative classification based on trabecular bone architecture. The authors described that a qualitative assessment based on three classes of trabecular network is more reliable than the classical bone quality index of Lekholm and Zarb (Lindh et al., 1996). Nevertheless, their classification was based on 2D contact radiographs, which limits a spatial characterization of the trabecular bone.

In the current study, morphometric bone parameters from a high-resolution CBCT were used to account for the full 3D trabecular structure. Previous studies have shown that trabecular bone morphometric parameters can be used in cluster analysis to automatically distinguish bone types (Nicolielo et al., 2018). Based on these parameters, an automatic classifier distinguished between three types of 3D trabecular pattern, namely, sparse, intermediate and dense. For the first time, however, the association between 3D trabecular pattern and early implant outcome was investigated. The present results showed that failure cases had significant more occurrence of sparse bone type, while intermediate bone type was more likely to occur in the survival group. These results are consistent with previous findings that showed that dense bone is associated with lower blood flow (Cha et al., 2015; Monje et al., 2015; Simons, De Smit, Duyck, Coucke, & Quirynen, 2015), while very soft bone may provide lack of implant stability (Ekfeldt et al., 2001; Martinez, Davarpanah, Missika, Celletti, & Lazzara, 2001).

Generally, the analysis of bone microstructure, as well as of bone volume, plays a major role in predicting the biomechanical properties and risk of bone fracture in osteoporotic patients (Borah et al., 2000; Jensen, Mosekilde, & Mosekilde, 1990; Kleerekoper, Villanueva, Stanciu, Rao, & Parfitt, 1985; Moon et al., 2004; Munakata, Tachikawa, Honda, Shiota, & Kasugai, 2011). In implantology, some studies showed correlation between trabecular structural parameters and implant stability (Gomes de Oliveira, Leles, Lindh, & Ribeiro-Rotta, 2012; Kang

et al., 2016). However, it remains a controversy since implant stability and high mechanical quality do not always represent high potential for biologic integration, and can also be a stressful factor for cells (Cha et al., 2015; Monje et al., 2015).

The structural characteristics of the bone is also related with the mechanical loading stimulations, such masticatory forces (Kim et al., 2013; Lorensen & Cline, 1987; Moon et al., 2004; Parfitt et al., 1983; Rhodes, Ford, Lynch, Liepins, & Curtis, 1999). The maxilla and mandible anterior regions have typically more compact trabeculae when compared with the respective posterior regions (Monje et al., 2015). In order not to account for regional structural differences, measurement sites need to be restricted to regions with the same loading influence, such the posterior area of the mandible.

Trabecular architecture is a very complex factor and can have multiple net configuration possibilities even within single bone sections (Ulm et al., 2009) and between different samples with similar bone volume fraction (Barak & Black, 2018). A sample with trabecular perforation can have the same BV/TV as a sample with thin trabeculae and integrate. However, the latter is more mechanically favorable (Ding, Odgaard, Linde, & Hvid, 2002; McDonnell et al., 2007; Silva & Gibson, 1997; Song, Liebschner, & Gunaratne, 2004). In the same way, both sparse and compact trabecular bone may present low connectivity. When sclerosis is present in dense bone, the trabecular separation is obliterate decreasing trabecular number and connectivity. Due to this heterogeneity, we have performed clustering analysis to discover coherent subgroups and meaningful categories of bone type. In this way three groups were distinguished and interpreted as sparse, intermediate and dense types. The intermediate bone type was close to the group average of both parameters that included bone quantity and structure, while the sparse and dense bone patterns showed opposing extremities.

Existing methods to assess the trabecular bone 3D architecture of the implant site depend on bone biopsy during implant site preparation. These are invasive methods and therefore unable to provide a realistic and clinically useful 3D reconstruction of the entire implant site (Van Dessel et al., 2016). The reliability of analysis methods in the current study, however, strongly depends on the quality of the scan, CBCT type and data acquisition protocol used. A voxel size smaller than 200 μm is required to accurately reflect the trabecular network, otherwise the trabecular bone may appear to be blurred due to partial volume artefacts (Van Dessel et al., 2013). This prevents proper segmentation and often leads to an overestimation of the amount of bone. Furthermore, it is important that the same CBCT scanner and acquisition protocol are used during the same study, so that any errors can be considered systematic and have no influence on the group comparisons.

Previous studies on implant failure/survival frequently report early and late implant failure (Borba, Deluiz, Lourenço, Oliveira, & Tannure, 2017; Ekfeldt et al., 2001; Esposito, Hirsch, Lekholm, & Thomsen, 1998; Han, Kim, & Han, 2014; Noda et al., 2015). We have opted to

focus on early failure, since it is more related to the biological capacity of the bone to achieve osseointegration; late implant failure, on the other hand, is thought to result from chronic bacterial infection, so-called “peri-implantitis”, or overload, due to the load-bearing capacity of the surrounding bone (Esposito, Thomsen, Ericson, Sennerby, & Lekholm, 2000).

Amongst limitations of this study are confounding effects inherent to retrospective studies design and small sample size. Early implant failure is mostly correlated with problems during surgical procedures (Han et al., 2014). Despite matching case and controls, meanwhile standardizing the surgical protocols applied by one and the same surgeon, it should be indicated that osteotomy of the implant site could be optimized based on surgical findings of hard versus softer bone. Under- and overpreparation of soft bone and hard bone, respectively. Such optimization strategy may have further influenced implant outcome. Prospective studies, such as randomized split-mouth designed, could provide less confounding effects, however, sample size could still remain a problem due to the low overall rates of implant failure.

Although this preliminary study cannot imply a direct causative relationship between the bone type and early implant survival, knowledge of preoperative trabecular bone structure can provide important indications for early implant failure risk. Especially, extremities, such as sparse and dense bone, should have attention when selecting one-stage or two-stage surgery procedure.

5.6 References

- Adell, R. (1981). A 15-year study of osseointegrated implants in the treatment of the edentulous jaw. *International Journal of Oral Surgery*. [https://doi.org/10.1016/S0300-9785\(81\)80077-4](https://doi.org/10.1016/S0300-9785(81)80077-4)
- Aranyarachkul, P., Caruso, J., Gantes, B., Schulz, E., Riggs, M., Dus, I., ... Crigger, M. (2005). Bone density assessments of dental implant sites: 2. Quantitative cone-beam computerized tomography. *The International Journal of Oral & Maxillofacial Implants*, 20(3), 416–424. <https://doi.org/10.1007/s13398-014-0173-7>
- Balshi, T., Wolfinger, G., Stein, B., & Balshi, S. (2015). A Long-term Retrospective Analysis of Survival Rates of Implants in the Mandible. *The International Journal of Oral & Maxillofacial Implants*, 30(6), 1348–1354. <https://doi.org/10.11607/jomi.3910>
- Barak, M. M., & Black, M. A. (2018). A novel use of 3D printing model demonstrates the effects of deteriorated trabecular bone structure on bone stiffness and strength. *Journal of the Mechanical Behavior of Biomedical Materials*, 78, 455–464. <https://doi.org/10.1016/j.jmbbm.2017.12.010>
- Bassi, F., Procchio, M., Fava, C., Schierano, G., & Preti, G. (1999). Bone density in human dentate and edentulous mandibles using computed tomography. *Clinical Oral Implants Research*, 10(5), 356–361. <https://doi.org/10.1034/j.1600-0501.1999.100503.x>
- Borah, B., Dufresne, T. E., Chmielewski, P. A., Johnson, T. D., Chines, A., & Manhart, M. D. (2004). Risedronate preserves bone architecture in postmenopausal women with osteoporosis as measured by three-dimensional microcomputed tomography. *Bone*, 34(4), 736–746. <https://doi.org/10.1016/j.bone.2003.12.013>
- Borah, B., Dufresne, T. E., Cockman, M. D., Gross, G. J., Sod, E. W., Myers, W. R., ... Stevens, M. L. (2000). Evaluation of changes in trabecular bone architecture and mechanical properties of minipig vertebrae by three-dimensional magnetic resonance microimaging and finite element modeling. *Journal of Bone and Mineral Research*, 15(9), 1786–1797. <https://doi.org/10.1359/jbmr.2000.15.9.1786>

- Borba, M., Deluiz, D., Lourenço, E. J. V., Oliveira, L., & Tannure, P. N. (2017). Risk factors for implant failure: a retrospective study in an educational institution using GEE analyses. *Brazilian Oral Research*, 31(0). <https://doi.org/10.1590/1807-3107bor-2017.vol31.0069>
- Cha, J. Y., Pereira, M. D., Smith, A. A., Houschyar, K. S., Yin, X., Mouraret, S., ... Helms, J. A. (2015). Multiscale analyses of the bone-implant interface. *Journal of Dental Research*, 94(3), 482–490. <https://doi.org/10.1177/0022034514566029>
- Chrcanovic, B., Albrektsson, T., & Wennerberg, A. (2017). Bone Quality and Quantity and Dental Implant Failure: A Systematic Review and Meta-analysis. *The International Journal of Prosthodontics*, 30(3), 219–237. <https://doi.org/10.11607/ijp.5142>
- Chrcanovic, B., Kisch, J., Albrektsson, T., & Wennerberg, A. (2016). Factors Influencing Early Dental Implant Failures. *Journal of Dental Research*, 95(9), 995–1002. <https://doi.org/10.1177/0022034516646098>
- Davies, J. (2003). Understanding peri-implant endosseous healing. *Journal of Dental Education*, 67(8), 932–949.
- Ding, M., Odgaard, A., Linde, F., & Hvid, I. (2002). Age-related variations in the microstructure of human tibial cancellous bone. *Journal of Orthopaedic Research*, 20(3), 615–621. [https://doi.org/10.1016/S0736-0266\(01\)00132-2](https://doi.org/10.1016/S0736-0266(01)00132-2)
- Ekfeldt, A., Christiansson, U., Eriksson, T., Linden, U., Lundqvist, S., Rundcrantz, T., ... Billstrom, C. (2001). A retrospective analysis of factors associated with multiple implant failures in maxillae. *Clinical Oral Implants Research*, 12(5), 462–467. <https://doi.org/10.1034/j.1600-0501.2001.120505.x>
- Esposito, M., Hirsch, J. M., Lekholm, U., & Thomsen, P. (1998). Biological factors contributing to failures of osseointegrated oral implants. (I). Success criteria and epidemiology. *European Journal of Oral Sciences*. <https://doi.org/10.1046/j.0909-8836..t01-2-.x>
- Esposito, M., Thomsen, P., Ericson, L. E., Sennerby, L., & Lekholm, U. (2000). Histopathologic observations on late oral implant failures. *Clinical Implant Dentistry and Related Research*, 2(1), 18–32. <https://doi.org/10.1111/j.1708-8208.2000.tb00103.x>
- Fanuscu, M. I., & Chang, T. L. (2004). Three-dimensional morphometric analysis of human

- cadaver bone: Microstructural data from maxilla and mandible. *Clinical Oral Implants Research*, 15(2), 213–218. <https://doi.org/10.1111/j.1600-0501.2004.00969.x>
- Goiato, M. C., Dos Santos, D. M., Santiago, J. F., Moreno, A., & Pellizzer, E. P. (2014). Longevity of dental implants in type IV bone: A systematic review. *International Journal of Oral and Maxillofacial Surgery*. <https://doi.org/10.1016/j.ijom.2014.02.016>
- Gomes de Oliveira, R. C., Leles, C. R., Lindh, C., & Ribeiro-Rotta, R. F. (2012). Bone tissue microarchitectural characteristics at dental implant sites. Part 1: Identification of clinical-related parameters. *Clinical Oral Implants Research*, 23(8), 981–986. <https://doi.org/10.1111/j.1600-0501.2011.02243.x>
- Han, H.-J., Kim, S., & Han, D.-H. (2014). Multifactorial Evaluation of Implant Failure: A 19-year Retrospective Study. *The International Journal of Oral & Maxillofacial Implants*, 29(2), 303–310. <https://doi.org/10.11607/jomi.2869>
- Henry, P. J., Laney, W. R., Jemt, T., Harris, D., Krogh, P. H. J., Polizzi, G., ... Herrmann, I. (1996). Osseointegrated implants for single-tooth replacement: a prospective 5-year multicenter study. *International Journal of Oral and Maxillofacial Implants*, 11(4), 450–455. <https://doi.org/10.11607/jomi.2937>
- Ho, J. T., Wu, J., Huang, H. L., Chen, M. Y. C., Fuh, L. J., & Hsu, J. T. (2013). Trabecular bone structural parameters evaluated using dental cone-beam computed tomography: Cellular synthetic bones. *BioMedical Engineering Online*, 12(1). <https://doi.org/10.1186/1475-925X-12-115>
- Huang, Y., Van Dessel, J., Depypere, M., EzEldeen, M., Iliescu, A. A., Santos, E. Dos, ... Jacobs, R. (2014). Validating cone-beam computed tomography for peri-implant bone morphometric analysis. *Bone Research*, 2, 14010. <https://doi.org/10.1038/boneres.2014.10>
- Ibrahim, N., Parsa, A., Hassan, B., van der Stelt, P., & Wismeijer, D. (2013). Diagnostic imaging of trabecular bone microstructure for oral implants: a literature review. *Dentomaxillofacial Radiology*, 42(3), 20120075. <https://doi.org/10.1259/dmfr.20120075>
- Jensen, K. S., Mosekilde, L., & Mosekilde, L. (1990). A model of vertebral trabecular bone

- architecture and its mechanical properties. *Bone*, 11(6), 417–423.
[https://doi.org/10.1016/8756-3282\(90\)90137-N](https://doi.org/10.1016/8756-3282(90)90137-N)
- Jonasson, G., Jonasson, L., & Kiliaridis, S. (2007). Skeletal bone mineral density in relation to thickness, bone mass, and structure of the mandibular alveolar process in dentate men and women. *European Journal of Oral Sciences*, 115(2), 117–123.
<https://doi.org/10.1111/j.1600-0722.2007.00438.x>
- Kang, S.-R., Bok, S.-C., Choi, S.-C., Lee, S.-S., Heo, M.-S., Huh, K.-H., ... Yi, W.-J. (2016). The relationship between dental implant stability and trabecular bone structure using cone-beam computed tomography. *Journal of Periodontal & Implant Science*, 46(2), 116–127. <https://doi.org/10.5051/jpis.2016.46.2.116>
- Kim, J. E., Shin, J. M., Oh, S. O., Yi, W. J., Heo, M. S., Lee, S. S., ... Huh, K. H. (2013). The three-dimensional microstructure of trabecular bone: Analysis of site-specific variation in the human jaw bone. *Imaging Science in Dentistry*, 43(4), 227–233.
<https://doi.org/10.5624/isd.2013.43.4.227>
- Kleerekoper, M., Villanueva, A. R., Stanciu, J., Rao, D. S., & Parfitt, A. M. (1985). The role of three-dimensional trabecular microstructure in the pathogenesis of vertebral compression fractures. *Calcified Tissue International*, 37(6), 594–597.
<https://doi.org/10.1007/BF02554913>
- Klintström, E., Klintström, B., Pahr, D., Brismar, T. B., Smedby, Ö., & Moreno, R. (2018). Direct estimation of human trabecular bone stiffness using cone beam computed tomography. *Oral Surgery, Oral Medicine, Oral Pathology and Oral Radiology*, 126(1), 72–82.
<https://doi.org/10.1016/j.oooo.2018.03.014>
- Lindh, C., Horner, K., Jonasson, G., Olsson, P., Rohlin, M., Jacobs, R., ... Devlin, H. (2008). The use of visual assessment of dental radiographs for identifying women at risk of having osteoporosis: the OSTEODENT project. *Oral Surgery, Oral Medicine, Oral Pathology, Oral Radiology and Endodontology*, 106(2), 285–293.
<https://doi.org/10.1016/j.tripleo.2007.09.008>
- Lindh, C., Petersson, A., & Rohlin, M. (1996). Assessment of the trabecular pattern before

- endosseous implant treatment: Diagnostic outcome of periapical radiography in the mandible. *Oral Surgery, Oral Medicine, Oral Pathology, Oral Radiology, and Endod*, 82(3), 335–343. [https://doi.org/10.1016/S1079-2104\(96\)80363-5](https://doi.org/10.1016/S1079-2104(96)80363-5)
- Lorensen, W. E., & Cline, H. E. (1987). Marching cubes: A high resolution 3D surface construction algorithm. In *Proceedings of the 14th annual conference on Computer graphics and interactive techniques - SIGGRAPH '87* (pp. 163–169). <https://doi.org/10.1145/37401.37422>
- Madrid, C., & Sanz, M. (2009). What impact do systemically administrated bisphosphonates have on oral implant therapy? A systematic review. *Clinical Oral Implants Research*. <https://doi.org/10.1111/j.1600-0501.2009.01772.x>
- Martinez, H., Davarpanah, M., Missika, P., Celletti, R., & Lazzara, R. (2001). Optimal implant stabilization in low density bone. *Clinical Oral Implants Research*, 12(5), 423–432. <https://doi.org/10.1034/j.1600-0501.2001.120501.x>
- McDonnell, P., McHugh, P. E., & O'Mahoney, D. (2007). Vertebral osteoporosis and trabecular bone quality. *Annals of Biomedical Engineering*, 35(2), 170–189. <https://doi.org/10.1007/s10439-006-9239-9>
- Merheb, J., Graham, J., Coucke, W., Roberts, M., Quirynen, M., Jacobs, R., & Devlin, H. (2015). Prediction of Implant Loss and Marginal Bone Loss by Analysis of Dental Panoramic Radiographs. *The International Journal of Oral & Maxillofacial Implants*, 30(2), 372–377. <https://doi.org/10.11607/jomi.3604>
- Minkin, C., & Marinho, V. C. (1999). Role of the osteoclast at the bone-implant interface. *Advances in Dental Research*, 13, 49–56. <https://doi.org/10.1177/08959374990130011401>
- Monje, A., Chan, H.-L., Galindo-Moreno, P., Elnayef, B., Suarez-Lopez del Amo, F., Wang, F., & Wang, H.-L. (2015). Alveolar Bone Architecture: A Systematic Review and Meta-Analysis. *Journal of Periodontology*, 86(11), 1231–1248. <https://doi.org/10.1902/jop.2015.150263>
- Moon, H. S., Won, Y. Y., Kim, K. D., Ruprecht, A., Kim, H. J., Kook, H. K., & Chung, M. K.

- (2004). The three-dimensional microstructure of the trabecular bone in the mandible. *Surgical and Radiologic Anatomy*, 26(6), 466–473. <https://doi.org/10.1007/s00276-004-0247-x>
- Munakata, M., Tachikawa, N., Honda, E., Shiota, M., & Kasugai, S. (2011). Influence of menopause on mandibular bone quantity and quality in Japanese women receiving dental implants. *Archives of Osteoporosis*, 6(1–2), 51–57. <https://doi.org/10.1007/s11657-011-0058-8>
- Nackaerts, O., Depypere, M., Zhang, G., Vandenberghe, B., Maes, F., & Jacobs, R. (2015). Segmentation of Trabecular Jaw Bone on Cone Beam CT Datasets. *Clinical Implant Dentistry and Related Research*, 17(6), 1082–1091. <https://doi.org/10.1111/cid.12217>
- Nicolielo, L. F. P., Van Dessel, J., van Lenthe, G. H., Lambrichts, I., & Jacobs, R. (2018). Computer-based automatic classification of trabecular bone pattern can assist radiographic bone quality assessment at dental implant site. *The British Journal of Radiology*, 91(1092), 20180437. <https://doi.org/10.1259/bjr.20180437>
- Noda, K., Arakawa, H., Kimura-Ono, A., Yamazaki, S., Hara, E. S., Sonoyama, W., ... Kuboki, T. (2015). A longitudinal retrospective study of the analysis of the risk factors of implant failure by the application of generalized estimating equations. *Journal of Prosthodontic Research*, 59(3), 178–184. <https://doi.org/10.1016/j.jpor.2015.04.003>
- Panmekiate, S., Ngonphloy, N., Charoenkarn, T., Faruangsang, T., & Pauwels, R. (2015). Comparison of mandibular bone microarchitecture between micro-CT and CBCT images. *Dentomaxillofacial Radiology*, 44(5). <https://doi.org/10.1259/dmfr.20140322>
- Parfitt, A. M., Mathews, C. H. E., Villanueva, A. B., Kleerekoper, M., Frame, B., & Rao, D. S. (1983). Relationships between surface, volume, and thickness of iliac trabecular bone in aging and in osteoporosis. Implications for the microanatomic and cellular mechanisms of bone loss. *Journal of Clinical Investigation*, 72(4), 1396–1409. <https://doi.org/10.1172/JCI111096>
- Pauwels, R., Nackaerts, O., Bellaiche, N., Stamatakis, H., Tsiklakis, K., Walker, A., ... Horner, K. (2013). Variability of dental cone beam CT grey values for density estimations. *British*

Journal of Radiology, 86(1021). <https://doi.org/10.1259/bjr.20120135>

Pham, D., Jonasson, G., & Kiliaridis, S. (2010). Assessment of trabecular pattern on periapical and panoramic radiographs: A pilot study. *Acta Odontologica Scandinavica*, 68(2), 91–97. <https://doi.org/10.3109/00016350903468235>

Quiryen, M., Gijbels, F., & Jacobs, R. (2003). An infected jawbone site compromising successful osseointegration. *Periodontology* 2000. <https://doi.org/10.1046/j.0906-6713.2002.03311.x>

Rhodes, J. S., Ford, T. R., Lynch, J. a, Liepins, P. J., & Curtis, R. V. (1999). Micro-computed tomography: a new tool for experimental endodontology. *International Endodontic Journal*, 32(3), 165–170. <https://doi.org/10.1046/j.1365-2591.1999.00204.x>

Ribeiro-Rotta, R. F., de Oliveira, R. C. G., Dias, D. R., Lindh, C., & Leles, C. R. (2014). Bone tissue microarchitectural characteristics at dental implant sites part 2: Correlation with bone classification and primary stability. *Clinical Oral Implants Research*, 25(2). <https://doi.org/10.1111/clr.12046>

Shahlaie, M., Gantes, B., Schulz, E., & Riggs, M. (2003). Bone Density Assessments of Dental Implant Sites : *The International Journal of Oral & Maxillofacial Implants*, 18(2), 224–231.

Silva, M. J., & Gibson, L. J. (1997). Modeling the mechanical behavior of vertebral trabecular bone: Effects of age-related changes in microstructure. *Bone*, 21(2), 191–199. [https://doi.org/10.1016/S8756-3282\(97\)00100-2](https://doi.org/10.1016/S8756-3282(97)00100-2)

Simons, W. F., De Smit, M., Duyck, J., Coucke, W., & Quiryen, M. (2015). The proportion of cancellous bone as predictive factor for early marginal bone loss around implants in the posterior part of the mandible. *Clinical Oral Implants Research*, 26(9), 1051–1059. <https://doi.org/10.1111/clr.12398>

Soares, M. Q. S., Van Dessel, J., Jacobs, R., da Silva Santos, P. S., Cestari, T. M., Garlet, G. P., ... Rubira-Bullen, I. R. F. (2018). Zoledronic Acid Induces Site-Specific Structural Changes and Decreases Vascular Area in the Alveolar Bone. *Journal of Oral and Maxillofacial Surgery*. <https://doi.org/10.1016/j.joms.2018.03.007>

Song, Y., Liebschner, M. A. K., & Gunaratne, G. H. (2004). A study of age-related architectural

- changes that are most damaging to bones. *Biophysical Journal*, 87(6), 3642–3647.
<https://doi.org/10.1529/biophysj.104.044511>
- Traini, T., Assenza, B., Roman, F. S., Thams, U., Caputi, S., & Piattelli, A. (2006). Bone microvascular pattern around loaded dental implants in a canine model. *Clinical Oral Investigations*, 10(2), 151–156. <https://doi.org/10.1007/s00784-006-0043-6>
- Trisi, P., & Rao, W. (1999). Bone classification: clinical-histomorphometric comparison. *Clinical Oral Implants Research*, 10(1), 1–7. <https://doi.org/10.1034/j.1600-0501.1999.100101.x>
- Ulm, C., Tepper, G., Blahout, R., Rausch-Fan, X., Hienz, S., & Matejka, M. (2009). Characteristic features of trabecular bone in edentulous mandibles. *Clinical Oral Implants Research*, 20(6), 594–600. <https://doi.org/10.1111/j.1600-0501.2008.01701.x>
- Van Dessel, J., Huang, Y., Depypere, M., Rubira-Bullen, I., Maes, F., & Jacobs, R. (2013). A comparative evaluation of cone beam CT and micro-CT on trabecular bone structures in the human mandible. *Dentomaxillofacial Radiology*, 42(8), 20130145. <https://doi.org/10.1259/dmfr.20130145>
- Van Dessel, J., Nicolielo, L., Huang, Y., Coudyzer, W., Salmon, B., Lambrichts, I., & Jacobs, R. (2017). Accuracy and reliability of different cone beam computed tomography (CBCT) devices for structural analysis of alveolar bone in comparison with multislice CT and micro-CT. *European Journal of Oral Implantology*, 10(1), 95–105.
- Van Dessel, J., Nicolielo, L., Huang, Y., Slagmolen, P., Politis, C., Lambrichts, I., & Jacobs, R. (2016). Quantification of bone quality using different cone beam computed tomography devices: Accuracy assessment for edentulous human mandibles. *European Journal of Oral Implantology*, 9(4), 411–424.
- Vervaeke, S., Collaert, B., Cosyn, J., Deschepper, E., & De Bruyn, H. (2015). A multifactorial analysis to identify predictors of implant failure and peri-implant bone loss. *Clinical Implant Dentistry and Related Research*. <https://doi.org/10.1111/cid.12149>

Chapter 6

Validation of a novel imaging approach using multi-slice CT and cone-beam CT to follow-up on condylar remodelling after bimaxillary surgery

This chapter is based on:

Nicolielo, L. F. P., Van Dessel, J., Shaheen, E., Letelier, C., Codari, M., Politis, C., ... Jacobs, R. (2017). Validation of a novel imaging approach using multi-slice CT and cone-beam CT to follow-up on condylar remodeling after bimaxillary surgery. *International Journal of Oral Science*, 9(3), 139-144. <https://doi.org/10.1038/ijos.2017.22>

6.1 Abstract

The main goal of this study was to introduce a novel three-dimensional procedure to objectively quantify both inner and outer condylar remodelling on preoperative multi-slice computed tomography (MSCT) and postoperative cone-beam computed tomography (CBCT) images. Second, the reliability and accuracy of this condylar volume quantification method was assessed. The mandibles of 20 patients (11 female and 9 male) who underwent bimaxillary surgery were semi-automatically extracted from MSCT/CBCT scans and rendered in 3D. The resulting condyles were spatially matched by using an anatomical landmark-based registration procedure. A standardised sphere was created around each condyle, and the condylar bone volume within this selected region of interest was automatically calculated. To investigate the reproducibility of the method, inter- and intra-observer reliability was calculated for assessments made by two experienced radiologists twice five months apart in a set of ten randomly selected patients. To test the accuracy of the bone segmentation, the inner and outer bone structures of one dry mandible, scanned according to the clinical set-up, were compared with the gold standard, micro-CT. Thirty-eight condyles showed a significant ($P < 0.05$) mean bone volume decrease of $26.4\% \pm 11.4\%$ ($502.9 \text{ mm}^3 \pm 268.1 \text{ mm}^3$). No significant effects of side, sex or age were found. Good to excellent ($\text{ICC} > 0.6$) intra- and inter-observer reliability was observed for both MSCT and CBCT. Moreover, the bone segmentation accuracy was less than one voxel (0.4 mm) for MSCT ($0.3 \text{ mm} \pm 0.2 \text{ mm}$) and CBCT ($0.4 \text{ mm} \pm 0.3 \text{ mm}$), thus indicating the clinical potential of this method for objective follow-up in pathological condylar resorption.

6.2 Introduction

Orthognathic surgery often creates changes in the location of the temporomandibular joint (TMJ). These positional alterations may induce functional stress on the mandibular head, thereby causing condylar remodelling, which is considered to be a possible aetiology of skeletal relapse after orthognathic surgery (Jung, Kim, Park, & Jung, 2015). When patients show clinical signs and symptoms of potential postsurgical condylar resorption, radiographic imaging is required to obtain additional diagnostic information to optimise patient treatment and to estimate the severity of the condition. High-resolution three-dimensional (3D) imaging is the standard radiographic evaluation tool. Magnetic resonance imaging is used to determine the actual position of the disc, while multi-slice computed tomography (MSCT) and Cone-Beam CT (CBCT) are used to evaluate osseous pathological changes at the condylar level (Geiger, Bae, Statum, Du, & Chung, 2014). MSCT is often the preferred imaging modality to plan orthognathic surgery, owing to its high contrast-to-noise-ratio. However, if a follow-up of the surgical stability is indicated, the patient is exposed to a high dose of radiation. Therefore, an alternative low- dose CBCT approach can be recommended. Recent advancements in CBCT technology have allowed sufficient resolution to accurately depict bone structures and render 3D models (Van Dessel et al., 2017, 2016). Unfortunately, this potential is not fully exploited in the routine dental practice. Most of the time, methods to assess condylar resorption remain limited to two-dimensional (2D) measurements (Chen et al., 2013; Ha, Kim, Park, Kim, & Son, 2013; Katsumata et al., 2006; Kim et al., 2010; Park et al., 2012). Or, when in 3D, inner trabecular structure is neglected (Cevitanes et al., 2010; Goncalves et al., 2013; Schilling et al., 2014; Xi, Schreurs, Heerink, Bergé, & Maal, 2014; Xi et al., 2015, 2013). To properly follow-up condylar changes over time, a precise and reliable diagnostic tool is mandatory. Therefore, the goal of the present study was to introduce a new 3D procedure to objectively quantify condylar remodelling in MSCT and CBCT images. As a second objective, the reliability and accuracy of this condylar volume quantification were evaluated.

6.3 Materials and methods

6.3.1 Clinical assessment of condylar remodelling

6.3.1.1 Data acquisition

Twenty patients (11 female and 9 male; mean age \pm standard deviations: 23 ± 10) who underwent bimaxillary surgery at the department of Oral and Maxillofacial Surgery (University Hospital Leuven, Leuven, Belgium) and presented signs and symptoms of temporomandibular

joint dysfunction (TMD) were retrospectively included in the study. All patients provided informed consent, and ethical approval was obtained from the medical ethics committee of University Hospitals KU Leuven, Leuven Belgium (S57587). All patients were orthodontically treated before and after surgery. No subjects had a previous history of maxillofacial trauma or any known autoimmune or metabolic bone disease.

Following the clinical protocol at our institution, preoperative images were acquired with Somatom Definition Flash MSCT (Siemens Healthcare, Erlangen, Germany) by using a high-resolution (400 μm) scanning protocol with the following exposure settings: 120 kVp, 250 mA, U75 kernel and a 500 \times 500 mm field of view (FOV). The voxel size of the MSCT was not isotropic, with a slice thickness of 500 μm . Low-dose ProMax 3D Max CBCT (Planmeca Oy, Helsinki, Finland) was used for the postoperative follow-up. All of the MSCT and CBCT scans were taken with a wax bite to ensure that the mandible was in a centric position (Swennen et al., 2007). A scout view was taken before the scan in order to include both condyles without truncation artefacts. Thereafter, a large 230 \times 260 mm FOV scan was acquired at 96 kVp, 5 mA and 400 μm resolution.

6.3.1.2 Image analysis

Preoperative MSCT and postoperative CBCT images underwent the same image processing procedure shown in *Figure 6.1*. Each MSCT and CBCT scan in DICOM format were imported into Mimics medical image processing software (Version 18.0, Materialise, Leuven, Belgium), and were resliced to an isotropic voxel dimension of 400 μm^3 . The mandibular bone was semi-automatically delineated by using a global threshold algorithm. The computer suggested bone threshold values were visually confirmed in order to allow for the best segmentation overlap with the original image. The segmented mandibles were rendered in 3D and saved in .stl format for further image processing purposes. Subsequently, the pre- and postoperative 3D models were imported in 3-Matic software (Version 9.0, Materialise, Leuven, Belgium), and a minimum of three anatomical landmarks per mandible were chosen by an experienced radiologist (L.F.P.N.). The anatomical landmarks were selected on the coronoid process and the mandibular ramus and angle, owing to expected changes in the mandibular body and symphysis morphology after orthognathic surgery and the presence of metal braces from orthodontic treatment. Based on the best fit of these landmarks, the computer calculated the optimal translation and rotation between the pre- and postoperative 3D mandibles by minimising the mean square distance between the coronoid and ramus surfaces. In this way, the left and right condyles were registered separately. To achieve uniform selection of each condyle from the mandible, a standardised sphere with its border passing through the lowest

point of the mandibular notch was created around the condyle. After consistent extraction of the condyle, the condylar bone volume was automatically calculated in mm³.

6.3.2 Validation of method reproducibility

The reproducibility of the condylar volume determination may be affected by subjective VOI and bone threshold selections. Therefore, inter- and intra-observer reliability were calculated between assessments made by two experienced radiologists (L.F.P.N. and C.L.) at two time points with a 5-month interval (T1 and T2) in a set of 10 randomly selected patients. The MSCT and CBCT data were thresholded by each observer, and 3D models were generated based on the individual segmented images. A VOI selection procedure was performed according to the clinical assessment described above. The resulting 3D models of the corresponding condyles selected by each observer were overlaid to calculate the discrepancies between both models using distance-to-curve and part-comparison analyses (*Figure 6.2*). First, the mean distance (in mm) between the lower borders was automatically quantified and used as a measurement of discrepancy in VOI selection. Second, the shortest distance (in mm) between each internal and surface part of the two models was automatically calculated after the removal of dissimilarities in VOI selection through model subtraction and used as a measurement of threshold selection discrepancy.

6.3.3 Validation of condylar mineralised bone assessment

To examine the accuracy of the analytic approach, one dry human mandible was obtained from the Institute for Biomedical Research, Hasselt University and was approved for research by the ethical committee of the University Hospitals KU Leuven (S55619). The same scan settings were used according to the clinical scanning protocol for TMJ visualisation with Somatom Definition Flash MSCT and ProMax 3D Max CBCT.

The left condyle was sectioned 1 cm below the lowest point of the sigmoid notch to allow micro-CT (SkyScan 1172, SkyScan, Kontich, Belgium) scanning, and further served as the gold standard for accuracy measurements. A high-resolution (35 µm) scan protocol was used at 100 kVp, 100 µmA, 1 mm aluminium, 180° rotation with an angular step of 0.7° and a frame averaging of 6, thus resulting in a total scan time of 9 min. The image stacks were reconstructed with an isotropic voxel size of 35 µm³ in NRecon software (version 1.6.5, Bruker micro-CT), which were used for further image analysis. An overview of the image processing steps is shown in *Figure 6.3*. The acquired CBCT and MSCT images were spatially aligned with the corresponding micro-CT images by using a mutual information algorithm (Maes, Collignon, Vandermeulen, Marchal, & Suetens, 1997).

After precise registration, each image was semi-automatically segmented and 3D rendered by using the same processing protocol as in the clinical evaluation. The mineralised condylar bone volume was automatically calculated and compared among the different imaging modalities. A more detailed part-comparison analysis was conducted to evaluate the structural dissimilarity of the inner and outer mineralised condylar bone between MSCT/CBCT and micro-CT images.

6.3.4 Statistical analysis

The sample size was calculated by using a postoperative reduction in condylar volume of $105 \text{ mm}^3 \pm 90 \text{ mm}^3$ after bilateral sagittal split advancement osteotomy, which was obtained from a previous study (Xi et al., 2015).

A power analysis in G*Power 3.1 suggested a sample size of 11 patients assuming 95% power with an α of 0.05 (Faul, Erdfelder, Buchner, & Lang, 2009). A repeated measures ANCOVA was used to examine the effects of time (preoperative MSCT/postoperative CBCT) and side (left/right) as within-subject factors on condylar volume (in mm^3). Sex and age were included as covariates. The intra-class correlation coefficient (ICC) was calculated between condylar volume, as a measure to evaluate the agreement within and between the observers. The two-way mixed single measures for consistency were reported. The reproducibility of the procedure was influenced by the differences in VOI selection and bone threshold selection. Measurement discrepancies and standard deviations were reported for condylar volume (in mm^3), VOI selection (in mm) and bone threshold selection (in mm). A one-way ANOVA was used to examine condylar volume differences between MSCT, CBCT and the gold standard, micro-CT.

The statistical analysis was conducted in IBM SPSS statistical software (Version 22.0, IBM, New York, USA). The significance level α was set for all statistical tests at 0.05.

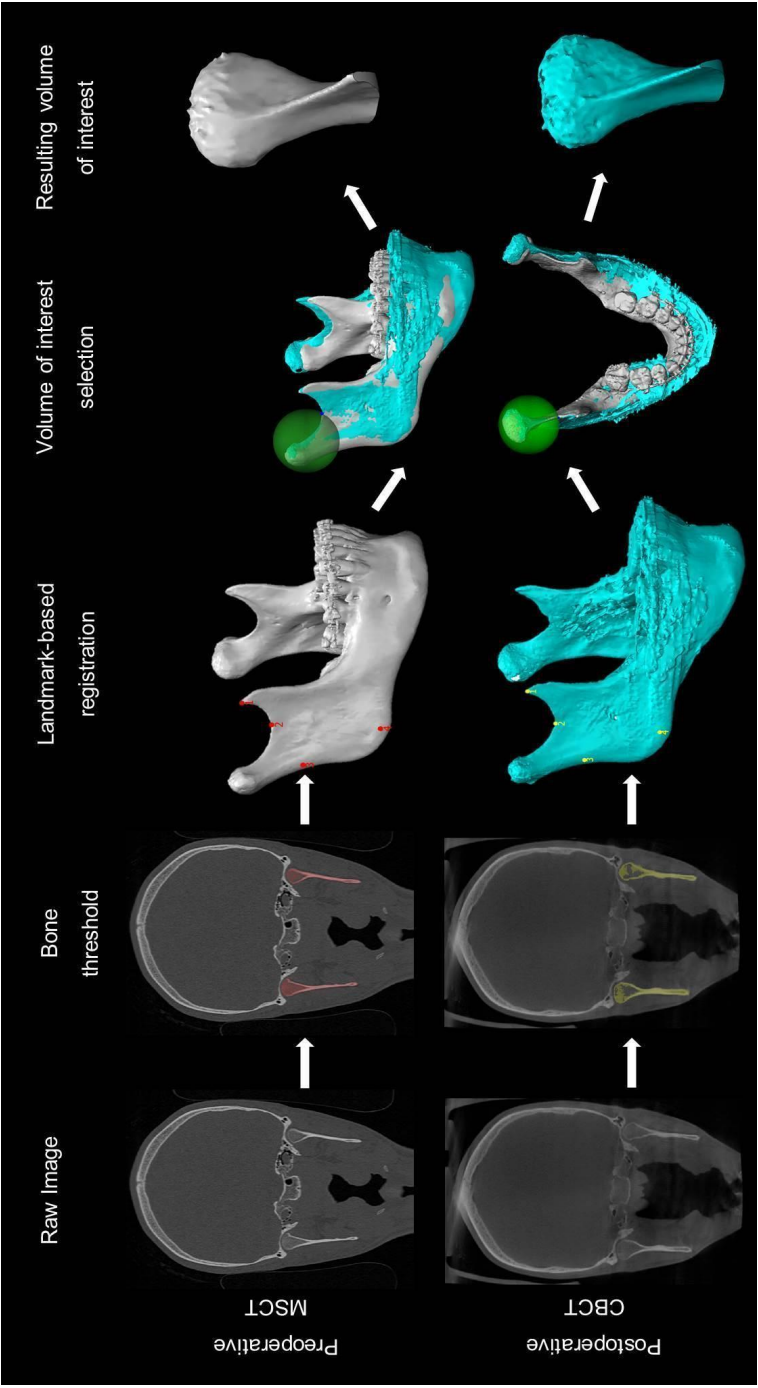


Figure 6.1. Workflow of the patient data image analysis. CBCT, cone-beam computed tomography; MSCT, multi-slice computed tomography.

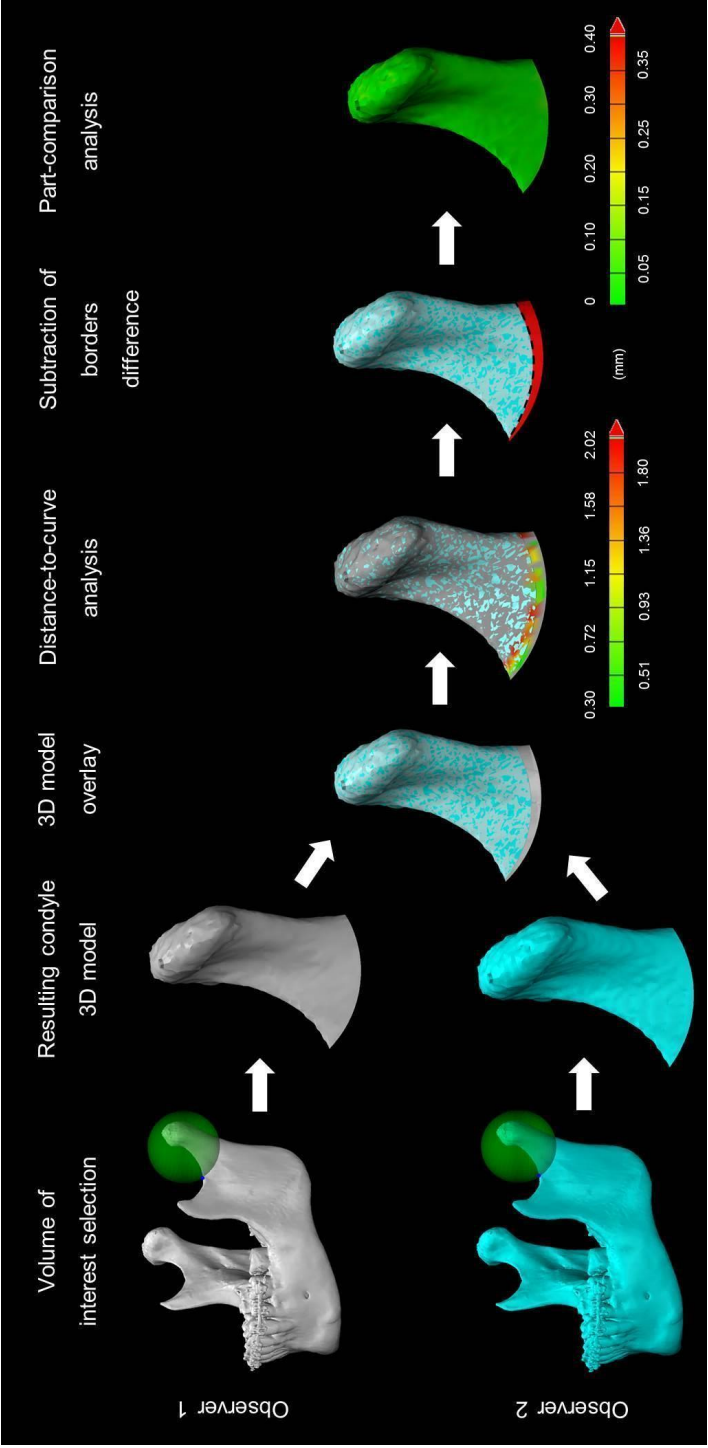


Figure 6.2. Workflow of the method reproducibility with MSCT data. 3D models generated by different observers were overlaid. A distance-to-curve analysis detected differences in the region of interest selection (mean: 1.25 mm, range: 0.3–2 mm). Before the part-comparison analysis, the error generated by the region of interest selection is subtracted (red colour). In this way, the calculation of the local differences between the 3D models is possible without counting the error of the region of interest selection. Part-comparison analysis from presented case shows a mean distance of 0.1 mm between the two condyles in the 3D models. 3D, three-dimensional; MSCT, multi-slice computed tomography.

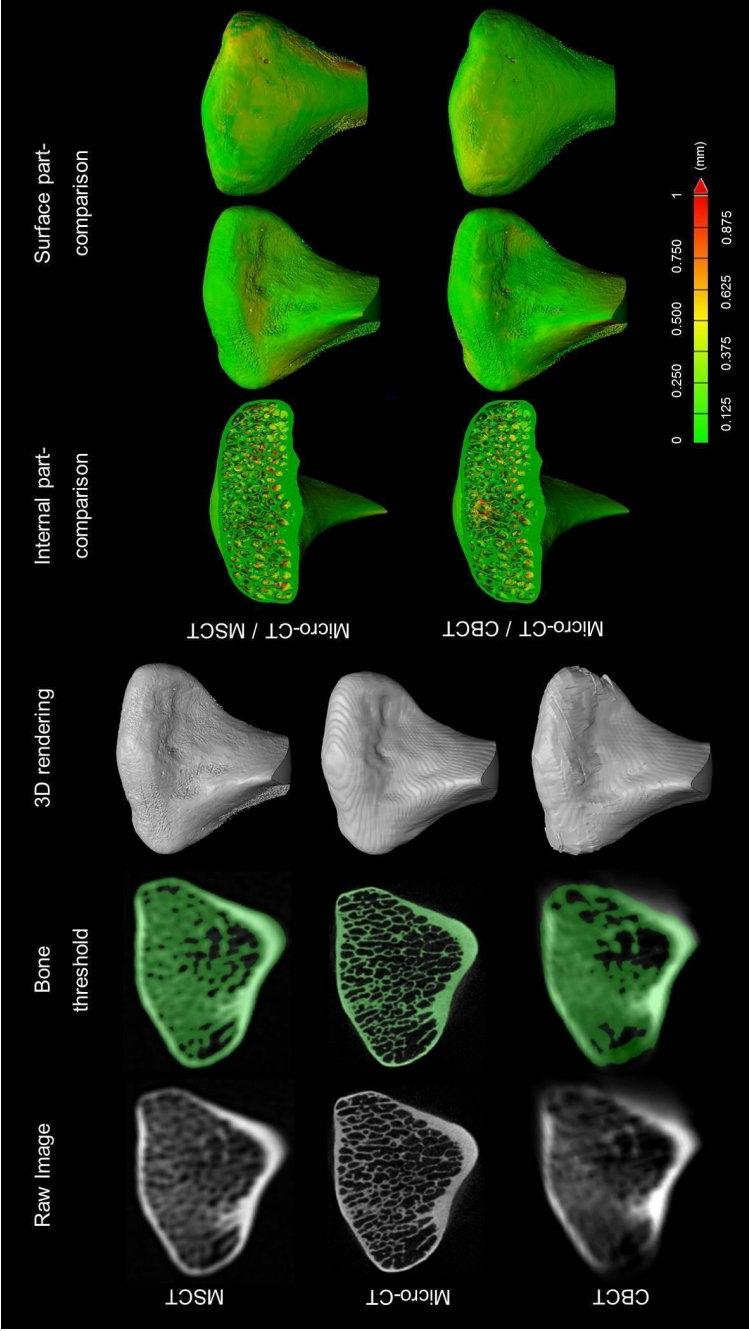


Figure 6.3. Accuracy of the condyle mineralised bone assessment. First column: The results of image registration between the different modalities. Second column: Image segmentation based on grey values. Third column: rendered 3D condylar models for all imaging modalities. The part-comparison analysis colour-codes the amount of overestimation in the inner and outer (surface) bone quantity between MSCT/CBCT and micro-CT. The green colour indicates an overestimation of less than one voxel between both 3D models and yellow and red indicate an overestimation of more than 0.375 mm. 3D, three-dimensional; CBCT, cone-beam computed tomography; MSCT, multi-slice computed tomography.

6.4 Results

6.4.1 Clinical assessment of condylar remodelling

The 40 condyles of 20 patients were analysed. All condyles, except for two from the same patient, exhibited remodelling of the mineralised volume of the condyle ranging up to a maximum of 46.5% (1 088.7 mm³) with a mean of 26.4% ±11.4% (502.9 mm³ ±268.1 mm³). Both the left and right condyles exhibited significant (P < 0.001) postoperative condylar remodelling volumes compared with their preoperative volumes. In individual subjects, differences in volumetric remodelling between the left and right condyles varied from 0.05% (4.8 mm³) to 14.9% (267.3 mm³) with a mean±standard deviations of 6.9%±4.8% (114.4 mm³ ±94.9 mm³), with no statistically significant difference (P = 0.55). No significant sex effect was observed in the present sample. In females, the condylar remodelling volume decreased on average by 27.0% ±13.4% (470.4 mm³ ±301.1 mm³), and in males, it decreased by 25.7% ±8.8% (542.6 mm³ ±223.3 mm³). Two condyles in one patient showed an increased volume of 7% (73.4 mm³) and 11% (105.0 mm³) in the left and right sides, respectively.

6.4.2 Validation of method reproducibility

Excellent evaluation reliability was obtained between observers at T2 (ICC=0.93 for MSCT; ICC=0.91 for CBCT) and within observer 1 (ICC=0.96 for MSCT; ICC=0.89 for CBCT). ICC values were excellent and good within observer 2 (ICC=0.96 for MSCT; ICC= 0.73 for CBCT) and between observers at T1 (ICC=0.89 for MSCT; ICC=0.6 for CBCT). Volume, VOI and segmentation discrepancies are shown in *Table 6.1*.

Table 6.1. The mean and standard deviations of the absolute discrepancy measurements of volume, VOI selection and segmentation between observers (inter) and within-observer (intra) in MSCT and in CBCT data.

Scanner type	Observer relation	Volume (mm ³)	VOI (mm)	Segmentation (mm)
MSCT	Intra	120.0 ± 92.6	0.9 ± 0.8	0.1 ± 0.2
	Inter	178.6 ± 149.3	0.8 ± 0.8	0.3 ± 0.3
CBCT	Intra	136.1 ± 143.5	0.5 ± 0.5	0.2 ± 0.2
	Inter	174.1 ± 201.1	0.7 ± 0.7	0.2 ± 0.2

*CBCT, cone-beam computed tomography; MSCT, multi-slice computed tomography; VOI, volume of interest.

6.4.3 Validation of condylar mineralised bone assessment

The micro-CT showed a lower condylar volume ($1\,167\text{ mm}^3$) compared with MSCT ($1\,834\text{ mm}^3$) and CBCT ($1\,732\text{ mm}^3$). The part-comparison analysis indicated an overestimation of the bone segmentation of $0.3\text{ mm} \pm 0.2\text{ mm}$ for MSCT and $0.4\text{ mm} \pm 0.3\text{ mm}$ for CBCT.

6.5 Discussion

In the present study, preoperative MSCT data and low-dose CBCT data at the 6-month postoperative follow-up from patients who underwent bimaxillary surgery were used to objectively assess condylar volume changes and to validate a new quantification method for condylar volume. The present method showed bone remodelling in 95% (38/40) of the condyles with an average of 26.4% mineralised bone loss. The reproducibility between the two observers was good to excellent and the accuracy with micro-CT indicated a bone segmentation overestimation of $< 0.4\text{ mm}$ on average, corresponding to less than one voxel. The reported incidence of condylar resorption after orthognathic surgery ranges from 1% to 31% depending on the defined criteria and various surgical and non-surgical risk factors (Borstlap, Stoelinga, Hoppenreijns, & van't Hof, 2004; De Clercq, Neyt, Mommaerts, Abeloos, & De Mot, 1994; Hoppenreijns, Freihof, Stoelinga, Tuinzing, & van't Hof, 1998). Young age and female sex are two of the most common patient-related risk factors for postoperative condylar resorption, mainly occurring in young female individuals in the second and third decades of life (De Clercq et al., 1994; Hoppenreijns et al., 1998; Wolford, 2001; Xi et al., 2015). In this study, no correlations between age, sex and condylar alterations were found, although more females in that age range were included. Unfortunately, the assessment of the age predilection is complicated, because most orthognathic surgery is performed in young patients. The female predisposition to condylar resorption, which occurs at a frequency of 9:1 (Hoppenreijns et al., 1998; Wolford, 2001), has been suggested to be related to a regulatory effect of oestrogen on bone metabolism in the TMJ. Moreover, as an important consideration, women seek medical help for dentofacial abnormalities more often than men.

Because of the study design and the implementation of only clinical and two-dimensional radiological data for the diagnosis of condylar alterations, most published studies have intrinsic limitations, although the diagnosis of condylar resorption in longitudinal studies is often based on a qualitative assessment of the mandibular condyles on OPG (Vidra, Rozema, Kostense, & Tuinzing, 2002). The major advantage of CT modalities compared with conventional radiographs is the possibility to render 3D models, thus allowing for linear, angular and volumetric measurements of the facial skeleton (Hoppenreijns, Stoelinga, Grace, & Robben, 1999; Plooi et al., 2009). The 3D rendering of the condyles has already been described in

average for the observer reproducibility, in agreement with previous studies (Xi et al., 2014, 2013), and less than one voxel for the accuracy measurements in both MSCT and CBCT (Van Dessel et al., 2013). This overestimation may influence the quantification results, because the literature has reported condylar resorptive changes of 0.4 mm (Chen et al., 2015) on average and up to at least 1.5 mm (Goncalves et al., 2013) after 1 year of orthognathic surgery. Although the present MSCT and CBCT protocols showed comparable overestimations, the standardisation of bone alteration measurements across time requires the use of the same scanning modality and protocol. Therefore, counterbalanced image quality and radiation dose are important. CBCT is considered to deliver a lower radiation dose to the patient, but the full head protocol may deliver a radiation dose comparable to that of MSCT with some machines (Hofmann, Schmid, Lell, & Hirschfelder, 2014; Stratis et al., 2016). The total condylar volume calculation is a sum of the segmentation and VOI selection. In this study, the size of the sphere was determined in each case according to the condyle size (which varied from 14 to 19 mm in radius). It was defined as the minimal size needed to involve the full condyle while the border of the sphere simultaneously passed through the lowest point of the sigmoid notch. This could occur only by manually centralising the sphere over the condyle. If the centre of the sphere shifted, the mandible head would be outside the sphere or the border would not pass through the lowest point of the sigmoid notch. According to our results, a higher discrepancy relative to VOI selection was observed compared with segmentation selection, especially with MSCT. VOI selection, which represents the total condyle volume, is a result of the anatomical marker choice, which is considered a reliable and reproducible anatomical marker that is not affected by natural growth or surgical interventions (Xi et al., 2013), with a 0.2 mm identification error (Xi et al., 2014). Although the identification of this anatomical point has a lower error, this error is distributed over the full condylar volume when placing the sphere around the condyle, thus potentially explaining the high variability in the distances between the limiting lower borders between the two models. In the clinical data, when comparing pre- and postoperative volumes, the VOI selection error can be overcome by the previous spatial alignment of the two condyles and the selection of the VOI simultaneously. In longitudinal studies, this spatial alignment can compensate for differences in the scanning head position and coordinate system, thus allowing for standardised measurements between images acquired at different time points. Currently, different methods are available to superimpose 3D images. Surface- and voxel-based registration have been reported to have similar accuracies in the assessment of surgical changes after orthognathic surgery (Almukhtar, Ju, Khambay, McDonald, & Ayoub, 2014). However, voxel-based registration relies on the greyscale intensity of the DICOM image voxels, thus suggesting the need for more efficient computers and a longer processing time (Almukhtar et al., 2014). This method may fail when superimposing two objects with significant morphological variability (Goncalves et al., 2013; Ruellas et al., 2016; Schilling et al., 2014).

After mandibular advancement, the ramus is the only anatomical part preserved from the osteotomy. Because the mandible width also changes after surgery, a simultaneous superimposition of both rami would not be possible without accounting for the mandible displacement. When landmark surface-based registration is applied, only one ramus can be superimposed at a time, and only differences in condylar volume can be assessed.

Our novel analysis method allows for the 3D quantification of the mineralised bone in the mandibular condyles, thus revealing differences between preoperative and postoperative situations. The proposed method may be of value during objective assessments and follow-ups of pathological condylar resorption after bimaxillary surgery.

6.6 References

- Almukhtar, A., Ju, X., Khambay, B., McDonald, J., & Ayoub, A. (2014). Comparison of the Accuracy of Voxel Based Registration and Surface Based Registration for 3D Assessment of Surgical Change following Orthognathic Surgery. *PLOS ONE*, 9(4), e93402. <https://doi.org/10.1371/journal.pone.0093402>
- Bayram, M., Kayipmaz, S., Sezgin, Ö. S., & Küçük, M. (2012). Volumetric analysis of the mandibular condyle using cone beam computed tomography. *European Journal of Radiology*, 81(8), 1812–1816. <https://doi.org/10.1016/j.ejrad.2011.04.070>
- Borstlap, W. A., Stoelinga, P. J. W., Hoppenreijns, T. J. M., & van't Hof, M. A. (2004). Stabilisation of sagittal split advancement osteotomies with miniplates: a prospective, multicentre study with two-year follow-up. Part I. Clinical parameters. *International Journal of Oral and Maxillofacial Surgery*, 33(5), 433–441. <https://doi.org/10.1016/j.ijom.2004.02.003>
- Cevidanes, L. H. S., Hajati, A.-K., Paniagua, B., Lim, P. F., Walker, D. G., Palconet, G., ... Phillips, C. (2010). Quantification of condylar resorption in temporomandibular joint osteoarthritis. *Oral Surgery, Oral Medicine, Oral Pathology, Oral Radiology, and Endodontology*, 110(1), 110–117. <https://doi.org/10.1016/j.tripleo.2010.01.008>
- Chen, S., Lei, J., Wang, X., Fu, K., Farzad, P., & Yi, B. (2013). Short- and Long-Term Changes of Condylar Position After Bilateral Sagittal Split Ramus Osteotomy for Mandibular Advancement in Combination With Le Fort I Osteotomy Evaluated by Cone-Beam Computed Tomography. *Journal of Oral and Maxillofacial Surgery*, 71(11), 1956–1966. <https://doi.org/10.1016/j.joms.2013.06.213>
- Chen, S., Liu, X., Li, Z., Liang, C., Wang, X., Fu, K., & Yi, B. (2015). Three-dimensional evaluation of condylar morphology remodeling after orthognathic surgery in mandibular retrognathism by cone-beam computed tomography. *Journal of Peking University(Health Sciences)*, 47(4), 703–707. <https://doi.org/10.3969/j.issn.1671-167X.2015.04.030>
- De Clercq, C., Neyt, L., Mommaerts, M. Y., Abeloos, J., & De Mot, B. M. (1994). Condylar

- resorption in orthognathic surgery: a retrospective study. *The International Journal of Adult Orthodontics and Orthognathic Surgery*, 9(3), 233–240.
- Faul, F., Erdfelder, E., Buchner, A., & Lang, A.-G. (2009). Statistical power analyses using G*Power 3.1: Tests for correlation and regression analyses. *Behavior Research Methods*, 41(4), 1149–1160. <https://doi.org/10.3758/BRM.41.4.1149>
- Geiger, D., Bae, W. C., Statum, S., Du, J., & Chung, C. B. (2014). Quantitative 3D ultrashort time-to-echo (UTE) MRI and micro-CT (μ CT) evaluation of the temporomandibular joint (TMJ) condylar morphology. *Skeletal Radiology*, 43(1), 19–25. <https://doi.org/10.1007/s00256-013-1738-9>
- Goncalves, J. R., Wolford, L. M., Cassano, D. S., da Porciuncula, G., Paniagua, B., & Cevidane, L. H. (2013). Temporomandibular Joint Condylar Changes Following Maxillomandibular Advancement and Articular Disc Repositioning. *Journal of Oral and Maxillofacial Surgery*, 71(10), 1759.e1-1759.e15. <https://doi.org/10.1016/j.joms.2013.06.209>
- Ha, M.-H., Kim, Y.-I., Park, S.-B., Kim, S.-S., & Son, W.-S. (2013). Cone-beam computed tomographic evaluation of the condylar remodeling occurring after mandibular set-back by bilateral sagittal split ramus osteotomy and rigid fixation. *The Korean Journal of Orthodontics*, 43(6), 263–270. <https://doi.org/10.4041/kjod.2013.43.6.263>
- Hofmann, E., Schmid, M., Lell, M., & Hirschfelder, U. (2014). Cone beam computed tomography and low-dose multislice computed tomography in orthodontics and dentistry: a comparative evaluation on image quality and radiation exposure. *Journal of Orofacial Orthopedics / Fortschritte Der Kieferorthopädie*, 75(5), 384–398. <https://doi.org/10.1007/s00056-014-0232-x>
- Hoppenreijts, T. J. M., Freihofer, H. P. M., Stoelinga, P. J. W., Tuinzing, D. B., & van't Hof, M. A. (1998). Condylar remodelling and resorption after Le Fort I and bimaxillary osteotomies in patients with anterior open bite. A clinical and radiological study. *International Journal of Oral and Maxillofacial Surgery*, 27(2), 81–91. [https://doi.org/10.1016/S0901-5027\(98\)80301-9](https://doi.org/10.1016/S0901-5027(98)80301-9)

- Hoppenreijts, T. J. M., Stoelinga, P. J. W., Grace, K. L., & Robben, C. M. G. (1999). Long-term evaluation of patients with progressive condylar resorption following orthognathic surgery. *International Journal of Oral and Maxillofacial Surgery*, 28(6), 411–418. <https://doi.org/10.1034/j.1399-0020.1999.280602.x>
- Jung, H.-D., Kim, S. Y., Park, H.-S., & Jung, Y.-S. (2015). Orthognathic surgery and temporomandibular joint symptoms. *Maxillofacial Plastic and Reconstructive Surgery*, 37(1), 14. <https://doi.org/10.1186/s40902-015-0014-4>
- Katsumata, A., Nojiri, M., Fujishita, M., Arijii, Y., Arijii, E., & Langlais, R. P. (2006). Condylar head remodeling following mandibular setback osteotomy for prognathism: A comparative study of different imaging modalities. *Oral Surgery, Oral Medicine, Oral Pathology, Oral Radiology, and Endodontology*, 101(4), 505–514. <https://doi.org/10.1016/j.tripleo.2005.07.028>
- Kim, Y.-I., Jung, Y.-H., Cho, B.-H., Kim, J.-R., Kim, S.-S., Son, W.-S., & Park, S.-B. (2010). The assessment of the short- and long-term changes in the condylar position following sagittal split ramus osteotomy (SSRO) with rigid fixation. *Journal of Oral Rehabilitation*, 37(4), 262–270. <https://doi.org/10.1111/j.1365-2842.2009.02056.x>
- Loubele, M., Maes, F., Schutyser, F., Marchal, G., Jacobs, R., & Suetens, P. (2006). Assessment of bone segmentation quality of cone-beam CT versus multislice spiral CT: a pilot study. *Oral Surgery, Oral Medicine, Oral Pathology, Oral Radiology, and Endodontology*, 102(2), 225–234. <https://doi.org/10.1016/j.tripleo.2005.10.039>
- Maes, F., Collignon, A., Vandermeulen, D., Marchal, G., & Suetens, P. (1997). Multimodality image registration by maximization of mutual information. *IEEE Transactions on Medical Imaging*, 16(2), 187–198. <https://doi.org/10.1109/42.563664>
- Nackaerts, O., Depypere, M., Zhang, G., Vandenberghe, B., Maes, F., & Jacobs, R. (2015). Segmentation of Trabecular Jaw Bone on Cone Beam CT Datasets. *Clinical Implant Dentistry and Related Research*, 17(6), 1082–1091. <https://doi.org/10.1111/cid.12217>
- Park, S.-B., Yang, Y.-M., Kim, Y.-I., Cho, B.-H., Jung, Y.-H., & Hwang, D.-S. (2012). Effect of Bimaxillary Surgery on Adaptive Condylar Head Remodeling: Metric Analysis and Image

- Interpretation Using Cone-Beam Computed Tomography Volume Superimposition. *Journal of Oral and Maxillofacial Surgery*, 70(8), 1951–1959. <https://doi.org/10.1016/j.joms.2011.08.017>
- Plooi, J. M., Naphausen, M. T. P., Maal, T. J. J., Xi, T., Rangel, F. A., Swennnen, G., ... Bergé, S. J. (2009). 3D evaluation of the lingual fracture line after a bilateral sagittal split osteotomy of the mandible. *International Journal of Oral and Maxillofacial Surgery*, 38(12), 1244–1249. <https://doi.org/10.1016/j.ijom.2009.07.013>
- Ruellas, A. C. de O., Yatabe, M. S., Souki, B. Q., Benavides, E., Nguyen, T., Luiz, R. R., ... Cevidanes, L. H. S. (2016). 3D Mandibular Superimposition: Comparison of Regions of Reference for Voxel-Based Registration. *PLOS ONE*, 11(6), e0157625. <https://doi.org/10.1371/journal.pone.0157625>
- Schilling, J., Gomes, L. C. R., Benavides, E., Nguyen, T., Paniagua, B., Styner, M., ... Cevidanes, L. H. S. (2014). Regional 3D superimposition to assess temporomandibular joint condylar morphology. *Dentomaxillofacial Radiology*, 43(1), 20130273. <https://doi.org/10.1259/dmfr.20130273>
- Stratis, A., Zhang, G., Jacobs, R., Bogaerts, R., Politis, C., Shaheen, E., & Bosmans, H. (2016). Head CBCT vs head MSCT imaging; comparing organ doses and radiation risks for a cohort of orthognathic patients. *Physica Medica*, 32(Suppl 3), 210. <https://doi.org/10.1016/j.ejmp.2016.07.709>
- Swennen, G. R. J., Mommaerts, M. Y., Abeloos, J., De Clercq, C., Lamoral, P., Neyt, N., ... Schutyser, F. (2007). The Use of a Wax Bite Wafer and a Double Computed Tomography Scan Procedure to Obtain a Three-Dimensional Augmented Virtual Skull Model. *Journal of Craniofacial Surgery*, 18(3), 533–539. <https://doi.org/10.1097/scs.0b013e31805343df>
- Van Dessel, J., Huang, Y., Depypere, M., Rubira-Bullen, I., Maes, F., & Jacobs, R. (2013). A comparative evaluation of cone beam CT and micro-CT on trabecular bone structures in the human mandible. *Dentomaxillofacial Radiology*, 42(8), 20130145. <https://doi.org/10.1259/dmfr.20130145>
- Van Dessel, J., Nicolielo, L. F., Huang, Y., Coudyzer, W., Salmon, B., Lambrichts, I., & Jacobs,

- R. (2017). Accuracy and reliability of different cone beam computed tomography (CBCT) devices for structural analysis of alveolar bone in comparison with multislice CT and micro-CT. *European Journal of Oral Implantology*, 10(1), 95–105.
- Van Dessel, J., Nicolielo, L. F., Huang, Y., Slagmolen, P., Politis, C., Lambrichts, I., & Jacobs, R. (2016). Quantification of bone quality using different cone beam computed tomography devices: Accuracy assessment for edentulous human mandibles. *European Journal of Oral Implantology*, 9(4), 411–424.
- Vidra, M. A. L., Rozema, F. R., Kostense, P. J., & Tuinzing, D. B. (2002). Observer consistency in radiographic assessment of condylar resorption. *Oral Surgery, Oral Medicine, Oral Pathology, Oral Radiology, and Endodontology*, 93(4), 399–403. <https://doi.org/10.1067/moe.2002.121706>
- Wolford, L. M. (2001). Idiopathic Condylar Resorption of the Temporomandibular Joint in Teenage Girls (Cheerleaders Syndrome). *Baylor University Medical Center Proceedings*, 14(3), 246–252. <https://doi.org/10.1080/08998280.2001.11927772>
- Xi, T., Schreurs, R., Heerink, W. J., Bergé, S. J., & Maal, T. J. J. (2014). A Novel Region-Growing Based Semi-Automatic Segmentation Protocol for Three-Dimensional Condylar Reconstruction Using Cone Beam Computed Tomography (CBCT). *PLOS ONE*, 9(11), e111126. <https://doi.org/10.1371/journal.pone.0111126>
- Xi, T., Schreurs, R., van Loon, B., de Koning, M., Bergé, S., Hoppenreijts, T., & Maal, T. J. J. (2015). 3D analysis of condylar remodelling and skeletal relapse following bilateral sagittal split advancement osteotomies. *Journal of Cranio-Maxillofacial Surgery*, 43(4), 462–468. <https://doi.org/10.1016/j.jcms.2015.02.006>
- Xi, T., van Loon, B., Fudalej, P., Bergé, S., Swennen, G., & Maal, T. J. J. (2013). Validation of a novel semi-automated method for three-dimensional surface rendering of condyles using cone beam computed tomography data. *International Journal of Oral and Maxillofacial Surgery*, 42(8), 1023–1029. <https://doi.org/10.1016/j.ijom.2013.01.016>

Chapter 7

General discussion and conclusions

7.1 General discussion

This PhD thesis has shown the potential of CBCT images for objective assessment of bone quality and quantity to assist maxillofacial procedures. In light of what was already discussed in the previous chapters, this general discussion aims to debate the new concepts of CBCT image analysis, providing a general opinion of what these techniques can bring to our reality and how we should conceive these new concepts, taking into account that radiology is fundamentally a science of observation and interpretation.

CBCT imaging has become more popular during the last two decades and has enhanced its efficiency as a tool for 3D imaging of the craniofacial area. This technology started from initial basic prototypes and evolved into a faster and more advanced method of imaging, targeted at specific clinical applications (e.g. small volume scanners used in endodontics Accutomo 3D; J.Morita Corporation, Kyoto, Japan). This evolution of CBCT imaging was made possible through optimising its detector technology in the first place, but also by maximising its computing ability, able to deal with large volumes of data (Arai, Tammisalo, Iwai, Hashimoto, & Shinoda, 1999; Mozzo, Procacci, Tacconi, Tinazzi Martini, & Bergamo Andreis, 1998; Nemtoi, Czink, Haba, & Gahleitner, 2013).

CBCT is very suited for imaging the maxillofacial area. It provides clear images of highly contrasted structures and is extremely useful for evaluating bone (Sukovic, 2003; Ziegler, Woertche, Brief, & Hassfeld, 2002). CBCT certainly offers a significant benefit over conventional CT imaging by allowing isotropic data, high-resolution 3D visualisation of the maxillofacial skeleton with adjustable FOV sizes and concomitant reduction in patient dose (D. Schulze, Heiland, Thurmann, & Adam, 2004). Furthermore, it can be post-processed into visualisations similar to traditional dental radiology representations, such as panoramic, cross-sectional, cephalometric, or bilateral multiplanar projections of the temporomandibular joint (Adibi, Zhang, Servos, & O'Neill, 2012). Although CBCT allows images to be displayed in a variety of formats, the interpretation of the volumetric data set involves more than the generation of 3D representations or application of clinical protocols providing specific images. Image science provides a lot of useful metrics in order to describe the morphology and functions of human skeleton. These metrics, for example: density, texture features, volume, surface areas, diffusion and perfusion parameters, chemical composition and metabolic activity, are convenient tools that can give detailed information to surgeons regarding the patient's specific medical situation (Rosenkrantz et al., 2015).

The use of quantitative metrics has many advantages and makes detecting new patterns more efficient. These advantages include an optimised standardisation, comparison and goal setting, as well as the facilitation of modern computational and statistical techniques in order to analyse complex datasets. However, before any quantitative method can be deployed in a

real-world setting, it must go through a process of validation to demonstrate its reliability and relevance. The findings of the research studies, which were conducted on the accuracy and reliability of CBCT images for bone morphometry, are introduced in **Chapters 2 and 3**. Despite the common drawbacks that occur in *ex vivo* studies, this step is essential to understand inherent limitations in CBCT imaging and processing techniques, including determining an appropriate voxel size, segmentation values, and volume of interest. Varying these parameters causes changes in all morphometric measurements; thus, careful consideration must be taken to choose application-specific parameters. Thin structures, such as trabecular bone, requires small voxel size that is not bigger than 200 μm to still show a reliable structure pattern. If not, partial volume effect will change its configuration significantly. Bone structure is also sensitive to noise and artefacts due to scatter, beam hardening and photon starvation from CBCT (R. Schulze et al., 2011).

The quantitative measures used in our studies are typically calculated from binary images, requiring segmentation of the CBCT images into bone and non-bone voxels (Bouxsein et al., 2010). Segmentation becomes problematic when noise and artefacts are more pronounced; therefore, segmentation methods have to be adapted to cope with such imaging degradation. We have opted for adaptive thresholding algorithm which is a more robust method that allows the segmentation threshold to vary in every pixel of the image and cope reasonably well with the non-uniformity of intensity values in CBCT images (Batenburg & Sijbers, 2009; Rashed, Wang, & Kudo, 2011).

Our validation studies have focussed mostly on the applicability of small FOVs due to our small samples. In a clinical practice, small FOV protocols may produce clearer images with better clarity because they can avoid structures out of the ROI that are more prone to beam hardening (Haridas, Mohan, Papisetti, & Ealla, 2016). On the other hand, small FOVs are often associated with a higher radiation dose that can generate images with increased noise and scatter. Thus, we must keep in mind that high-resolution images do not always provide better image quality (Valentin, 2007), and some CBCT machines can provide enough image quality with lower resolution for trabecular bone segmentation.

As we move towards more sophisticated methods, capable to extract more radiological data, handling of high-quality 3D medical data becomes cumbersome and time-consuming for clinical settings. Therefore, efforts are still necessary to improve and automatise workflows. Computer-assisted techniques have been used because they reduce the time to analyse complex data and increase diagnostic accuracy (Kavitha, Asano, Taguchi, Kurita, & Sanada, 2012). **Chapter 4** showed that a computer-based method can assist automatic bone quality classification using 3D features of the trabecular bone that have low individual detectability. Incorporation of an effective workflow in the clinical practice, however, it is taking place slowly and deliberately. Much of this is due to the lack of standardisation in data generation and

collection for multicentre studies (Ker, Wang, Rao, & Lim, 2018). As healthcare professionals, we must consider taking the most advantage of 3D features to generate relevant clinical data that will further guide diagnosis, surgical planning and monitoring.

In **Chapters 5 and 6** the applicability of our methods was demonstrated in clinical data with standardised image acquisition protocol between and within subjects. Standardisation is important so that analysis errors can be considered to occur systematically and therefore, it is not necessary to prevent correct relative comparisons between groups and over time (Waarsing, Day, & Weinans, 2004). As mentioned above, high-resolution protocols are not always necessary to perform bone structure analysis. Medium and large FOV protocols can produce smoother images due to scatter reduction. Still, the applicability of these quantification methods remains challenging for low-dose CBCT modality as well as images with metal and movement artefacts, as regularly founded in orthognathic and implant rehabilitated patients. Our findings could help further optimisation of CBCT acquisition protocols (Jacobs, Salmon, Codari, Hassan, & Bornstein, 2018; McGuigan, Duncan, & Horner, 2018), as well as the developing of more robust pre- and post-processing image algorithms for jaw bone structure analysis.

Although clinical studies are challenging due to inherent confounding, they are essential to help translate the quantitative methods in a clinical-setting. Additionally, in **Chapters 5 and 6**, the relationship between 3D bone morphometric parameters and treatment outcomes were investigated. While **Chapter 5** showed significant bone structural differences between early failed and survived implant sites, **Chapter 6** demonstrated significant changes in condylar mineralisation pre- and post- bimaxillary surgery. This is not the first time that bone structure quantification helps as prognostic test. Previously studies have shown the usefulness of bone parameters in predicting bone fracture in several clinical contexts, such as osteoporosis, diabetes and hyperparathyroidism (Harvey et al., 2015). Though quantification in radiology is surely an efficient method that is gaining popularity in the medical field, it is important to regard this quantification as a tool to support qualitative description and narrative context. As pre- and post-processing techniques entail an inevitable loss of vital information, it is primordial to contextualise the results of metrics and consider quantification in radiology as a medium to qualitatively describe and interpret images.

Even though CBCT imaging has advanced significantly over the past decade, there are still a few challenges to deal with. On a technical level, these challenges are related to the balances and trade-offs between spatial resolution, sample size, signal-to-noise ratio, radiation exposure and acquisition time. On a clinical level, these challenges include how the advantages of a broader understanding of bone structural features actually improves procedures outcomes and survival.

7.1.1 Future perspectives

7.1.1.1 Image analysis workflow

The 3D quantitative methods presented in this PhD thesis have proven valuable for scientific research. Although a variety of commercial medical imaging equipment now comes loaded with simple forms of image processing and analysis algorithms, which might range from basic thresholding to manual registration and ROI selection, radiologists and technologists use them to some extent. On the other hand, computer and software's to assist medical image analysis have rapidly evolved with more complex and efficient algorithms, which requires a steep learning curve and remains distant from clinicians. Thus, future research should be still directed for both improving and optimising image analysis workflow to simplify clinical applications. At the same time, efforts should be made in the standardisation and indication of image acquisition protocols to improve data quality.

7.1.1.2 Bone vascularity

With the rapid evolution of innovative methods, combination of image modalities through registration is expanding in the medical image field. For example, association of anatomic CT imaging with dynamic contrast-enhanced MRI (DCE-MRI) can characterise bone vascularity in the setting of acute trauma and bone repair (Chan et al., 2011; Chu et al., 2013; Dyke et al., 2015; Ma et al., 2012; Ma, Lv, Griffith, Yuan, & Leung, 2013; Michoux et al., 2012; Ng et al., 2013). As well as positron emission tomography can demonstrate quantitative measurements of bone blood flow and metabolism derived from dynamic ^{18}F -NaF imaging (Piert et al., 2001). These non-invasive measurements correlate well with invasive assessments of bone turnover, showing that subtle functional variation can be identified prior to the major structural change detectable by X-ray. It would be advantageous to use bone analysis in combination to blood flow assessment for early detection of bone diseases and healing disorders (Davies, 2003; Lethaus et al., 2013; Traini et al., 2006) in the context of maxillofacial procedures.

7.1.1.3 3D finite element models and bone printing

Finite element analysis (FEA) has been extensively used to predict bone displacements and estimate stress distributions at the implant-to bone interface and cortical bone structures. Thanks to the use of this technique, one can ascertain mechanical characteristics of dental implants on bone tissue, which one can never measure in vivo. However, the complex geometrical characterization of bone (especially of the trabecular bone) has forced researchers

to make important simplifications. Early FEA studies modelled bone as a simplified two-dimensional (2D) rectangular setup and often disregarded the trabecular bone network because they simply did not have the means to visualize it. These 2D evaluation methods were limited in level of accuracy and reliability, as the structure of the bone cannot be taken into account (Korioth & Versluis, 1997). The results presented in this thesis could support future studies on accuracy assessment of different clinical CBCT machines for stress and strain distribution using both full trabecular and cortical bone structures models. CBCT-based finite element models could provide an improved approach for predicting the ultimate stress and strain of trabecular bone which is needed to perform FEA simulations in biomechanical analyses with dental implants rehabilitations.

Three-dimensionally printed anatomical models are rapidly becoming an integral part of pre-operative planning and treatment (custom-made prostheses) of complex surgical cases (Diment, Thompson, & Bergmann, 2017; Eley, Richards, Dobson, Linney, & Watt-Smith, 2011; Martelli et al., 2016). This is largely due to improvement in 3D models accuracy supported by better image quality and segmentation techniques. Nevertheless, bone prototypes in maxillofacial care are still mostly CT-based. We hope that this thesis serves as basis for applications in CBCT-based 3D bone printing in parallel with advancements in scanners technology and bioprinting materials.

7.2 Conclusions

In conclusion, the findings of this PhD thesis showed that CBCT-based bone structural analysis could offer a reliable and objective support to human understanding of bone quality and quantity in oral and maxillofacial procedures. More specifically:

- CBCT can be used for 3D analysis of both dentate and edentulous alveolar bone structure when considering adequate CBCT imaging protocol and device;
- Computer-aided trabecular bone pattern assessment based on morphometric parameters could assist objectivity in clinical bone quality classification;
- Although *in vivo* CBCT high-resolution images of trabecular bone microstructure are technically challenging, 3D morphometric analysis of jaw bone structure can offer a standardised method to plan and follow-up oral and maxillofacial procedures.

7.3 References

- Adibi, S., Zhang, W., Servos, T., & O'Neill, P. N. (2012). Cone beam computed tomography in dentistry: what dental educators and learners should know. *Journal of Dental Education*, 76(11), 1437–1442. <http://www.ncbi.nlm.nih.gov/pubmed/23144478>
- Arai, Y., Tammisalo, E., Iwai, K., Hashimoto, K., & Shinoda, K. (1999). Development of a compact computed tomographic apparatus for dental use. *Dentomaxillofacial Radiology*, 28(4), 245–248. <https://doi.org/10.1038/sj.dmfr.4600448>
- Batenburg, K. J., & Sijbers, J. (2009). Adaptive thresholding of tomograms by projection distance minimization. *Pattern Recognition*, 42(10), 2297–2305. <https://doi.org/10.1016/j.patcog.2008.11.027>
- Bouxsein, M. L., Boyd, S. K., Christiansen, B. A., Guldberg, R. E., Jepsen, K. J., & Müller, R. (2010). Guidelines for assessment of bone microstructure in rodents using micro-computed tomography. *Journal of Bone and Mineral Research*, 25(7), 1468–1486. <https://doi.org/10.1002/jbmr.141>
- Chan, W. P., Liu, Y.-J., Huang, G.-S., Lin, M.-F., Huang, S., Chang, Y.-C., & Jiang, C.-C. (2011). Relationship of Idiopathic Osteonecrosis of the Femoral Head to Perfusion Changes in the Proximal Femur by Dynamic Contrast-Enhanced MRI. *American Journal of Roentgenology*, 196(3), 637–643. <https://doi.org/10.2214/AJR.10.4322>
- Chu, S., Karimi, S., Peck, K. K., Yamada, Y., Lis, E., Lyo, J., ... Holodny, A. I. (2013). Measurement of Blood Perfusion in Spinal Metastases With Dynamic Contrast-Enhanced Magnetic Resonance Imaging. *Spine*, 38(22), E1418–E1424. <https://doi.org/10.1097/BRS.0b013e3182a40838>
- Davies, J. E. (2003). Understanding peri-implant endosseous healing. *Journal of Dental Education*, 67(8), 932–949. <http://www.ncbi.nlm.nih.gov/pubmed/12959168>
- Diment, L. E., Thompson, M. S., & Bergmann, J. H. M. (2017). Clinical efficacy and effectiveness of 3D printing: a systematic review. *BMJ Open*, 7(12), e016891. <https://doi.org/10.1136/bmjopen-2017-016891>

- Dyke, J. P., Lazaro, L. E., Hettrich, C. M., Hentel, K. D., Helfet, D. L., & Lorich, D. G. (2015). Regional analysis of femoral head perfusion following displaced fractures of the femoral neck. *Journal of Magnetic Resonance Imaging*, 41(2), 550–554. <https://doi.org/10.1002/jmri.24524>
- Eley, K. A., Richards, R., Dobson, D., Linney, A., & Watt-Smith, S. R. (2011). Re: development of in-house rapid manufacturing of three-dimensional models in maxillofacial surgery. *British Journal of Oral and Maxillofacial Surgery*, 49(4), 326–327. <https://doi.org/10.1016/j.bjoms.2010.09.019>
- Haridas, H., Mohan, A., Papisetti, S., & Ealla, K. K. R. (2016). Computed tomography: Will the slices reveal the truth. *Journal of International Society of Preventive and Community Dentistry*, 6(8), 85–92. <https://doi.org/10.4103/2231-0762.189734>
- Harvey, N. C., Glüer, C. C., Binkley, N., McCloskey, E. V., Brandi, M.-L., Cooper, C., ... Kanis, J. A. (2015). Trabecular bone score (TBS) as a new complementary approach for osteoporosis evaluation in clinical practice. *Bone*, 78, 216–224. <https://doi.org/10.1016/j.bone.2015.05.016>
- Jacobs, R., Salmon, B., Codari, M., Hassan, B., & Bornstein, M. M. (2018). Cone beam computed tomography in implant dentistry: recommendations for clinical use. *BMC Oral Health*, 18(1), 88–103. <https://doi.org/10.1186/s12903-018-0523-5>
- Kavitha, M. S., Asano, A., Taguchi, A., Kurita, T., & Sanada, M. (2012). Diagnosis of osteoporosis from dental panoramic radiographs using the support vector machine method in a computer-aided system. *BMC Medical Imaging*, 12(1), 1–11. <https://doi.org/10.1186/1471-2342-12-1>
- Ker, J., Wang, L., Rao, J., & Lim, T. (2018). Deep Learning Applications in Medical Image Analysis. *IEEE Access*, 6, 9375–9389. <https://doi.org/10.1109/ACCESS.2017.2788044>
- Keyak, J. H., Rossi, S. A., Jones, K. A., & Skinner, H. B. (1997). Prediction of femoral fracture load using automated finite element modeling. *Journal of Biomechanics*, 31(2), 125–133. [https://doi.org/10.1016/S0021-9290\(97\)00123-1](https://doi.org/10.1016/S0021-9290(97)00123-1)
- Korioth, T. W. P., & Versluis, A. (1997). Modeling the mechanical behavior of the jaws and

- them related structures by finite element (FE) analysis. *Critical Reviews in Oral Biology and Medicine*. <https://doi.org/10.1177/10454411970080010501>
- Lang, T. F., Guglielmi, G., van Kuijk, C., De Serio, A., Cammisa, M., & Genant, H. K. (2002). Measurement of bone mineral density at the spine and proximal femur by volumetric quantitative computed tomography and dual-energy x-ray absorptiometry in elderly women with and without vertebral fractures. *Bone*, 30(1), 247–250. [https://doi.org/10.1016/S8756-3282\(01\)00647-0](https://doi.org/10.1016/S8756-3282(01)00647-0)
- Lang, T. F., Keyak, J. H., Heitz, M. W., Augat, P., Lu, Y., Mathur, A., & Genant, H. K. (1997). Volumetric quantitative computed tomography of the proximal femur: Precision and relation to bone strength. *Bone*, 21(1), 101–108. [https://doi.org/10.1016/S8756-3282\(97\)00072-0](https://doi.org/10.1016/S8756-3282(97)00072-0)
- Lethaus, B., Poort, L., Yamauchi, K., Kloss-Brandstätter, A., Boeckmann, R., & Kessler, P. (2013). Qualitative bone CT as a tool to assess vascularization in irradiated bone: an animal study. *Clinical Oral Implants Research*, 24(7), 746–749. <https://doi.org/10.1111/j.1600-0501.2012.02480.x>
- Lotz, J. C., Gerhart, T. N., & Hayes, W. C. (1990). Mechanical Properties of Trabecular Bone from the Proximal Femur. *Journal of Computer Assisted Tomography*, 14(1), 107–114. <https://doi.org/10.1097/00004728-199001000-00020>
- Ma, H. T., Griffith, J. F., Zhao, X., Lv, H., Yeung, D. K. W., & Leung, P.-C. (2012). Relationship between marrow perfusion and bone mineral density: A pharmacokinetic study of DCE-MRI. In *2012 Annual International Conference of the IEEE Engineering in Medicine and Biology Society* (pp. 377–379). IEEE. <https://doi.org/10.1109/EMBC.2012.6345947>
- Ma, H. T., Lv, H., Griffith, J. F., Yuan, J., & Leung, P.-C. (2013). Bone marrow perfusion of proximal femur varied with BMD - A longitudinal study by DCE-MRI. In *2013 35th Annual International Conference of the IEEE Engineering in Medicine and Biology Society (EMBC)* (pp. 2607–2610). IEEE. <https://doi.org/10.1109/EMBC.2013.6610074>
- Martelli, N., Serrano, C., van den Brink, H., Pineau, J., Prognon, P., Borget, I., & El Batti, S. (2016). Advantages and disadvantages of 3-dimensional printing in surgery: A systematic

- review. *Surgery*, 159(6), 1485–1500. <https://doi.org/10.1016/j.surg.2015.12.017>
- McGuigan, M. B., Duncan, H. F., & Horner, K. (2018). An analysis of effective dose optimization and its impact on image quality and diagnostic efficacy relating to dental cone beam computed tomography (CBCT). *Swiss Dental Journal*, 128(4), 297–316. https://www.sso.ch/fileadmin/upload_sso/2_Zahnaerzte/2_SDJ/SDJ_2018/SDJ_Pubmed_2018/sdj-2018-04-02.pdf
- Michoux, N., Simoni, P., Tombal, B., Peeters, F., Machiels, J.-P., & Lecouvet, F. (2012). Evaluation of DCE-MRI postprocessing techniques to assess metastatic bone marrow in patients with prostate cancer. *Clinical Imaging*, 36(4), 308–315. <https://doi.org/10.1016/j.clinimag.2011.10.002>
- Mozzo, P., Procacci, C., Tacconi, A., Tinazzi Martini, P., & Bergamo Andreis, I. A. (1998). A new volumetric CT machine for dental imaging based on the cone-beam technique: preliminary results. *European Radiology*, 8(9), 1558–1564. <https://doi.org/10.1007/s003300050586>
- Nemtoi, A., Czink, C., Haba, D., & Gahleitner, A. (2013). Cone beam CT: a current overview of devices. *Dentomaxillofacial Radiology*, 42(8), 20120443. <https://doi.org/10.1259/dmfr.20120443>
- Ng, A. W. H., Griffith, J. F., Taljanovic, M. S., Li, A., Tse, W. L., & Ho, P. C. (2013). Is dynamic contrast-enhanced MRI useful for assessing proximal fragment vascularity in scaphoid fracture delayed and non-union? *Skeletal Radiology*, 42(7), 983–992. <https://doi.org/10.1007/s00256-013-1627-2>
- Piert, M., Zittel, T. T., Becker, G. A., Jahn, M., Stahlschmidt, A., Maier, G., ... Bares, R. (2001). Assessment of Porcine Bone Metabolism by Dynamic [18F]Fluoride Ion PET: Correlation with Bone Histomorphometry. *Journal of Nuclear Medicine*, 42(7), 1091–1100. <http://jnm.snmjournals.org/content/42/7/1091.long>
- Rashed, E. A., Wang, Z., & Kudo, H. (2011). Adaptive thresholding for robust iterative image reconstruction from limited views projection data. In *2011 IEEE Nuclear Science Symposium Conference Record* (pp. 4249–4252). IEEE.

<https://doi.org/10.1109/NSSMIC.2011.6153815>

- Rosenkrantz, A. B., Mendiratta-Lala, M., Bartholmai, B. J., Ganeshan, D., Abramson, R. G., Burton, K. R., ... Lenchik, L. (2015). Clinical Utility of Quantitative Imaging. *Academic Radiology*, 22(1), 33–49. <https://doi.org/10.1016/j.acra.2014.08.011>
- Schulze, D., Heiland, M., Thurmann, H., & Adam, G. (2004). Radiation exposure during midfacial imaging using 4- and 16-slice computed tomography, cone beam computed tomography systems and conventional radiography. *Dentomaxillofacial Radiology*, 33(2), 83–86. <https://doi.org/10.1259/dmfr/28403350>
- Schulze, R., Heil, U., Groß, D., Bruellmann, D., Dranischnikow, E., Schwanecke, U., & Schoemer, E. (2011). Artefacts in CBCT: a review. *Dentomaxillofacial Radiology*, 40(5), 265–273. <https://doi.org/10.1259/dmfr/30642039>
- Sukovic, P. (2003). Cone beam computed tomography in craniofacial imaging. *Orthodontics and Craniofacial Research*, 6(s1), 31–36. <https://doi.org/10.1034/j.1600-0544.2003.259.x>
- Traini, T., Assenza, B., Roman, F. S., Thams, U., Caputi, S., & Piattelli, A. (2006). Bone microvascular pattern around loaded dental implants in a canine model. *Clinical Oral Investigations*, 10(2), 151–156. <https://doi.org/10.1007/s00784-006-0043-6>
- Valentin, J. (2007). Managing patient dose in multi-detector computed tomography(MDCT). ICRP Publication 102. *Annals of the ICRP*, 37(1), 1–79, iii. <http://www.ncbi.nlm.nih.gov/pubmed/18069128>
- Waarsing, J. H., Day, J. S., & Weinans, H. (2004). An Improved Segmentation Method for In Vivo μ CT Imaging. *Journal of Bone and Mineral Research*, 19(10), 1640–1650. <https://doi.org/10.1359/JBMR.040705>
- Ziegler, C. M., Woertche, R., Brief, J., & Hassfeld, S. (2002). Clinical indications for digital volume tomography in oral and maxillofacial surgery. *Dento Maxillo Facial Radiology*. <https://doi.org/10.1038/sj/dmfr/4600680>

Summary

In oral and maxillofacial surgery, 3D radiographs have become a breakthrough technique required for diagnosis and treatment planning and follow-up. Nevertheless, 3D capabilities are not fully explored and bone assessment still relies on subjective and 2D methods. Due to the rapid technological advances in dentomaxillofacial radiology, new image analysis based on 3D Cone-Beam Computed Tomography (CBCT) scans could take into account not only bone quantity but also structure.

The primary goal of this thesis was to assess 3D clinical methodologies to quantify and qualify bone for oral maxillofacial procedures. More specifically developing and assessing accuracy and reliability of 3D methods, and the relation of bone morphometric parameters with treatment outcomes.

The first chapter starts with an overview of the evolution of 2D to 3D radiographic clinical evaluation of maxillofacial bone, followed by the aims and hypotheses of this doctoral thesis.

In **Chapters 2 and 3** the accuracy and reliability of several CBCT machines to assess 3D alveolar bone structure was investigated in comparison with the gold standard micro-CT and the clinical reference MSCT. Although overall morphometric analysis showed significant overestimation for all CBCTs and MSCT when compared to micro-CT, a significant structure pattern similarity was found for most of CBCT modalities and high-resolution MSCT, making it a clinical alternative for structure analysis of alveolar bone.

Subsequently, in **Chapter 4**, a machine learning method was developed and evaluated to assist objectivity in clinical bone quality classification. This computer-based classification performed better than a classic subjective evaluation, with 79% prediction accuracy. These findings confirm that objective methods are necessary for evaluation of trabecular bone structure in 3D.

Based on the acknowledge in cluster analysis of the previous study, the relation of trabecular bone morphometric parameters and implant survival was investigated in **Chapter 5**. This matched-control study showed a significant relationship between trabecular bone pattern and implant survival, where especially extreme bone qualities could lead to early implant failure.

In the last study, **Chapter 6**, a 3D method to follow-up condylar remodelling after bimaxillary surgery was proposed and validated. This novel analysis method revealed differences between preoperative and postoperative condyle mineralized bone with less than one voxel-size error and good to excellent reproducibility. It can offer objectivity in the assessment and follow-up of pathological condylar resorption after orthognathic surgeries.

Finally, **Chapter 7** presents an overall discussion and conclusion from the studies described in the previous chapters. The findings of this doctoral thesis showed that CBCT imaging is a

valuable clinical tool to produce reliable analysis of maxillofacial bone if the correct scan protocol is used and errors are taken into account. With the current methods, bone imaging analysis workflow can be developed to answer relevant maxillofacial research questions.

Samenvatting

In de orale en maxillofaciale heelkunde is driedimensionele (3D) beeldvorming een belangrijke techniek voor diagnose, planning en de follow-up van de behandeling. Desondanks zijn de voordelen van deze 3D weergave nog niet volledig geëxploiteerd en gebeurt de beoordeling van botkwaliteit voornamelijk op basis van tweedimensionale (2D) radiografieën. Doch, door de snelle technologische vooruitgang in de dentomaxillofaciale radiologie, nieuwe beeldanalyses op basis van 3D Cone-Beam Computed Tomography (CBCT) scans zouden niet alleen botkwantiteit maar ook structuur in rekening kunnen brengen.

Het hoofddoel van dit proefschrift was het ontwikkelen en valideren van nieuwe innovatieve methoden die een automatische en objectieve evaluatie van botkwaliteit toe laten in het kader van orale en maxillofaciale chirurgische procedures. In **hoofdstuk 1** wordt er een overzicht gegeven van de evolutie van 2D naar 3D radiografische evaluatie van bot, gevolgd door de doelstellingen en hypothesen van dit proefschrift.

In **hoofdstukken 2 en 3** werd de nauwkeurigheid en betrouwbaarheid van 3D botkwaliteit evaluatie doormiddel van morfometrische bot parameters in zeven CBCT-machines vergeleken met de gouden standaard micro-CT en het klinisch alternatief, de multi-slice CT (MSCT). Zowel CBCT als MSCT waren geassocieerd met een klinische en statistisch significante meetfout. Het structurele patroon van het alveolaire bot bleef echter vergelijkbaar met dat van de micro-CT en MSCT voor 5 van de 7 CBCT machines. Deze studies tonen aan dat het merendeel van de CBCT machines alveolaire botkwaliteit kwantitatief kunnen beoordelen, met een nauwkeurigheid en betrouwbaarheid die micro-CT benadert.

In **Hoofdstuk 4** werden morfometrische bot parameters uit 100 CBCT scans gebruikt in machine-learning technieken om zo een automatische en objectieve klinische classificatie van botkwaliteit te ontwikkelen. Er werden drie soorten trabeculaire botclusters geïdentificeerd: dun, middelmatig en dens bot. Deze computer-gebaseerde classificatie presteerde beter dan een klassieke subjectieve evaluatie uitgevoerd door 4 onafhankelijken dentomaxillofaciale radiologen. Computerondersteunde beoordeling van het trabeculaire botpatroon op basis van morfometrische parameter zou kunnen helpen in de voorspelling van behandelingssucces bij orale en maxillofaciale ingrepen.

Voortbouwend op de vorige studie, werd in **Hoofdstuk 5** de relatie onderzocht tussen trabeculaire botmorfometrische parameters en implantaatoverleving. Deze klinische case-control studie toonde een significante relatie aan tussen het trabeculaire botpatroon en de implantaatoverleving, waarbij vooral extreme botkwaliteiten kunnen leiden tot vroeg implantaatfalen.

In het laatste onderzoek, **Hoofdstuk 6**, werd een 3D-methode voor de follow-up van de condylar-hermodellering na bimaxillaire chirurgie ontwikkeld en gevalideerd. Deze nieuwe analysemethode onthulde verschillen tussen de mineralisatie van de preoperatieve en postoperatieve condylus op basis van een zeer nauwkeurige evaluatieprocedure (meetfout beperkt tot 1 voxel) met goede tot uitstekende reproduceerbaarheid. Deze nieuwe evaluatietechniek kan gebruikt worden om klinische objectief condylaire veranderingen te bestuderen na orthognathische chirurgie (vb. detectie en follow-up pathologische condylaire resorptie).

Ten slotte presenteert **Hoofdstuk 7** een algemene discussie en conclusie uit de studies die in de voorgaande hoofdstukken zijn beschreven. De bevindingen van dit proefschrift hebben aangetoond dat CBCT-beeldvorming een waardevol klinisch hulpmiddel is om een betrouwbare analyse van maxillofaciaal bot te produceren als het juiste scanprotocol wordt gebruikt en met fouten rekening wordt gehouden. Met de huidige methoden kan botanalyse workflow worden ontwikkeld om relevante maxillofaciale onderzoeksvragen te beantwoorden.

Curriculum vitae



Laura Nicolielo was born in Porto Velho, Brazil on April 18th 1985. After completing the Dental School education at the University of São Paulo (USP) in 2009, she followed training in Oral Surgery in 2010. In 2011, she started her master studies in Applied Dental Sciences with focus on Oral Radiology & Pathology also at USP. At the same time, she specialized in Oral Implantology accomplishing both master and specialist titles in 2013.

After applying for a full PhD position with the Brazilian National Grant (CAPES – BEX 9419/13-6), she simultaneously started in October 2013 Postgraduate in Advanced Medical Image and PhD training in the OMFS-IMPATh Research Group at KU Leuven, under supervision of Prof. Dr. Reinhilde Jacobs and Prof. Dr. Ivo Lambrichts (UHasselt). During this period, her research was focussed on developing 3D radiological methods for objective analysis in dentistry.

Publications

Nicolielo, L. F. P., Van Dessel, J., Jacobs, R., Quirino Silveira Soares, M., & Collaert, B. (2019). Relationship between trabecular bone architecture and early dental implant failure in the posterior region of the mandible. *Clinical Oral Implants Research*. doi: 10.1111/clr.13551

Celikten, B., Jacobs, R., de Faria Vasconcelos, K., Huang, Y., Shaheen, E., **Nicolielo, L.F.P.**, Orhan, K. (2019). Comparative evaluation of cone beam CT and micro-CT on blooming artifacts in human teeth filled with bioceramic sealers. *Clinical Oral Investigations*, 23(8) 3267-3273. doi: 10.1007/s00784-018-2748-8.

Vasconcelos, K.F., Codari, M., Queiroz, P.M., **Nicolielo, L.F.P.**, Freitas, D.Q., Sforza, C., Jacobs, R., Haiter-Neto, F. (2019). The performance of metal artifact reduction algorithms in cone beam computed tomography images considering the effects of materials, metal positions, and fields of view. *Oral Surgery Oral Medicine Oral Pathology Oral Radiology*, 127(1), 71-76. doi: 10.1016/j.oooo.2018.09.004

Nicolielo, L.F.P., Van Dessel, J., van Lenthe, G.H., Lambrichts, I., Jacobs, R. (2018). Computer-based automatic classification of trabecular bone pattern can assist radiographic bone quality assessment at dental implant site. *British Journal of Radiology*, 91(1092), 20180437. doi: 10.1259/bjr.20180437.

Orhan, K., Jacobs, R., Celikten, B., Huang, Y., de Faria Vasconcelos, K., **Nicoliello, L.F.P.**, Buyuksungur, A., Van Dessel, J. (2018). Evaluation of Threshold Values for Root Canal Filling Voids in Micro-CT and Nano-CT Images. *Scanning*, 2018:9437569. doi: 10.1155/2018/9437569.

Oenning, A.C., Salmon, B., Vasconcelos, K.F., **Pinheiro Nicoliello, L.F.**, Lambrichts, I., Sanderink, G., Pauwels, R.; DIMITRA Group, Jacobs, R. (2018). DIMITRA paediatric skull phantoms: development of age-specific paediatric models for dentomaxillofacial radiology research. *Dentomaxillofacial Radiology*, 47(3), 20170285. doi: 10.1259/dmfr.20170285.

Codari, M., de Faria Vasconcelos, K., **Ferreira Pinheiro Nicoliello, L.**, Haiter Neto, F., Jacobs, R. (2017). Quantitative evaluation of metal artifacts using different CBCT devices, high-density materials and field of views. *Clinical Oral Implants Research*, 28(12), 1509-1514. doi: 10.1111/clr.13019.

Nicoliello, L.F.P., Jacobs, R., Ali Albdour, E., Hoste, X., Abeloos, J., Politis, C., Swennen, G. (2017). Is oestrogen associated with mandibular condylar resorption? A systematic review. *International Journal of Oral & Maxillofacial Surgery*, 46(11), 1394-1402. doi:10.1016/j.ijom.2017.06.012.

Celikten, B., Jacobs, R., de Faria Vasconcelos, K., Huang, Y., **Nicoliello, L.F.P.**, Orhan, K. (2017). Assessment of Volumetric Distortion Artifact in Filled Root Canals Using Different Cone-beam Computed Tomographic Devices. *Journal of Endodontics*, 43(9), 1517-1521. doi: 10.1016/j.joen.2017.03.035.

Huang, Y., Celikten, B., de Faria Vasconcelos, K., **Ferreira Pinheiro Nicoliello, L.**, Lippiatt, N., Buyuksungur, A., Jacobs, R., Orhan, K. (2017) Micro-CT and nano-CT analysis of filling quality of three different endodontic sealers. *Dentomaxillofacial Radiology*, 46(8), 20170223. doi: 10.1259/dmfr.20170223.

De Mol, A., **Nicoliello, L.**, Ghekiere, O., Jacobs, R., Politis, C. (2017). Dislocation of a mandibular condyle in the middle cranial fossa, diagnosed 54 years after trauma. *Journal of Surgical Case Reports*, 2017(7), rjx149. doi: 10.1093/jscr/rjx149.

Nicoliello, L.F.P., Van Dessel, J., Shaheen, E., Letelier, C., Codari, M., Politis, C., Lambrichts, I., Jacobs, R. (2017). Validation of a novel imaging approach using multi-slice CT and cone-

beam CT to follow-up on condylar remodeling after bimaxillary surgery. *International Journal of Oral Science*, 9(3), 139-144. doi: 10.1038/ijos.2017.22.

Politis, C., Agbaje, J., Van Hevele, J., **Nicoliello, L.**, De Laat, A., Lambrichts, I., & Jacobs, R. (2017). Report of Neuropathic Pain After Dental Implant Placement: A Case Series. *The International Journal of Oral & Maxillofacial Implants*, 32(2), 439-444. doi: 10.11607/jomi.5241.

Gendviliene, I., Legrand, P., **Nicoliello, L.F.P.**, Sinha, D., Spaey, Y., Politis, C., Jacobs, R. (2017). Conservative management of large dentigerous cysts with a novel approach for follow up. *Stomatologija*, 19 (1), 24-32.

Van Dessel, J., **Nicoliello, L.F.**, Huang, Y., Coudyzer, W., Salmon, B., Lambrichts, I., Jacobs, R. (2017). Accuracy and reliability of different cone beam computed tomography (CBCT) devices for structural analysis of alveolar bone in comparison with multislice CT and micro-CT. *European Journal of Oral Implantology*, 10(1), 95-105.

Van Dessel, J., **Nicoliello, L.F.**, Huang, Y., Slagmolen, P., Politis, C., Lambrichts, I., Jacobs, R. (2016). Quantification of bone quality using different cone beam computed tomography devices: Accuracy assessment for edentulous human mandibles. *European Journal of Oral Implantology*, 9(4), 411-424.

Vasconcelos, K.F., **Nicoliello, L.F.**, Nascimento, M.C., Haiter-Neto, F., Bóscolo, F.N., Van Dessel, J., EzEldeen, M., Lambrichts, I., Jacobs, R. (2015). Artefact expression associated with several cone-beam computed tomographic machines when imaging root filled teeth. *International Endodontic Journal*, 48(10), 994-1000. doi: 10.1111/iej.12395.

Nicoliello, L.F., Van Dessel, J., Jacobs, R., Martens, W., Lambrichts, I., Rubira-Bullen, I.R. (2014). Presurgical CBCT assessment of maxillary neurovascularization in relation to maxillary sinus augmentation procedures and posterior implant placement. *Surgical and Radiologic Anatomy*, 36(9), 915-24. doi: 10.1007/s00276-014-1309-3.

Nicoliello, L.F.P., Tinoco-Araujo, J.E., Chinellato, L.E.M., Santos, P.S.S. (2013). "Manifestações Oraís em Pacientes Portadores da Síndrome da Imunodeficiência Adquirida (Sida/Aids): Uma Revisão Atualizada". *Prática Hospitalar*. Ano XV Nº 85 Jan-Fev/2013.

Articles in preparation

Van Dessel, J., **Nicoliello, L.F.P.**, Jacobs, R., van Lenthe, G.H. Accuracy of three-dimensional finite element modelling of trabecular and cortical bone structures using cone beam computed tomography. *In preparation*.

Meeting abstracts, presented at international scientific conferences and symposia

Nicoliello, L.F.P., Van Dessel, J., van Lenthe, G.H., Lambrichts, I., Jacobs, R. (2018). Computer-aided bone quality classification. In: XVI European Congress of Dento Maxillo Facial Radiology, Lucerne, Switzerland.

Nicoliello, L.F.P., Van Dessel, J., Codari, M., Kakar, A., Shaheen, E., Politis, C., Jacobs, R. (2016). A novel imaging approach to follow-up of condylar remodeling following bimaxillary surgery. In: XV European Congress of Dento Maxillo Facial Radiology, Cardiff, Wales. [Selected for Oral Research Award].

Nicoliello, L.F.P., Van Dessel, J., Codari, M., De Mol, A., Kakar, A., Politis, C., Jacobs, R. (2016). A novel imaging approach to follow-up of condylar remodeling following bimaxillary surgery. In: MKA Spring Symposium – Orthognathic Surgery & Harmonization of the Face, Brussels, Belgium.

Legrand, P., Gendviliene, I., **Nicoliello, L.F.P.**, Jacobs, R. (2015). Conservative management of large dentigerous cyst with a novel approach for treatment follow up. In: The 8th Baltic Morphology Scientific Conference: Interdisciplinary nature of contemporary morphology, Vilnius, Lithuanian. [1st place in E-Poster Presentation Award].

Lamira, A., Jacobs, R., **Nicoliello, L.F.P.**, Souza Neto, M.D. (2015). Root canal anatomy of mandibular molars assessed by MicroCT. In: International Congress of Dento Maxillo Facial Radiology, Santiago, Chile.

Van Dessel, J., Huang, Y., **Nicoliello, L.F.P.**, Slagmolen, P., Jacobs, R. (2015). The reliability of cone-beam computed tomography to analyze trabecular and cortical bone structures: an in-vitro study. In: European Association for Osseointegration Congress, Stockholm, Sweden.

Vasconcelos, K.F., **Nicoliello, L.F.P.**, Nascimento, M.C., Haiter-Neto, F., Bóscolo, F.N., Van Dessel, J. (2014). Estudo dos padrões de artefatos em imagens obtidas por meio de

tomografia computadorizada de feixe cônico. In: XIX Jornada da Associação Brasileira de Radiologia Odontológica (JABRO), Vitória, Brasil.

De Clercq, C., Abeloos, J., **Nicolielo, L.F.P.**, Van Dessel, J., Barbier, L., Jacobs, R. (2014). Quantitative assessment of bone volume in reconstructed atrophic jaws. In: XIV ECDMFR Cluj-Napoca, Romania. [Selected for the Travel Grant Award].

Van Dessel, J., Huang, Y., **Nicolielo, L.F.P.**, Slagmolen, P., Jacobs, R. (2014). Accuracy of different cone-beam CT devices for trabecular bone structure analysis: an in vitro study. In: XIV ECDMFR, Cluj-Napoca, Romania. [1st place in Oral Research Award].

Van Dessel, J., Huang, Y., **Nicolielo, L.F.P.**, Slagmolen, P., Jacobs, R. (2014). Accuracy of different cone-beam CT devices for trabecular bone structure analysis: an in vitro study. In: 1st EADMFR Junior Meeting, Umeå, Sweden.

Nicolielo, L.F.P., Van Dessel, J., Lauris, J.R.P., Martens, W., Lambrichts, I., Jacobs, R., Rubira-Bullen, I. (2013). Study of the superior alveolar canals using Cone- Beam Computed Tomography. In: 19th International Congress of Dento-Maxillo-Facial Radiology (IADMFR), Bergen, Norway.

Nicolielo, L.F.P., Bravo-Calderon, D.M., Pagin, O., Oliveira, D.T., Santos, P.S.S. (2012). Parafunctional habit lesion: a diagnostic challenge. In: 16th International Congress on Oral Pathology and Medicine and 20th Brazilian Congress of Oral Medicine and Pathology, São Pedro, Brasil.

Nicolielo, L.F.P., Ikuta, C.R.S., Fernandes, L., Rubira-Bullen, I.R.F., Damante, J.H. (2012). Dor irradiada para o ouvido em portador de carcinoma espinocelular no assoalho da boca. In: V Jornada de Cirurgia e Traumatologia Bucomaxilofacial do Hospital Erasto Gaertner, Curitiba, Brasil.

Nicolielo, L.F.P., Pagin, O., Centurion, B.S., Imada, T.S.N., Poleti, M.L., Capelozza, A.L.A., Rubira-Bullen, I.R.F. (2011). Variabilidade dos valores de pixels de placas de fósforo do Sistema VistaScan. In: 28th Reunião Anual da Sociedade Brasileira de Pesquisa Odontológica, Águas de Lindóia, Brasil.

Nicolielo, L.F.P., Duarte, B.G., Ferreira Júnior, O., Salgueiro, D.G., Goncales, E.S., Sant'Ana, E. (2010). Posição ectópica dos segundo e terceiro molares inferiores (Kissing Molars). In: 23rd Congresso Odontológico de Bauru, Bauru, Brasil.

Scientific Acknowledgment

The author of this thesis was supported by Coordination for the Improvement of Higher Education Personnel (CAPES) program Science without borders from the Brazilian government (BEX 9419/13-6). Jeroen Van Dessel is a Research Foundation Flanders (FWO) research fellow (11.ZU.117N).

Chapter 2: Jeroen Van Dessel: Drafting article, critical revision and approval of article, data collection and analysis, statistics;

Laura Nicolielo: Critical revision and approval of article, data collection and analysis, statistics;

Yan Huang: Critical revision and approval of article, data collection and analysis;

Pieter Slagmolen: Data analysis, critical revision and approval of article;

Constantinus Politis, Ivo Lambrichts and Reinhilde Jacobs: Critical revision & approval of article.

Further acknowledgment to Imelda Hospital, Bonheiden, Belgium for kindly enabling the scanning on the i-CAT Next Generation system, to Walter Coudyzer for his help with the multi-slice CT and to the University Paris Descartes, Paris, France for kindly enabling the scanning on the GiANO 3D.

Chapter 3: Jeroen Van Dessel: Drafting, critical revision and approval of article, data collection and analysis, statistics;

Laura Nicolielo: Critical revision and approval of article, data collection and analysis, statistics;

Yan Huang: Critical revision and approval of article, data collection and analysis;

Walter Coudyzer: Data collection, critical revision and approval of article;

Benjamin Salmon: Data collection, critical revision and approval of article;

Ivo Lambrichts and Reinhilde Jacobs: Critical revision and approval of article.

Further acknowledgment go to Dr Dirk Withofs, Imelda Hospital, Bonheiden, Belgium for kindly enabling the scanning on the i-CAT Next Generation system, and to statistician Wim Coucke and engineer Pieter Slagmolen for their professional advice.

Chapter 4: Laura Nicolielo: Drafting article, critical revision and approval of article, data collection and analysis, statistics;

Jeroen Van Dessel: Critical revision and approval of article, data collection and analysis, statistics;

Harry van Lenthe: Data collection, critical revision and approval of article;

Ivo Lambrichts and Reinhilde Jacobs: Critical revision and approval of article.

Further acknowledgment to Omar El Mahraoui, Dr Yan Huang, Dr Mariana Quirino Silveira Soares and Dr Karla de Faria Vasconcelos for their help with the subjective observations.

Chapter 5: Laura Nicolielo: Drafting, critical revision and approval of article, data collection and analysis, statistics;

Jeroen Van Dessel: Critical revision and approval of article, statistics;

Reinhilde Jacobs: Critical revision and approval article;

Mariana Quirino Silveira Soares: Approval of article, data collection, statistics;

Bruno Collaert: Critical revision and approval of article, data collection and analysis;

Chapter 6: Laura Nicolielo: Drafting, critical revision and approval of article, data collection and analysis, statistics;

Jeroen Van Dessel: Critical revision and approval of article, statistics;

Eman Shaheen and Marina Codari: Data analysis, critical revision and approval of article;

Carolina Letelier: Data collection, critical revision and approval of article;

Constantinus Politis and Reinhilde Jacobs: Critical revision and approval of article.

Further acknowledgment to Walter Coudyzer from the Department of Radiology, University Hospitals Leuven, for kindly enabling the scanning with Somatom Definition Flash multi-slice computed tomography.

Personal Contribution

Laura Nicolielo conceived, planned and carried out the experiments, interpreted the results and wrote all manuscripts in consultation with the supervisors and co-authors.

Conflict of Interest

The authors declare no conflict of interest.

Laura Nicolielo was born in Porto Velho, Brazil on April 18th 1985. After completing the Dental School education at the University of São Paulo (USP) in 2009, she followed training in Oral Surgery in 2010. In 2011, she started her master studies in Applied Dental Sciences with focus on Oral Radiology & Pathology also at USP. At the same time, she specialized in Oral Implantology accomplishing both master and specialist titles in 2013. After applying for a full PhD position with the Brazilian National Grant, she simultaneously started in October 2013 Postgraduate in Advanced Medical Image and PhD training in the OMFS-IMPATh Research Group at KU Leuven, under supervision of Prof. Dr. Reinhilde Jacobs and Prof. Dr. Ivo Lambrichts (UHasselt). During this period, her research was focussed on developing 3D radiological methods for objective analysis in dentistry. Currently she is working as general dentist in Belgium.

Jaw bone evaluation through radiographs is an important procedure during diagnosis, planning and follow-up of treatments in maxillofacial surgery. Because of its easy acquisition and low radiation dose, conventional two-dimensional radiographs are the primary choice. With advances in three-dimensional radiographs technology and radiation dose reduction, Cone-Beam Computed Tomography (CBCT) became increasingly important for more detailed imaging of jaw bone structures, offering more realistic images with less distortion problems occasioned by two-dimensional techniques. The advantages of this three-dimensional technology, however, are not fully explored in clinical settings and evaluation of bone quality and quantity remains dubious. In the present thesis, we aimed to evaluate the capabilities of CBCT technology for objective analysis of jaw bone structures. Our findings showed that CBCT is an accurate and reliable clinical method for dentate and edentulous jaw bone structures. Moreover, the use of three-dimensional quantification methods can offer standardization for planning and following up of maxillofacial treatments.

